

Multispectral Image Deblurring

By

Elsie V. Morales Irizarry

A project report submitted in partial fulfillment
For the degree of

MASTER OF ENGINEERING

In

Electrical Engineering

UNIVERSITY OF PUERTO RICO
MAYAGÜEZ CAMPUS
2007

Approved by:

Miguel Vélez Reyes, Ph.D.
President, Graduate Committee

Date

Shawn D. Hunt, Ph.D.
Member, Graduate Committee

Date

Rafael Rodríguez Solís, Ph.D.
Member, Graduate Committee

Date

Fernando Gilbes, Ph.D.
Representative of Graduate Studies

Date

Isidoro Couvertier, Ph.D.
ECE Department Head

Date

ABSTRACT

Multispectral Image Restoration

By

Elsie V. Morales Irizarry

In this project, we implemented iterative algorithms for deblurring multispectral images. Deblurring was performed in a per channel basis. The algorithms were applied to LANDSAT-4 imagery of Puerto Rico. Deblurring methods resulted in sharpening of spatial features particularly in the infrared channels. Effects on classification were studied and it is shown that deblurring allowed correct classification of small spatial features lost due to sensor and atmospheric blurring.

RESUMEN

Restauración de Imágenes Multiespectrales

Por

Elsie V. Morales Irizarry

En este proyecto, implementamos algoritmos iterativos para reconstrucción de imágenes. La corrección de imágenes se llevó a cabo pixel a pixel. Estos algoritmos fueron aplicados imágenes de LANDSAT-4 del área sur de Puerto Rico. Los métodos usados dieron como resultado cambios de las características espaciales, especialmente en los canales infrarrojos. Los efectos en clasificaciones también fueron estudiados, y se probó que la corrección de imágenes permitió clasificaciones correctas en características u objetos pequeños que antes de la corrección no se podían notar debido a la distorsión causada por el sensor y la atmósfera.

“To all those persons who believed and believe in me . . .”

ACKNOWLEDGEMENTS

This project was supported by the **NASA University Research Centers Program** under Grant NCC5-518 and the **NSF Engineering Research Centers Program** under Grant ECC-9986821. The project presented herein used facilities of the **Center for Subsurface Sensing and Imaging Systems** at the University of Puerto Rico at Mayagüez.

TABLE OF CONTENTS

LIST OF TABLES	viii
LIST OF FIGURES	ix
1 Introduction	1
1.1 Problem Statement	2
1.2 Objectives	3
1.3 Report Outline	3
2 Background and Literature Review	5
2.1 Literature Review	5
2.2 Multispectral Imagery (MSI)	8
2.3 Spatial Restoration	10
2.3.1 Sensor Point Spread Function (PSF)	11
2.4 Image Restoration Algorithms	15
2.4.1 Van Cittert Method	16
2.4.2 Gold Method	16
2.4.3 Lucy-Richardson Algorithm	17
2.4 Conclusions	17
3 Experimental Results: Restored Images	18
3.1 Methodology	18
3.2 Image Restoration Routine Description	20
3.4 Restored Image, With Atmospheric Correction Results	32
3.5 Atmospheric Corrected Original and Restored Images Results	41
3.6 Effects of Stopping Criteria	49
3.7 Conclusions	57
4 Experimental Results: Effects on Classifications	58
4.1 Description of Classification Process	58
4.2 Restored Image Classification	62
4.3 Restored Image with Atmospheric Corrections Classification	65
4.4 Atmospheric Corrected-Restored Image Classification	67
4.5 Effects on Classification of Stopping Criteria	68
4.6 Conclusions	72
5 CONCLUSIONS AND FUTURE WORK	74
5.1 Summary	74
5.2 Conclusions	75
5.3 Future Work	76

BIBLIOGRAPHY	78
Appendix A	80
MATLAB Algorithm for the image without atmospheric corrections	80
Appendix B	87
MATLAB Algorithm for the image with atmospheric corrections	87
Appendix C	90
MATLAB Algorithm for the image with atmospheric corrections before restoration	90

LIST OF TABLES

Table 2.1 MSI Spatial Resolution (in meters).....	9
Table 3.1 LANDSAT-4 EIFOV values at nadir. EIFOV values adapted from [13].....	21
Table 3.2 Mean, standard deviation and correlation coefficients in percent of reflectance for the original image.....	29
Table 3.3 Mean, standard deviation and correlation coefficients in percent of reflectance for the restored image with atmospheric correction.....	38
Table 3.4 Mean, standard deviation and correlation coefficients in percent of reflectance for the atmospheric corrected-restored image.....	46
Table 3.5 Mean, standard deviation and correlation coefficient in percent of reflectance for the difference between images.....	53
Table 4.1 Tesing/training samples used for classification of the restored image.....	61
Table 4.2 Confusion matrix for the original image without atmospheric correction.....	63
Table 4.3 Confusion matrix for the restored image without atmospheric correction.....	64
Table 4.4 Confusion matrix for the original image with atmospheric correction.....	68
Table 4.5 Confusion matrix for the restored image with atmospheric correction.....	68
Table 4.6 Confusion matrix for the restored image with 5 iterations.....	72
Table 4.7 Confusion matrix for the restored image with 10 iterations.....	72

LIST OF FIGURES

Figure 1.1 Radiation distribution once entered the atmosphere.....	3
Figure 2.1 Original image (a), a blurred plus white gaussian noise (b) and a motion blurred (c) image.....	6
Figure 2.2 Spatial PSF response larger than GIFOV. (Figure adapted form [6]).....	7
Figure 2.3 Electreomagnetic spectrum.....	10
Figure 2.4 Atmospherc windows.....	10
Figure 2.5 Multispectral image acquisition model.....	11
Figure 2.6 Effects of the PSF on a point source image. (Adapted from [20]).....	11
Figure 2.7 Airy Pattern and its radial profile. (Adapted from [16]).....	12
Figure 2.8 Image motion during scan. (Adapted from [16]).....	13
Figure 2.9 Detector PSF. (Adapted from [16]).....	14
Figure 3.1 Figure 3.1. Block diagram of the methodology for the analysis of real data.....	19
Figure 3.2. DIRSIG simulated Image, (a). Blurred image with a Gaussian filter, (b); and restored image, using a Wiener filter, (c).....	20
Figure 3.3 Image Restoration Routine.....	21
Figure 3.5 Iterations results for band 5: 3rd iteration (a), 5th iteration(b), and 10th iteration (c).....	23
Figure 3.6 Original (a, d, g, j, m, p) and restored (b, e, h, k, n, q) images in grayscale. Difference of the images (c, f, i, l, o, r). Original (s) and Restored (t) image in RGB. Original (u) and Restored (v) image in CIR.....	24-25
Figure 3.7 Regions of the image where the PSF correction were more notable. Original (a, c, e), restored (b, d, f)...	27
Figure 3.8 Spectral profiles for original (a); and restored (b).....	28
Figure 3.9 Scatterplots per bands, bands 1 and 2 (a), bands 3 and 4 (b), and bands 5 and 7 (c).....	31
Figure 3.10 Plots of percent of reflectance per bands, bands 1 and 2 (a), bands 3 and 4 (b), and bands 5 and 6 (c), from original and restored images.....	32
Figure 3.11 Original (a, d, g, j, m, p) and restored (b, e, h, k, n, q) images in grayscale. Difference of the images (c, f, i, l, o, r). Original (s) and Restored (t) image in RGB. Original (u) and Restored (v) image in CIR.....	33-34
Figure 3.12 Regions of the image where the PSF correction were more notable. Original (a, c, e), restored (b, d, f).	36
Figure 3.13 Spectral profiles for original (a); and restored (b).....	37
Figure 3.14 Scatterplots per bands, bands 1 and 2 (a), bands 3 and 4 (b) and bands 5 and 7 (c).....	39
Figure 3.15 Plots of percent of reflectance per bands, bands 1 and 2 (a), bands 3 and 4 (b), and bands 5 and 6 (c), from original and restored images.....	40
Figure 3.16 Original (a, d, g, j, m, p) and restored (b, e, h, k, n, q) images in grayscale. Difference of the images (c, f, i, l, o, r). Original (s) and Restored (t) image in RGB. Original (u) and Restored (v) image in CIR.....	42-43

Figure 3.17 Regions of the image where the PSF correction were more notable. Original (a, c, e), restored (b, d, f).	44
Figure 3.18 Spectral profiles for original (a); and restored (b).	45
Figure 3.19 Scatterplots per bands, bands 1 and 2 (a), bands 3 and 4 (b) and bands 5 and 7 (c).	47
Figure 3.20 Plots of percent of reflectance per bands, bands 1 and 2 (a), bands 3 and 4 (b), and bands 5 and 6 (c), from original and restored images.	48
Figure 3.21 Original (a, d, g, j, m, p) and restored (b, e, h, k, n, q) images in grayscale for the fifth iteration. For the tenth iteration (c, f, i, l, o, r) are the resulting images. Original (s), Restored with 5 iterations (t), and Restored with 10 iterations (u) images in RGB. Original (v), Restored with 5 iterations (w), and Restored with 10 iterations (x) images in CIR.	51-52
Figure 3.22 Scatterplots per bands, for 5 iterations, bands 1 and 2 (a), bands 3 and 4 (c), bands 5 and 7 (e), and for 10 iterations, bands 1 and 2 (b), bands 3 and 4 (d), and bands 5 and 7 (f).	54
Figure 3.23 Plots of percent of reflectance per bands, for along-track transect of the image with 5 iterations; bands 1 and 2 (a), bands 3 and 4 (c), and bands 5 and 6 (e). Image with 10 iterations, bands 1 and 2 (b), bands 3 and 4 (d), and bands 5 and 6 (f), from original and restored images. Image with the transect used (g).	55
Figure 3.24 Plots of percent of reflectance per bands, for cross-track transect of the image with 5 iterations; bands 1 and 2 (a), bands 3 and 4 (c), and bands 5 and 6 (e). Image with 10 iterations, bands 1 and 2 (b), bands 3 and 4 (d), and bands 5 and 6 (f), from original and restored images. Image with the transect used (g).	56
Figure 4.1 Puerto Rico Natural Vegetation and Land Cover, 1991-1992.	59
Figure 4.2 Landsat image compared to IKONOS images, urban, barren and agriculture class (a), mangrove, barren, lowland semideciduous forest and water (b), and urban and inland water classes (c).	60
Figure 4.3 Thematic map for the image without atmospheric corrections. Image with ROIs (a), color map of classes (b), original (c) and restored (d) thematic maps.	62
Figure 4.4 Original (a), Restored (b), difference between images (c) and IKONOS image.	65
Figure 4.5 Original (a), Restored (b), difference between images (c) and IKONOS image.	66
Figure 4.6 Thematic map for the images with 5 and 10 iterations. Thematic map of the original (a), 3 iterations (b), 5 iterations (c) and 10 iterations (d) images.	69
Figure 4.7 Zoom of the thematic map for the images with 3, 5 and 10 iterations. Original (a), 3 iterations (b), 5 iterations (c) and 10 iterations (d) images.	70
Figure 4.8 Zoom of the thematic map for the images with 3, 5 and 10 iterations. Original (a), 3 iterations (b), 5 iterations (c) and 10 iterations (d) images.	71

1 Introduction

Remote sensing has been used for years, in astronomy, medicine, and in earth observations, just to mention a few applications. Multispectral imaging (MSI) consist of several channels of data, some of them with three to seven channels, with high spatial resolution. There are some advantages that characterize this technology for remote sensing. However, multispectral remote sensing images suffer from degradation, caused by the optics of the sensor, the platform motion, the detector, and the electronics of the sensor.

Spectral and spatial restoration are used to reveal information that is present but hidden in the data due to sensor degradation. Deconvolution is a useful technique to restore blurred images. There are many deconvolution methods, the one proposed by Jansson in [10] has been proven to be very effective. Other methods, also described in [10], include maximum likelihood, maximum entropy, and the alternating projection methods have also achieved certain success [16]. All these methods do require the knowledge of the instrument point spread function (PSF).

This work aims at implementing algorithms for multispectral image restoration and study the effects of deblurring in classification performance. We will also compare atmospherically corrected and non-corrected images before and after the restoration process to further study the effect of this combination of processing operations in classification performance.

1.1 Problem Statement

Multispectral Imaging (MSI) is used for object detection and environmental monitoring. MSI data consist of several spectral channels of data, some of them with three to seven channels, with varying spatial resolution. No matter which sensors we are using, the images are degraded since they have been affected by the atmosphere and the sensor, among other factors, resulting in producing as a result blurred images. Figure 1.1 illustrates how the radiation is distributed once it enters the atmosphere. Once the solar radiation enters the atmosphere it is reflected, transmitted, absorbed and emitted by the atmosphere itself and all the objects found in its path. For example, radiation can be reflected by aerosols and clouds; also, it can be absorbed by the earth surface, water bodies, and vegetation, just to mention a few. Then this radiation is emitted or reflected back to the atmosphere and collected by the sensor. The radiation collected by the sensor and all the contributions of the sensor cause blurred images. Some of the sources of degradation, besides the atmosphere, can be the sensor optics, the electronics, the motion of the sensor platform, and the motion of the target.

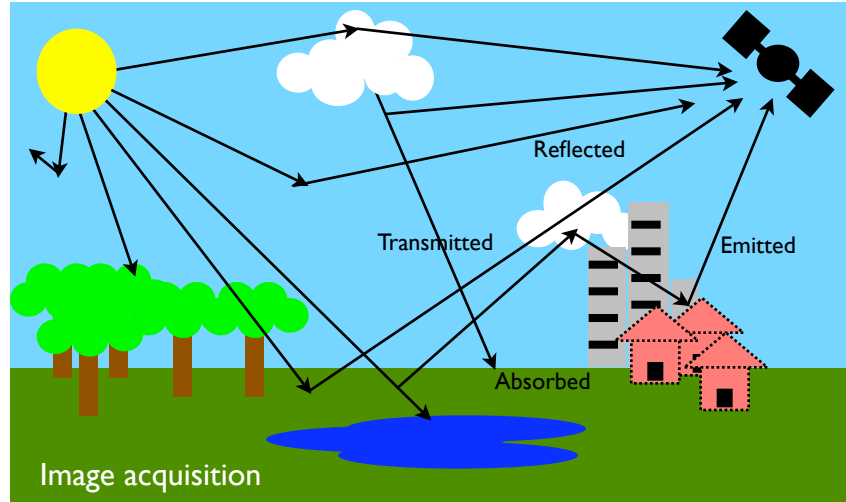


Figure 1.1 Radiation distribution once entered the atmosphere.

One of the consequences of degradation is that the pixels of the collected image are not pure, it has contributions of the pixels around it, causing blurred images. To solve this problem, an inverse procedure is used to recover original image from the degraded measurement. In this work, we implement restoration algorithms to restore blurred multispectral images.

1.2 Objectives

The main objective is to implement restoration algorithms for multispectral imagery and to study the effect of restoration in classification accuracy. Other objectives were:

- Create and develop a software application for multispectral image restoration.
- Study restoration and classification performance with and without atmospheric corrections.

1.3 Report Outline

This project report is organized as follow. In Chapter 2, we present the background and literature review for this project, a description of MSI data, the PSF, and of image restoration methods is also given. Chapter 3 is the application and performance analysis of the restoration algorithm

to real data. Experimental results are discussed. In Chapter 4, we present experimental results studying the effects of restoration in image classification. Chapter 5 contains conclusions and recommendations for future work.

2 Background and Literature Review

The image restoration problem is treated and solutions are presented to remove the degradations caused by the PSF of the sensor on multispectral images. In almost all the cases, an inverse procedure is used to recover an estimate of the original image from degraded measurements. An iterative restoration method derived through the Bayes theorem for conditional probabilities is presented.

2.1 Literature Review

“Digital image restoration is a field of engineering that studies methods used to recover an original scene from degraded observations” [1]. Digital image restoration has been used for years; based on the literature it began with the efforts of scientists from United States and the Soviet Union in the 1950s and 1960s [1]. In these programs, the scientists were taking photographs of the Earth and the solar system, but these images were subject to many degradations. Restoration at the time was highly expensive. Scientists began to look for less expensive meth-

ods to perform image restoration. Image degradation is also a problem that can be found in many areas, such as television, astronomy, optics, and medicine. Image restoration techniques have wide application.

The most common forms of degradation found in the literature are blur and noise. Figure 2.1 shows the original image (a), a blurred plus white gaussian noise (b) and a motion blurred (c) image. An inverse procedure is used to try to recover the original image from the degraded measurement. Some of the sources of degradations can be the sensor optics and its electronics, the motion of the sensor platform when, and the motion of the target.

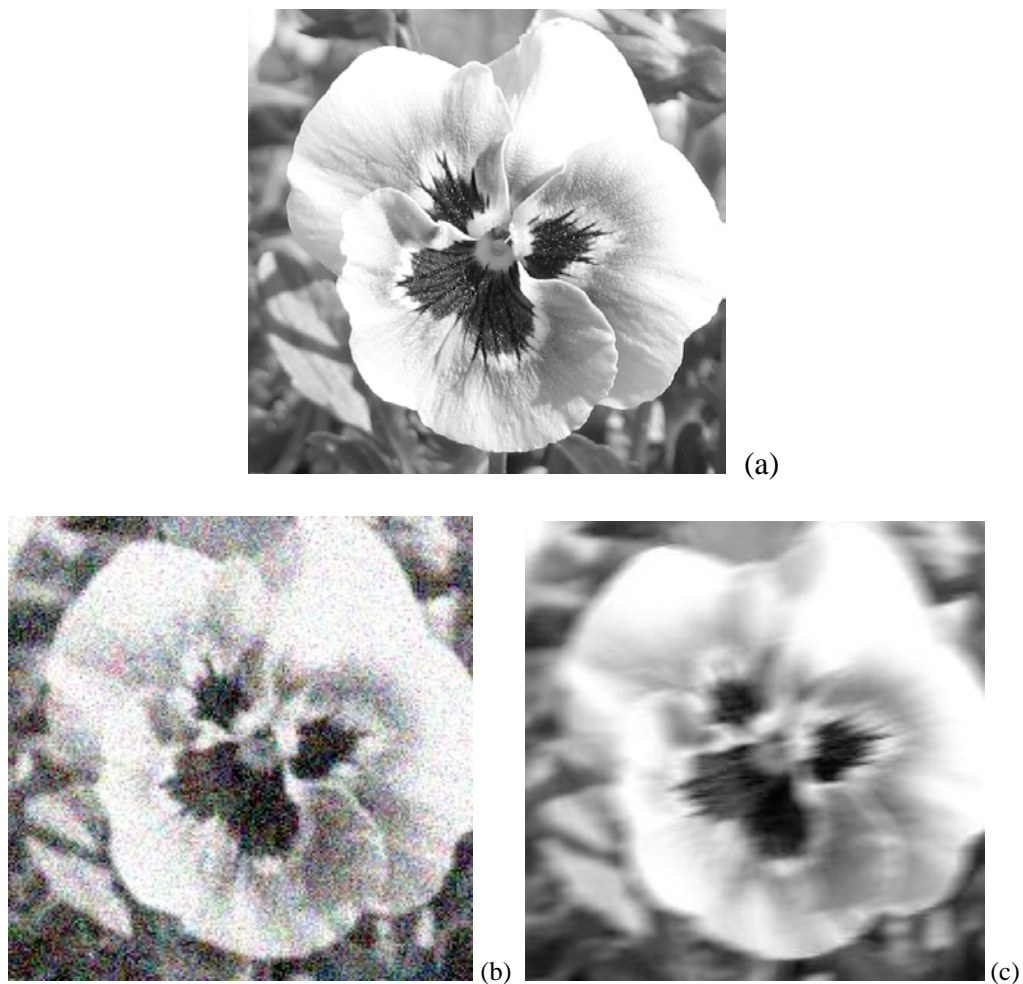


Figure 2.1 Original image (a), a blurred plus white gaussian noise (b) and a motion blurred (c) image.

Spatial Response: Larger than GIFOV

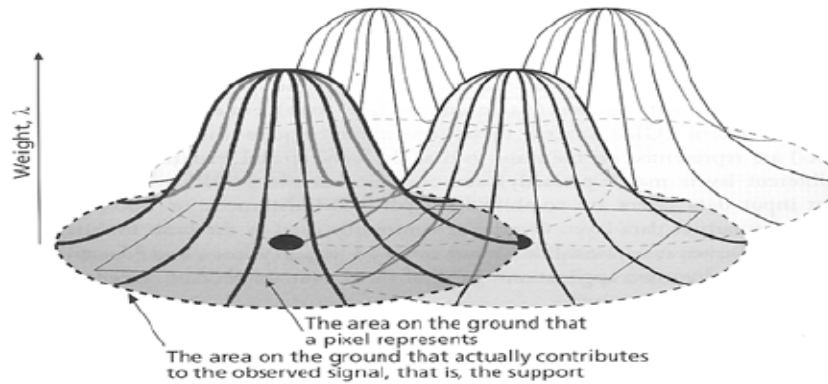


Figure 2.2 Spatial PSF response larger than GIFOV. (Figure adapted from [6]).

The recorded signal of each pixel of a satellite image has information from the pixels around it as described by the PSF of the sensor system [9]. Figure 2.2 illustrates the area on the ground that contributes to the obtained signal. Also, Huang et al., found in [9] that the impact of the PSF not only depends on it, but also depends on the spatial variability of the input pattern. Results from [9] show that generally, the PSF brightens dark objects and darkens bright objects.

It was found in [9] and [17] that the classification error of the classifier decreased after the restoration method and by deriving estimates for pixels twice their dimensional pixels size. Degradations or neighboring pixels contributions to the pixel under study can be ignored only when the pixel size is small relative to the area of land cover [17].

In [7] and [19], the process of restoring multichannel or multispectral image by using the Wiener Filter was presented. Galatsanos et al., in [7] used spatial and spectral correlation in order to correct for image degradation. It was found in [19] by Wu et al., that the process of image restoration is useful in increasing the accuracy of spectral unmixing. They used simulated data in

order to convolve this image with an original TM image. The description of the construction and properties of a two-dimensional random field, in this case with independent Poisson processes can be found in [15].

Four different iterative methods for spectral restoration: the Van Cittert, Jansson, Gold's and Lucy-Richardson method were described in [18]. They analyzed simulated and real data from AVIRIS NW Indian Pines Hyperspectral Image and found that all the methods gave similar results but the Jansson method was the best giving higher classification accuracy.

2.2 Multispectral Imagery (MSI)

Remote Sensing collection systems records electromagnetic (EM) radiation which may be solar reflected or thermal energy emitted by an object. This collection of EM radiation is subject to the amount of radiation that exits through the atmosphere or the atmospheric windows. EM radiation transmission is affected by the atmospheric attenuation. The latter is the effect that shows the ability of the atmosphere to reflect, absorb or scatter energy because of particulate matter, aerosols and water vapor found in the atmosphere. Atmospheric windows are those areas of the atmosphere that allow for transmission of the EM radiation. Figure 2.4 illustrates the atmospheric windows.

Multispectral imagery has been used for years in so many areas; military, medicine, land use/land cover, astronomy, among others. MSI was developed as a result of the operational success of Color Infrared (CIR) imagery used in the 1960's. These kind of imagery was used to distinguish artificial features, such as camouflage, from a background of natural vegetation [21]. The first satellite that used MSI for land remote sensing was the Earth Resources Technology Satellite-A (ERTS-S), later renamed as Landsat 1. Six additional Landsat satellites have been

launched; Landsat 1, 2, 3 and 4 are no longer operating, Landsat 6 failed achieving orbit and Landsat 5 and 7 are still operating. Landsat 7 has the Enhanced Thematic Mapper Plus (ETM+) which produces data in six spectral bands with a spatial resolution of 30 m, also has one pan-chromatic band with 15 m spatial resolution, and a long wave infrared band with 60 m spatial resolution.

Table 2.1 MSI Spatial Resolution (in meters).

Satellite	Spectral Bands (μm) and Spatial Resolution	Satellite	Spatial Resolution
Landsat ETM+	Vis. 0.45 - 0.52: 30 m Vis. 0.52 - 0.60: 30 m Vis. 0.63 - 0.69: 30 m NIR 0.76 - 0.90: 30 m NIR 1.55 - 1.75: 30 m Thermal 10.40 - 12.50: 120 m MIR 2.08 - 2.35: 30 m	AVHRR	Vis. 0.58 - 0.68: 1000 m NIR 0.72 - 1.10: 1000 m Thermal IR 3.55 - 3.93: 1000 m Thermal IR 10.50 - 11.50: 1000 m Thermal IR 11.50 - 12.50: 1000 m
SPOT 4	Vis. 0.50 - 0.59: 20 m Vis. 0.61 - 0.68: 20 m Vis. 0.79 - 0.89: 20 m MIR 1.58 - 1.75: 20 m PAN 0.51 - 0.73: 10 m	IKONOS	Vis. 0.45 - 0.53: 4 m Vis. 0.52 - 0.61: 4 m Vis. 0.64 - 0.72: 4 m NIR 0.77 - 0.88: 4 m PAN 0.45 - 0.90: 1 m

There are other MSI satellites, such as “SPOT” (Satellite Pour L’Observation de la Terre), AVHRR, and IKONOS among others. Table 2.1 lists spatial resolutions of some land sensorsⁱ.

MSI capture images in the visible spectrum, Near IR and the thermal infrared regions of the electromagnetic spectrum, see Figure 2.3. Numeric values or brightness values (also known as digital numbers (DN)) are recorded for the identification of brightness associated with light reflected from different material in each spectral band [21]. If the objective is to discriminate be

ⁱ For more information about multispectral sensors and the acronyms of these sensors see [12] and their respective websites.

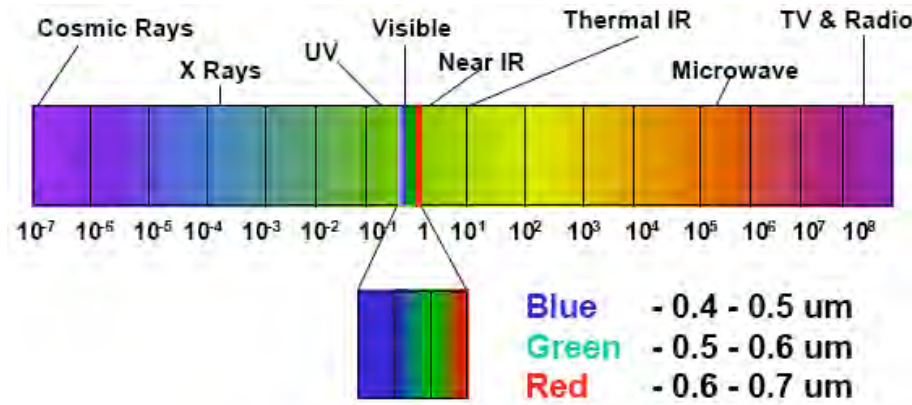


Figure 2.3 Electromagnetic Spectrum

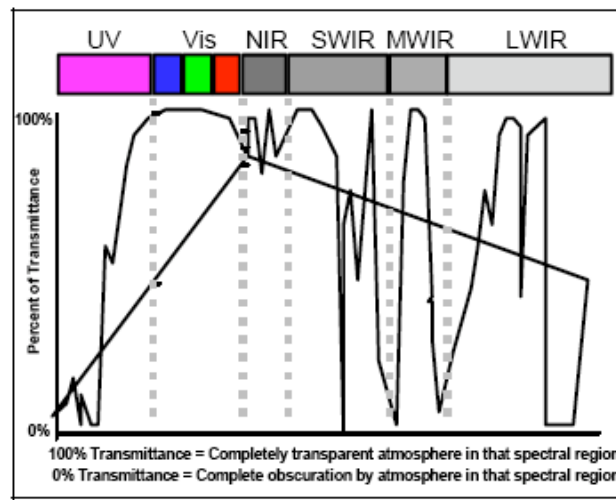


Figure 2.4 Atmospheric Windows.

tween various material on an image, it is necessary to chose the appropriate bands across the spectrum.

2.3 Spatial Restoration

Image degradation is a problem that can be found in so many areas, such as television, astronomy, optics, and medicine, just to mention a few. Figure 2.5 shows a block diagram representing the image acquisition restoration process, where $f(x,y)$ represents the input image, $h(x,y)$ is the sensor spatial weighting function, $g(x,y)$ is the degraded image and $\hat{f}(x,y)$ represents the restored image. There are many sources of degradations but the most common are blur and noise.

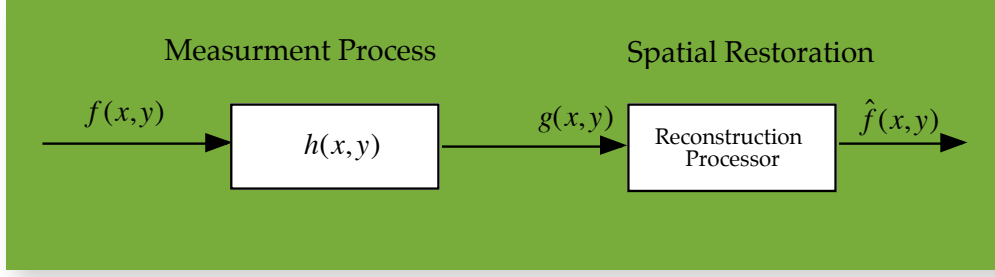


Figure 2.5 Multispectral image acquisition model.

In the following sections, we will describe the PSF as a spatial responsivity of the sensor and some iterative methods used for image restoration.

2.3.1 Sensor Point Spread Function (PSF)

In the spatial domain, the sensor modifies the properties of a scene in two ways. First as blurring the image due to the optics, the electronics of the sensor and the detector contributions; the second way is by distorting the geometry of the scene [16]. These distortions occur on a small spatial scale, small details are blurred compared with larger details or features on the image. This blurring is a result of the net sensor Point Spread Function (PSF_{net}). Figure 2.6 illustrates the effects of the PSF on a point source image.

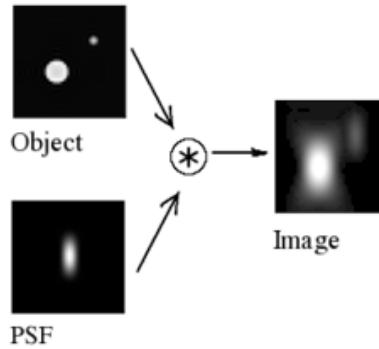


Figure 2.6 Effects of the PSF on a point source image. (Adapted from [20]).

Several components characterize the PSF_{net} . The first component is the blurring induced by the optical PSF. The second component is the image motion PSF, which is introduced when

the image is being formed by the optics on the detectors. The detectors also introduce blurring due to the detector PSF. The last component is the blurring induced by the electronics PSF.

In [16] the optical PSF is defined as the spatial energy distribution in the image of a point source. The image energy is spread over a small area in the focal plane. The resulting optical PSF given in a laboratory is called the Airy Pattern, which is a bright central disk surrounded by concentric rings with decreasing brightness (Figure 2.7). The optical PSF is given by the following equation [16]

$$PSF(r') = \left[2 \frac{J_1(r')}{r'} \right]^2 \quad (1)$$

where J_1 is the Bessel function of the first kind and the normalized radius is given by

$$r' = \frac{\pi D}{\lambda f} r = \frac{\pi r}{\lambda N} \quad (2)$$

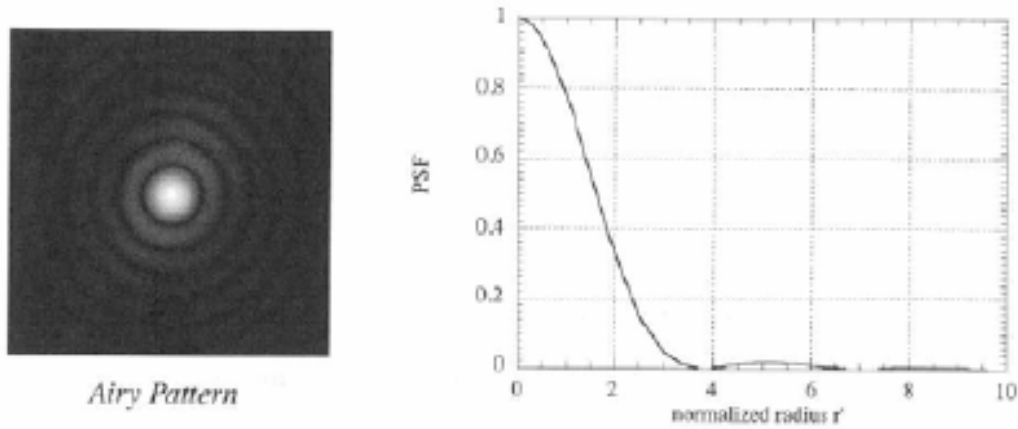


Figure 2.7 Airy Pattern and its radial profile. (Adapted from [16]).

Blurring is also caused by image motion, occurs when the image moves across the detectors during the integration time for a pixel signal. Image motion is modeled by a square pulse PSF in one direction (Figure 2.8); the latter is defined for whiskbroom and pushbroom scanners as follows

$$\text{whiskbroom scanner: } PSF_{IM}(x, y) = \text{rect}(x / s) \quad (3)$$

$$\text{pushbroom scanner: } PSF_{IM}(x, y) = \text{rect}(y / s) \quad (4)$$

where s is the spatial smear of the image in the focal plane, s is given by

$$\text{whiskbroom scanner: } s = \text{scan velocity} \times \text{integration time} \quad (5)$$

$$\text{pushbroom scanner: } s = \text{platform velocity} \times \text{integration time} \quad (6)$$

These equations describe the image motion PSF. Figure 2.8 shows a diagram of image motion during scan.

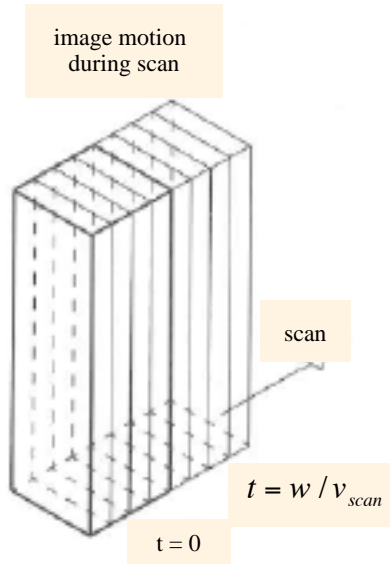


Figure 2.8 Image motion during scan. (Adapted from [16]).

The third component of the net PSF is the detector PSF (Figure 2.9), which is given by

$$PSF_{det}(x, y) = \text{rect}(x / w) \text{rect}(y / w) \quad (7)$$

The last response that compose the net PSF is the electronics PSF. When the signal is been scanned and read from the detectors the electronics PSF operate in the temporal domain of the signal.

The net sensor PSF is the convolution of the individual responses and the equation is given by

$$PSF_{net}(x, y) = PSF_{opt} * PSF_{det} * PSF_{IM} * PSF_{el} . \quad (8)$$

The net sensor PSF generally, is wider than the ground instantaneous field of view (GIFOV)

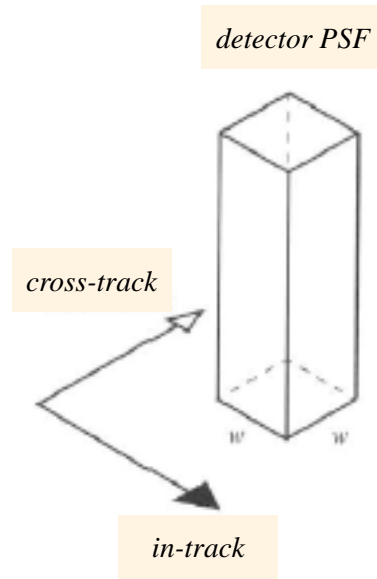


Figure 2.9 Detector PSF. (Adapted from [16]).

because of these individual responses described above. In many cases, the net PSF is separable in the cross-track and in-track directions as follows

$$PSF_{net}(x, y) = PSF_i(x)PSF_c(y) . \quad (9)$$

The degraded image in the spatial domain is modeled as a convolution between the original image and the imaging PSF (9).

$$g(x,y) = PSF_{net} * f(x,y) + n(x,y) \quad (10)$$

where $g(x,y)$ is the degraded image, $f(x,y)$ is the original image, and $n(x,y)$ is the additive noise.

For now, we will assume $n(x,y) = 0$, then we have for a linear imaging system,

$$g(x,y) = h(x,y) * f(x,y) \quad (11)$$

where $h(x,y)$ is the PSF of the sensor.

We can also express the latter equation (11) as a matrix, $\mathbf{g} = \mathbf{H}\mathbf{f} + \mathbf{n}$, where \mathbf{H} is the matrix for the PSF and \mathbf{f} is the matrix of the original image, if $\mathbf{n} = \mathbf{0}$, then

$$\mathbf{g} = \mathbf{H}\mathbf{f}. \quad (12)$$

2.4 Image Restoration Algorithms

In this project we aim to minimize the effects of the PSF on the image (12).

$$\hat{\mathbf{f}} = \arg \min_{\mathbf{f}} \|\mathbf{H}\mathbf{f} - \mathbf{g}\| \quad (13)$$

There are different types of restoration methods found in the literature, these are divided in direct and iterative algorithms. The Wiener filter is a direct method for image reconstruction, this filter aims to minimize the mean square error (MSE) between the estimated and the original image.

The MSE is given by

$$e^2 = E\left\{\left(\mathbf{f} - \hat{\mathbf{f}}\right)^2\right\} \quad (14)$$

where $E\{\bullet\}$ is the expected value of the argument [2]. For more information on Wiener filter see [2]. In the following sections, we describe some iterative methods used for image restoration.

2.4.1 Van Cittert Method

This method is considered one of the earliest and simplest methods for image restoration. For a general discrete system it is given by,

$$\hat{\mathbf{f}}^{k+1} = \hat{\mathbf{f}}^k + \mu(\mathbf{g} - \mathbf{H}\hat{\mathbf{f}}^k) \quad (15)$$

where k represents the iteration number, μ is a relaxation factor, $\hat{\mathbf{f}}^k$ is the estimated image at the k -th iteration, \mathbf{g} is the degraded image and \mathbf{H} is the blurring operator [18]. \mathbf{H} must satisfy a diagonal dominance condition, in order to converge. This condition is given by

$$\mathbf{H}_{ii} > \sum_{j \neq i}^{N-1} \mathbf{H}_{ij} \quad (16)$$

2.4.2 Gold Method

This iterative method can be obtain from the Van Cittert method by letting the relaxation factor equal to the following equation:

$$\mu_i = \frac{\mathbf{f}_i^k}{(\mathbf{H}\mathbf{f}^k)_i} \quad (17)$$

If we substitute μ in (15) we have

$$\hat{\mathbf{f}}_i^{k+1} = \frac{\mathbf{g}}{(\mathbf{H}\hat{\mathbf{f}}^k)_i} \hat{\mathbf{f}}_i^k \quad (18)$$

where $(\mathbf{H}\hat{\mathbf{f}}^k)_i$ is the i -th component of the vector $\mathbf{H}\hat{\mathbf{f}}^k$.

2.4.3 Lucy-Richardson Algorithm

The Lucy-Richardson algorithm is an iterative method for recovering an image that has been blurred by a known PSF. This iterative method is derived through the Bayes theorem for conditional probabilities and is given by

$$\hat{f}_k = \hat{f}_k \left(\frac{\mathbf{g}}{\hat{f}_k * h} \times h \right) \quad (19)$$

where \times denotes correlation, $*$ denotes convolution and \hat{f}_k is the estimate of the original image at step k of the iterations[23]. The Lucy-Richardson algorithm converges to the maximum likelihood solution for Poisson noise statistics. Moreover; if the SNR is too low it amplifies the noise. We will use this method for image reconstruction.

2.4 Conclusions

In this Chapter, background information and literature review were presented. In addition, description and examples of blurred images were shown. The PSF for a remote sensing system was presented and a summary of restoration algorithm is given.

3 Experimental Results: Restored Images

In this chapter, application of the restoration algorithm applied to LANDSAT-4 imagery is presented. Analysis of three restored images are shown; a restored image compare with the original image, a restored image with atmospheric corrections after the application of the restoration algorithm and an atmospherically corrected image restored with the Lucy-Richardson algorithm.

3.1 Methodology

Application of the Lucy-Richardson restoration method to simulated and real data. Analyze the results obtained, and compare the restored image with the original image in order to see the spatial differences, then compute classification accuracies statistics before and after the restoration process (Described in Chapter 4). MATLAB® and ENVI® were used for this purpose. Figure 3.1 shows a chart of the processing stages applied to the LANDSAT-4 imagery.

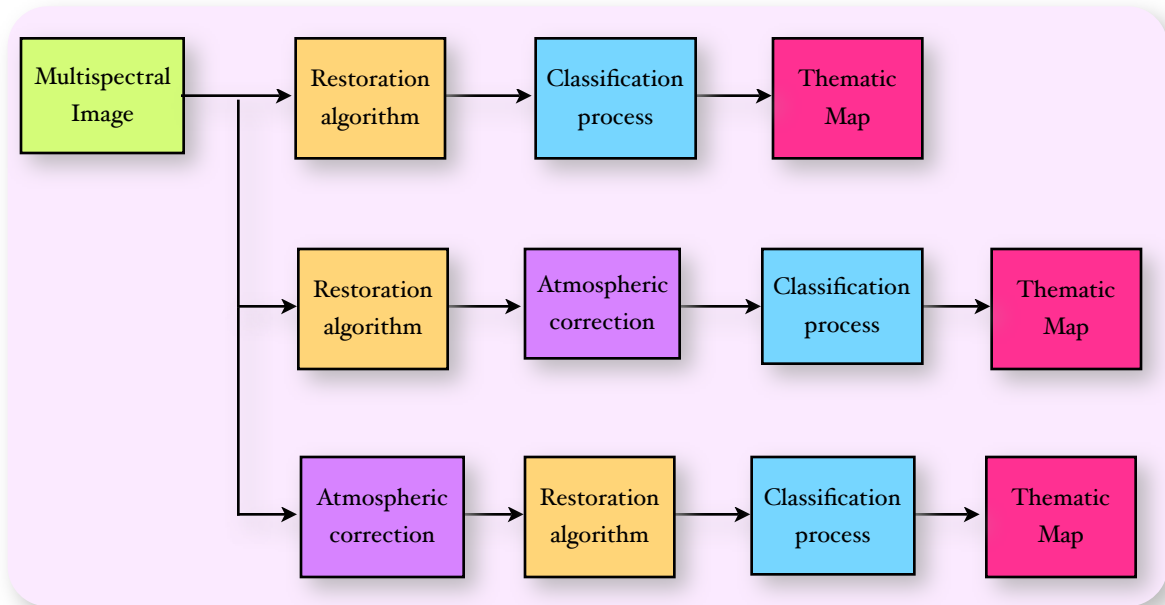


Figure 3.1. Block diagram of the methodology for the analysis of real data.

In order to have a simulated image, we used DIRSIG to simulate a simple image based on a scene from Rochester, NY (43° N, 78° W) taken on June 14, 2005 at 2:00 p.m.. The simulation used a fixed/static platform over the scene and it was pointing at nadir. Figure 3.2(a) shows the simulated image without any degradation. Then, in MATLAB®, a Gaussian filter with a 5×5 window and standard deviation equal to one was applied to the image. The latter creates a blurred image (Figure 3.2(b)). Figure 3.2(c) shows the restored image, after we applied a Wiener filter. It can be notice that the restored image still have some blur, in this project we aim to eliminate as much as degradation caused by PSF as we can in order to have a more accurate classification process.

For the real data analysis we used an image acquired by the Landsat TM 4 sensor on January 20, 1999 over the southern region of Puerto Rico, we used the region of the Guayanilla bay

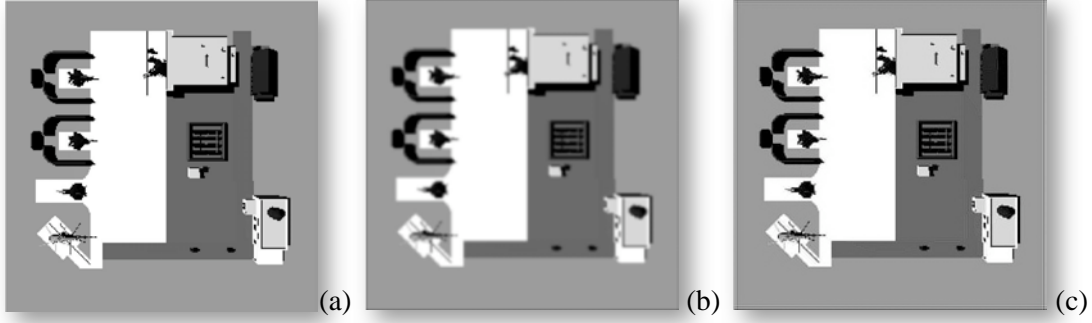


Figure 3.2. DIRSIG simulated Image, (a). Blurred image with a Gaussian filter, (b); and restored image, using a Wiener filter, (c).

(18.1°N, 66.2°W). The image file includes seven bands, but for our analysis we chose the first five bands and band 7. In the following sections, results from real data are shown.

3.2 Image Restoration Routine Description

The code used was organized in two stages. In stage 1 the PSF matrix is computed and the restoration method is applied to obtain the restored image. A header file is generated for future analysis in ENVI®. The second stage, is for results analysis. It calculates the differences of the images obtained in stage 1. Also, in stage 2, mean and standard deviation values of the difference between images, scatterplots comparing the different bands are produced. Figure 3.3 presents a flow chart of the routine with the stages. It begin by loading the blurred image acquired by LANDSAT TM 4. Compute the PSF matrix using parameters from the literature [13].

The PSF of LANDSAT TM 4 is a separable PSF. The along-track and cross-track follow a normal gaussian shape. The cross-track (PSF(x)) and in-track (PSF(y)) PSF are described by

$$PSF(x) = \frac{1}{\sqrt{2\pi}\sigma_x} e^{-\frac{x^2}{2\sigma_x^2}} \quad (1)$$

$$PSF(y) = \frac{1}{\sqrt{2\pi}\sigma_y} e^{-\frac{y^2}{2\sigma_y^2}} \quad (2)$$

The values for sigma give the Effective Instantaneous Field of View (EIFOV) of the sensor. For the first four bands of LANDSAT TM 4, the EIFOVs are 35.9 m and 32.1 m, cross-track and along-track directions, respectively [12]. For bands 5 and 7 the EIFOVs are, 35.7 m and 33.3 m cross-track and along-track, respectively [12]. Table 3.1 shows the EIFOV values for LANDSAT TM 4.

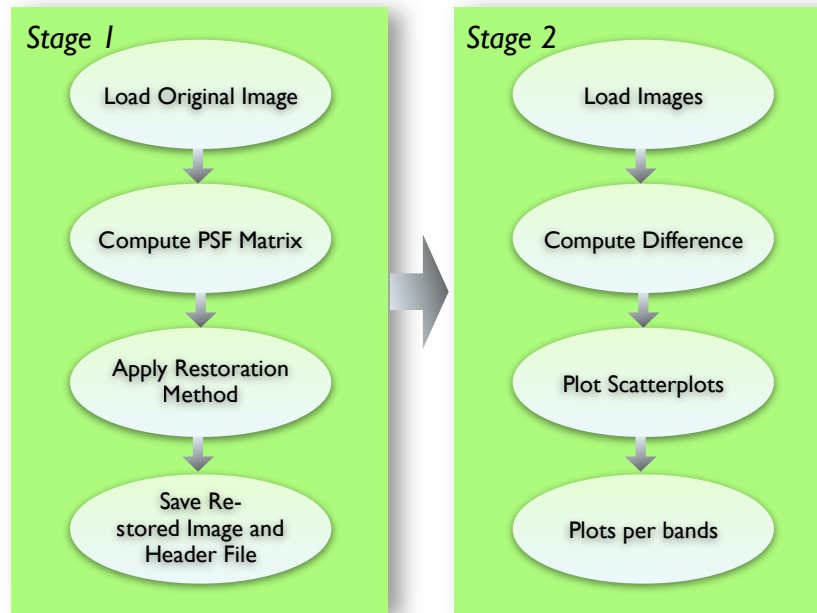


Figure 3.3 Image Restoration Routine.

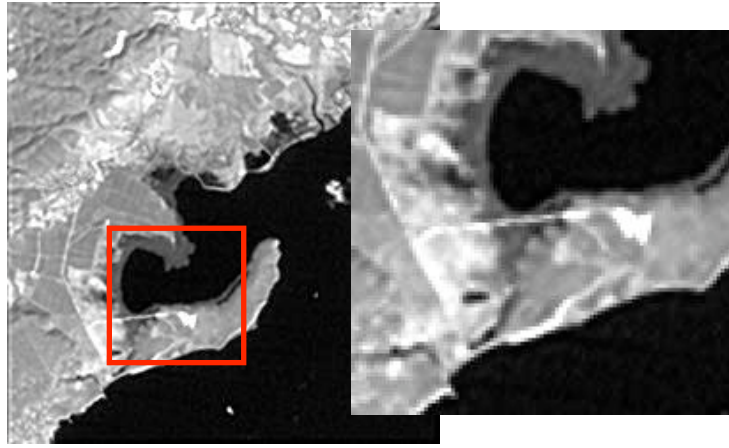
Table 3.1 Landsat TM 4 EIFOV values at Nadir. EIFOV values adapted from [13].

Landsat - 4 Spectral Bands	FOV [m]	EIFOV [m]	
		cross-track (x-dir)	along-track (y-dir)
1, 2, 3, 4	30	35.9	32.1
5, 7	30	35.7	33.3
6	120	141.1	123.9

3.3 Restored Image Without Atmospheric Corrections Results

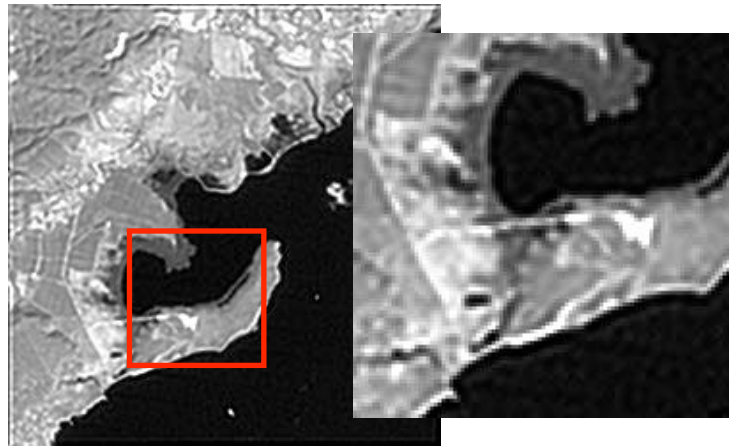
For this project, we used an image from LANDSAT TM 4 to perform the restoration process. Figure 3.5 show examples of the iterations results for band 5 in grayscale. We found that the third iteration show very good results, in further iterations the algorithm diverges and the details are lost. We found that in grayscale (band 5) the changes are more notable than in RGB (bands 3, 2, 1). Figure 3.6 shows the results without atmospheric corrections of the original and restored images in RGB, CIR (bands 4, 3, 2), and from band 1-5 in grayscale, we also show the difference between these images with a color bar in percent of reflectance that goes from black to white meaning, zero to some changes.

If we compare these images (Figure 3.6) in large scale, we can see that the color on the RGB are enhanced to brighter colors. The mountains, their shadows and urban areas are much defined than in the original image; even the clouds and their shadows are brighter. If we see the grayscale image, the details are also enhanced. The borders are more defined in the restored image than in the original, giving us an idea of where start or ends a region. For example; the areas that looks like agriculture lands can be defined easily in the restored image. Other features, are the coastal border and some water bodies on land, the urban regions, and the ridges of the mountains.



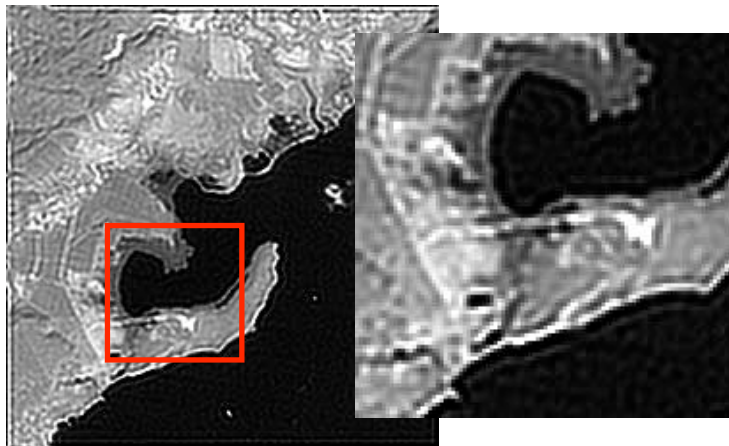
3rd iteration

(a)



5th iteration

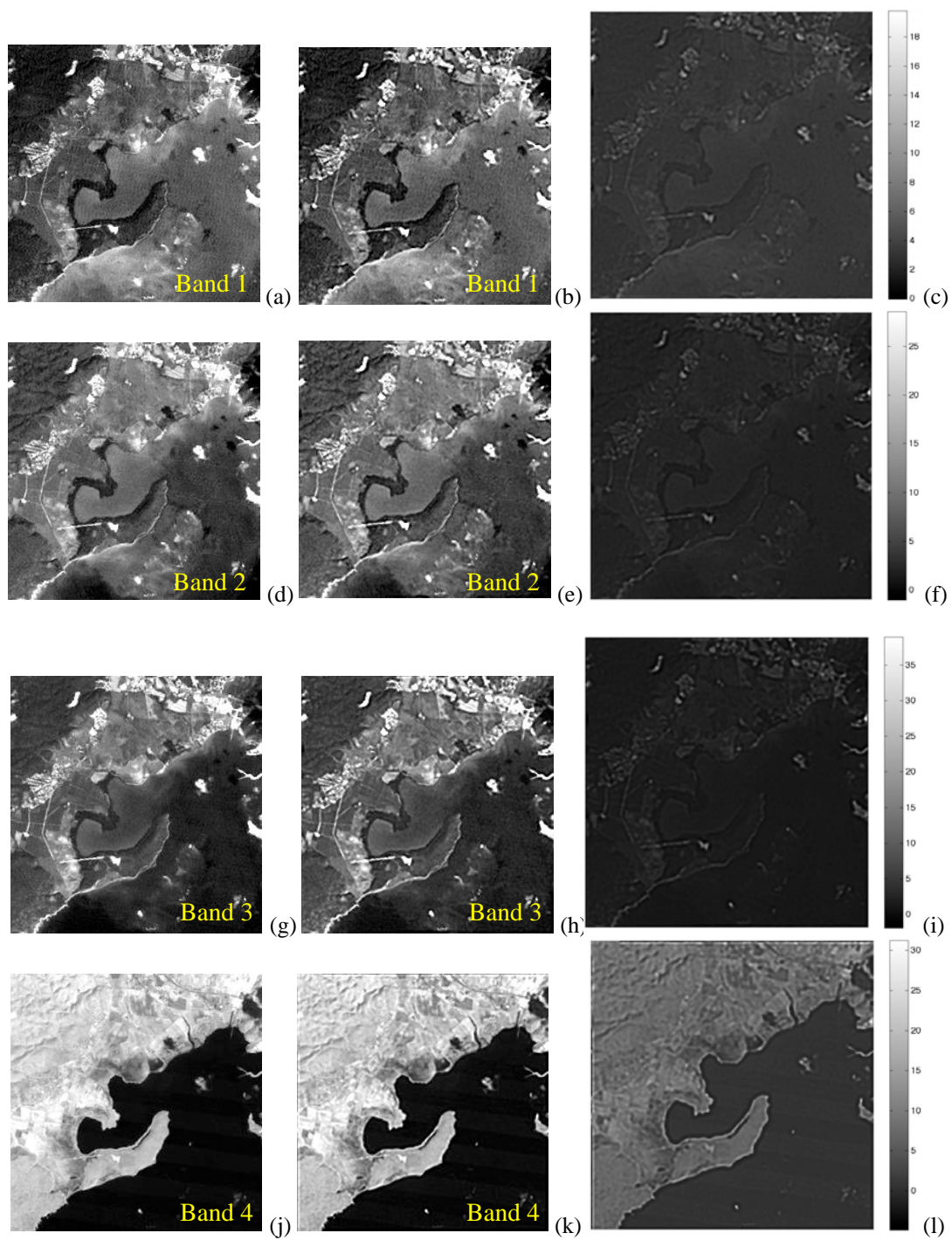
(b)



10th iteration

(c)

Figure 3.5 Iterations results for band 5: 3rd iteration (a), 5th iteration(b), and 10th iteration (c)



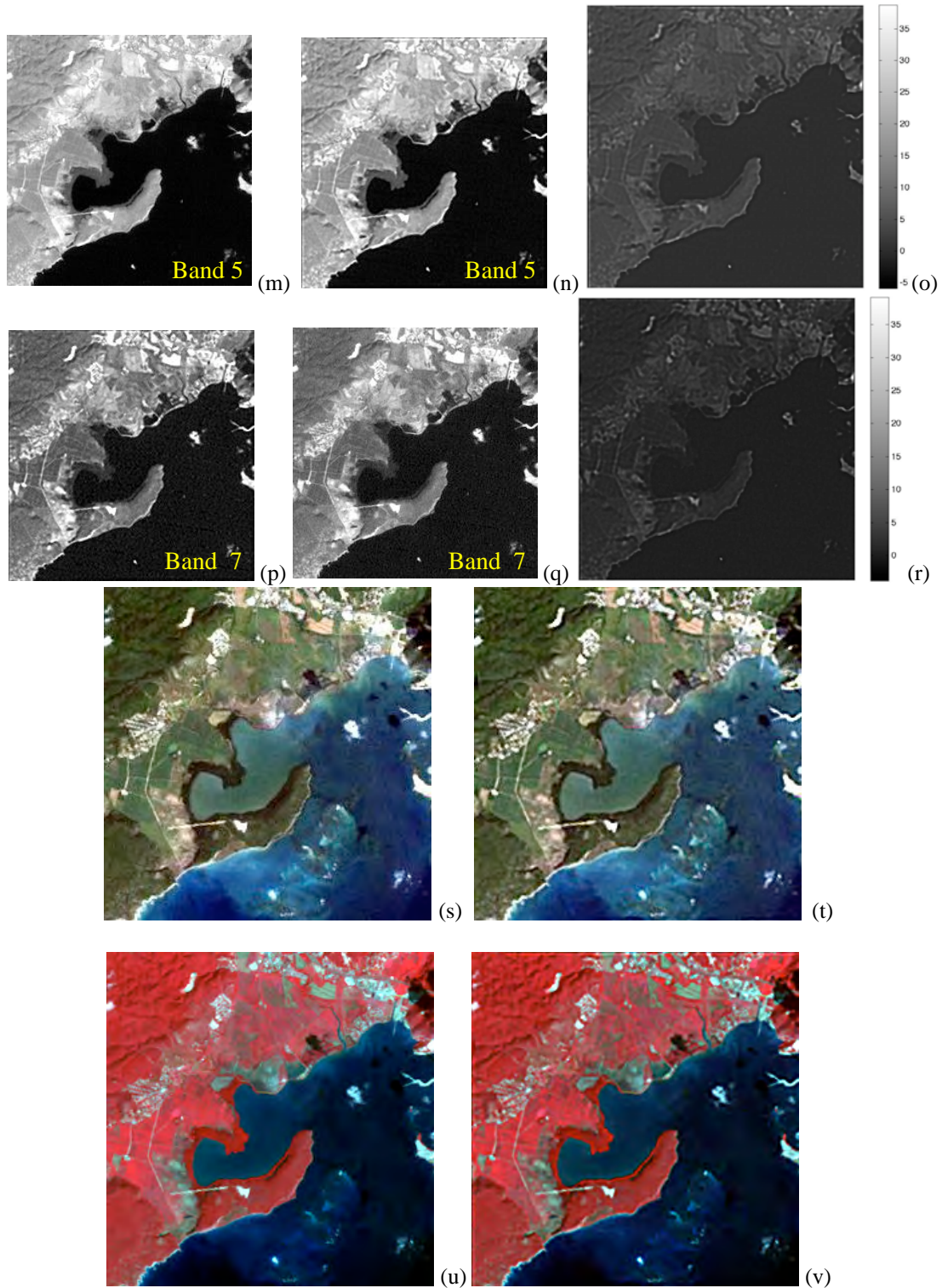


Figure 3.6 Original (a, d, g, j, m, p) and restored (b, e, h, k, n, q) images in grayscale. Difference of the images (c, f, i l, o r). Original (s) and Restored (t) image in RGB. Original (u) and Restored (v) image in CIR.

The point spread function is usually evaluated and studied by using point sources of light, we cropped some regions from the original and restored images that looks like a point; and other small areas showing borders and lines. In figure 3.7, we illustrate these areas from the image where the PSF correction was more notable. We chose keys around the coast, and two different areas from the coast in order to show the results of the restoration process. It is clear that the shape or geometry of the object is more defined in the restored image. It was found that, the darker pixels are brighter and the brighter pixels are darker. This changes can be seen on the RGB images.

Image restoration changes, can also be appreciated on the spectral profiles. Figure 3.8 illustrate plots with the spectral reflectance profiles before and after the restoration. These are characteristic profiles of some features of the image, such as, water, urban areas, pasture and agriculture fields (“Pasture”), and lowland dry semideciduous forest “(Forest)”. An average profile along the bands was used to draw the plots; ENVI® was used to obtain these results. Reflectance is a ratio of reflected flux from a certain surface to reflected flux from a Lambertian surface. In other words, is the measure of the portion of light that reflects from an object.

In these plots, we can see the spectral separability, for example, water and the other three signatures are very close in the original image plot, but are very separated in the restored one. The water is not a good reflector, because of that we are having small reflectance values. Other, characteristics of these spectral profiles are the initial values of the curves. For example, the urban feature have reflectance values of about 0.22 and 0.27 for the original and restored image, respectively. This is a result of the PSF restoration process, the image become brighter.

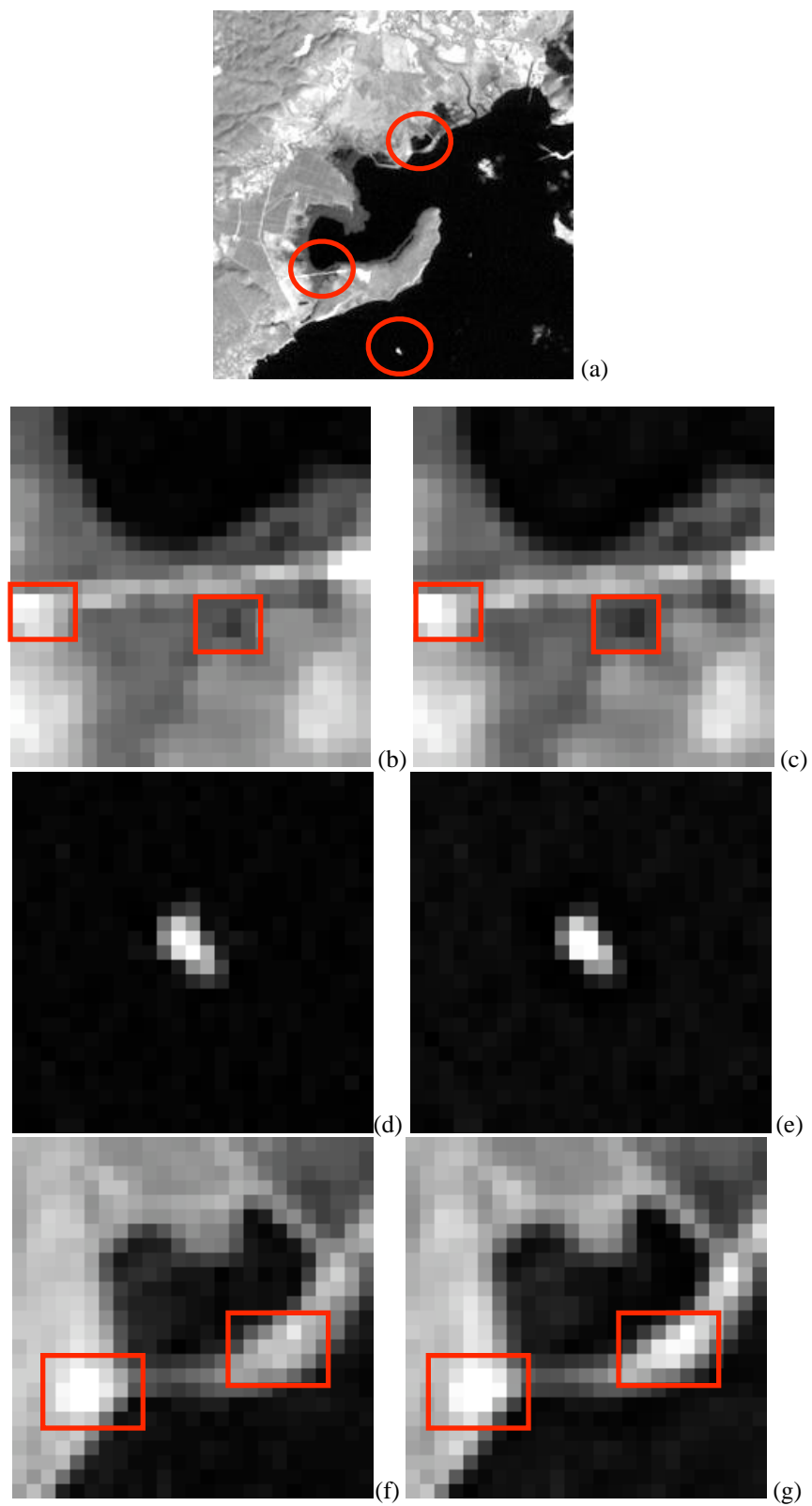


Figure 3.7 Regions of the image where the PSF correction were more notable (a). Original (b, d, f), restored (c, e, g).

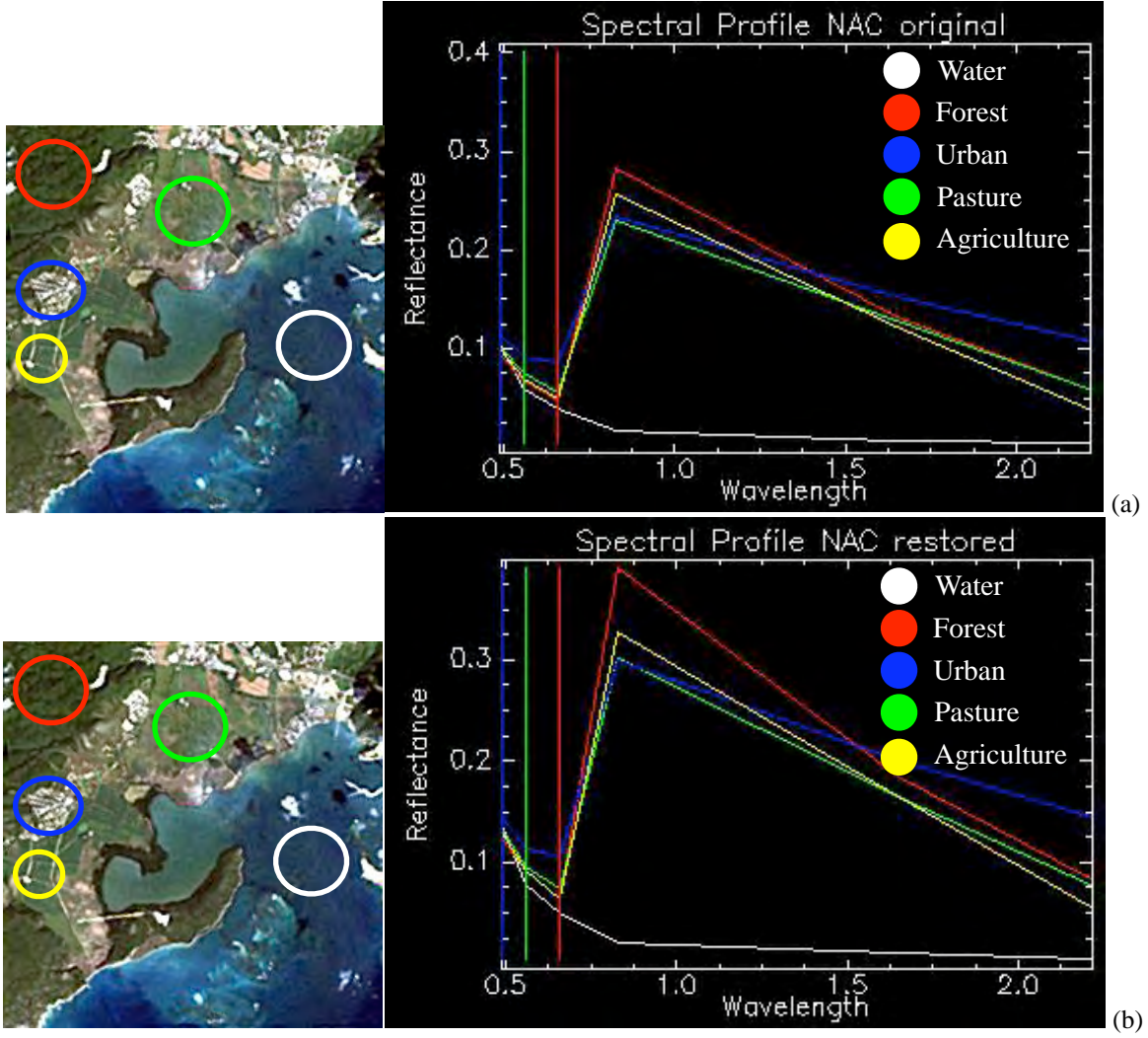


Figure 3.8 Spectral profiles for original (a); and restored (b).

In Section 3.2, we described the two stages for the algorithm used to restore images; in the second stage, the main objective is to develop quantitative evaluations of the restored images obtained in order to compare the changes due to the restoration process.

In order to measure the performance of the restoration method, we quantify the impact of the PSF by calculating the mean, standard deviation and correlation coefficient of the difference between the two images, original and restored. In Table 3.2 we show the results for these calculations and the correlation coefficient between the bands of both images, original and restored.

Table 3.2 Mean, standard deviation and correlation coefficient in percent of reflectance for the original image.

	Band 1	Band 2	Band 3	Band 4	Band 5	Band 7
Mean	0.7344	0.8817	1.2401	4.0357	2.7563	1.9062
Standard deviation	3.2865	2.1964	1.6751	4.2623	2.4862	1.3678
Correlation coefficient	0.9849	0.9847	0.9845	0.9938	0.9926	0.9891

Once we have the differences between the images, we developed scatterplots comparing the same bands from the two images (for example, band 1 of the original image and band 1 of the restored image). Figure 3.9 show the reflectance values (%) of the original and restored. With these scatterplots, we show the expected results when a restoration algorithm is applied to an image, the dark pixels were brighter and bright pixels were less bright when compared to the pixels of the original image.

The last step of the second stage of the algorithm is dedicated to plot the bands of the images and compare the changes due to the PSF corrections. Figure 3.10 show plots of the changes in reflectance values of the bands from the original and restored images. In these plots we aim to show the enhancement due to the PSF restoration, the red plot is for the reflectance values of the restored image and the blue plot is for the original image. In all bands the reflectance raised about 4%, meaning that the image is brighter after the restoration.

In the following sections we show results of images atmospherically corrected before and after the restoration process.

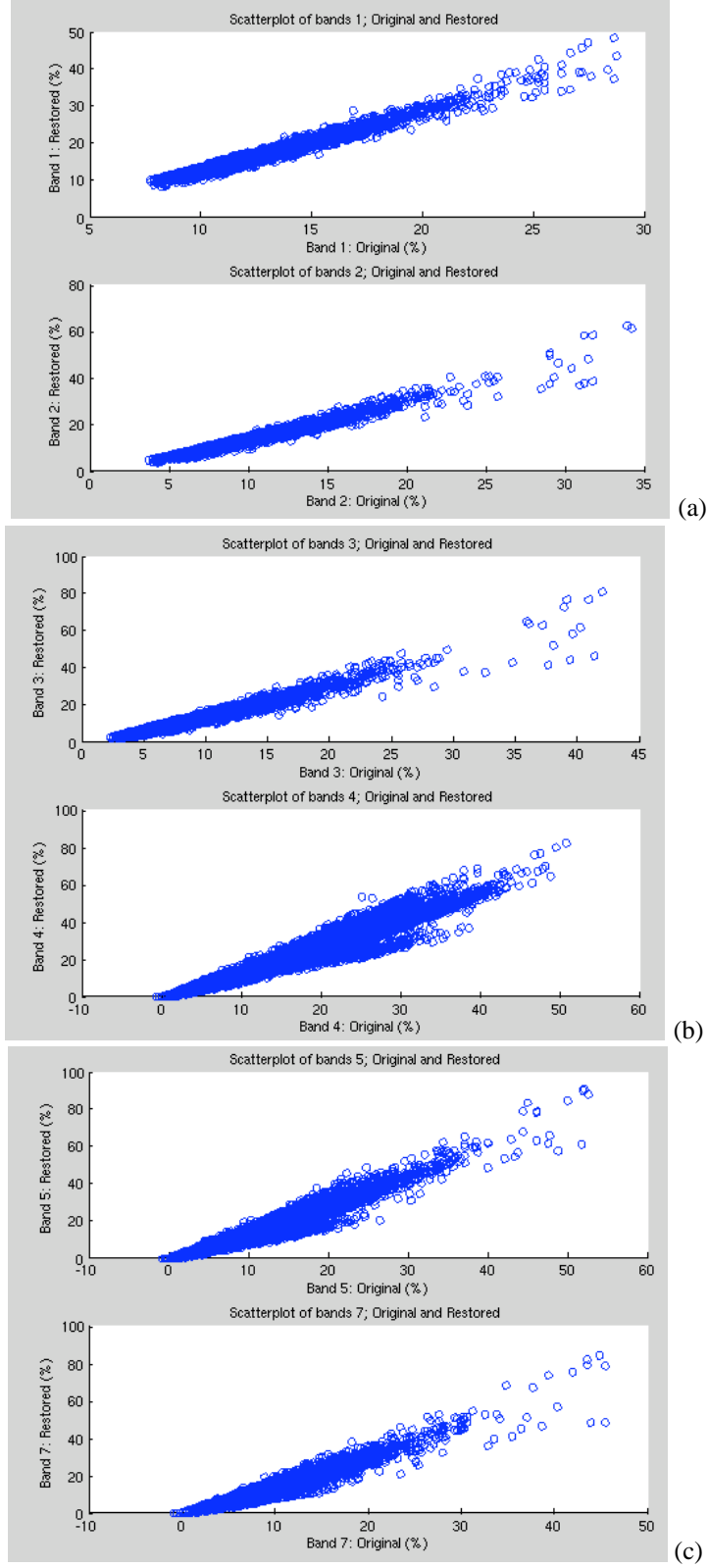


Figure 3.9 Scatterplots per bands, bands 1 and 2 (a), bands 3 and 4 (b), and bands 5 and 7 (c).

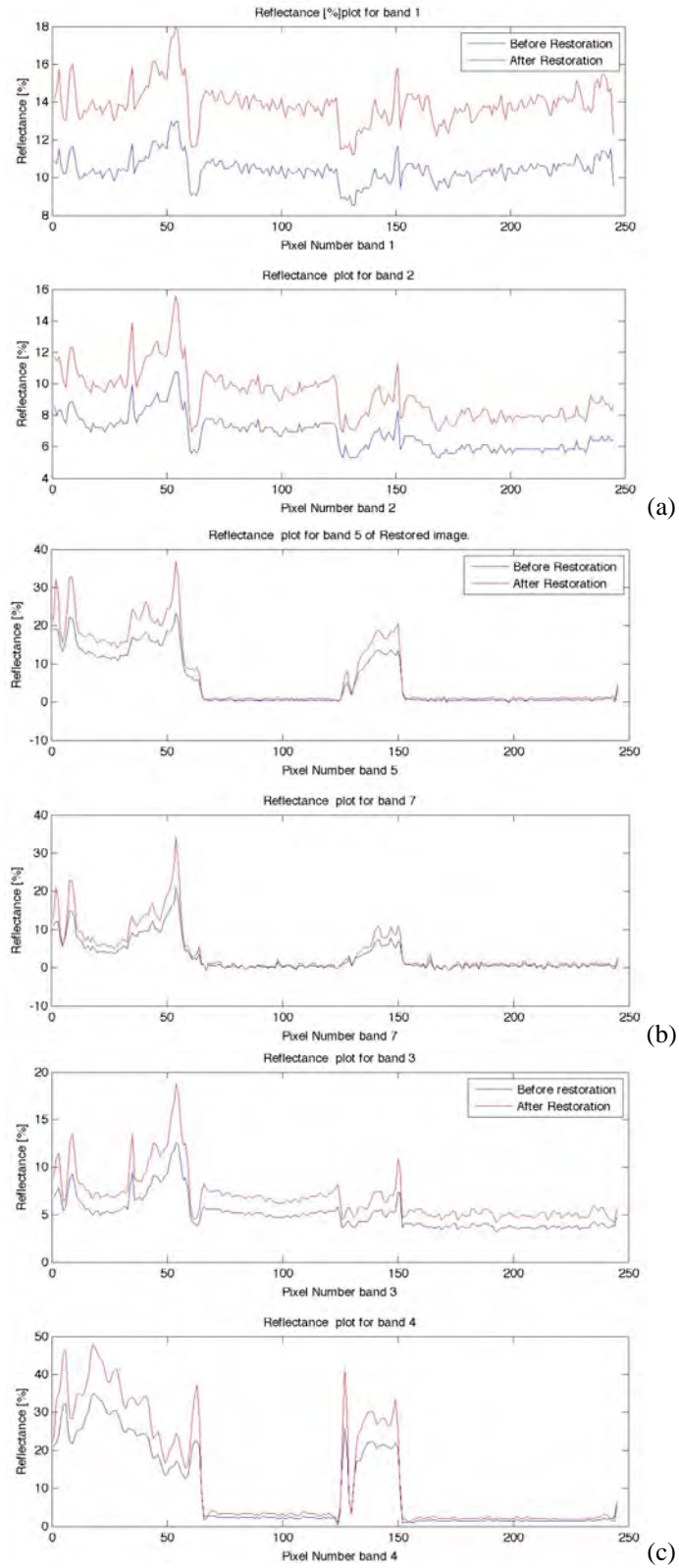


Figure 3.10 Plots of percent of reflectance per bands, bands 1 and 2 (a), bands 3 and 4 (b), and bands 5 and 6 (c), from original and restored images.

3.4 Restored Image, With Atmospheric Correction Results

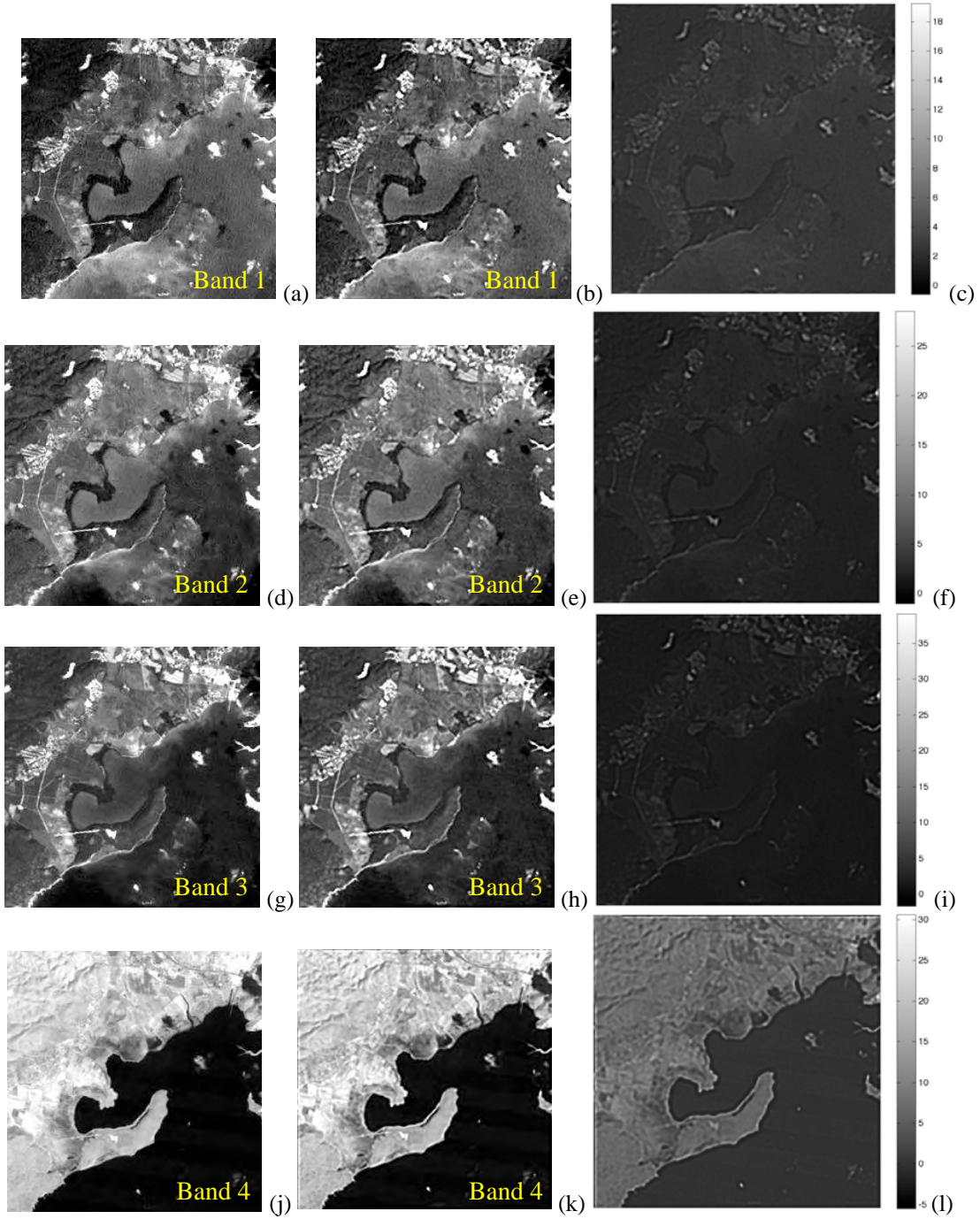
In this section, we present results of the restored image, with atmospheric corrections. In this work, we also aim to study the effects caused by an atmospheric correction method on the image and on the classification (See Chapter 4), before and after the restoration process. We used the original and restored images from the latter section and applied the dark-object method for atmospheric correction. This method is one of the oldest and simplest methods for this purpose. It consist of subtract the image pixel value of each band by its minimum value. These pixels have negligible surface reflectance values, usually called “dark-objects”. The procedure described by [12] to correct for atmosphere in TM imagery is as follows:

- Identify dark pixels in the middle-IR (band 7, around $2.1\mu\text{m}$) by using a low-threshold reflectance value.
- Calculate surface reflectance values of bands 1 (blue) and 3 (red) using the following equations [12]:

$$\begin{aligned}\rho_{red} &= 0.5\rho_{2.1} \\ \rho_{blue} &= 0.25\rho_{2.1}\end{aligned}\tag{7}$$

- Determine the optical depths of bands 1 and 3.
- Determine the optical depths of other bands.
- By using a moving-window interpolation technique, estimate the spatial distribution of the optical depth.

In order to use the method described, the image data was changed to reflectance values. We used ENVI® to get these results. Our purpose is to show results from PSF restoration, in this section we will compare the restored images with the original image from Section 3.3.



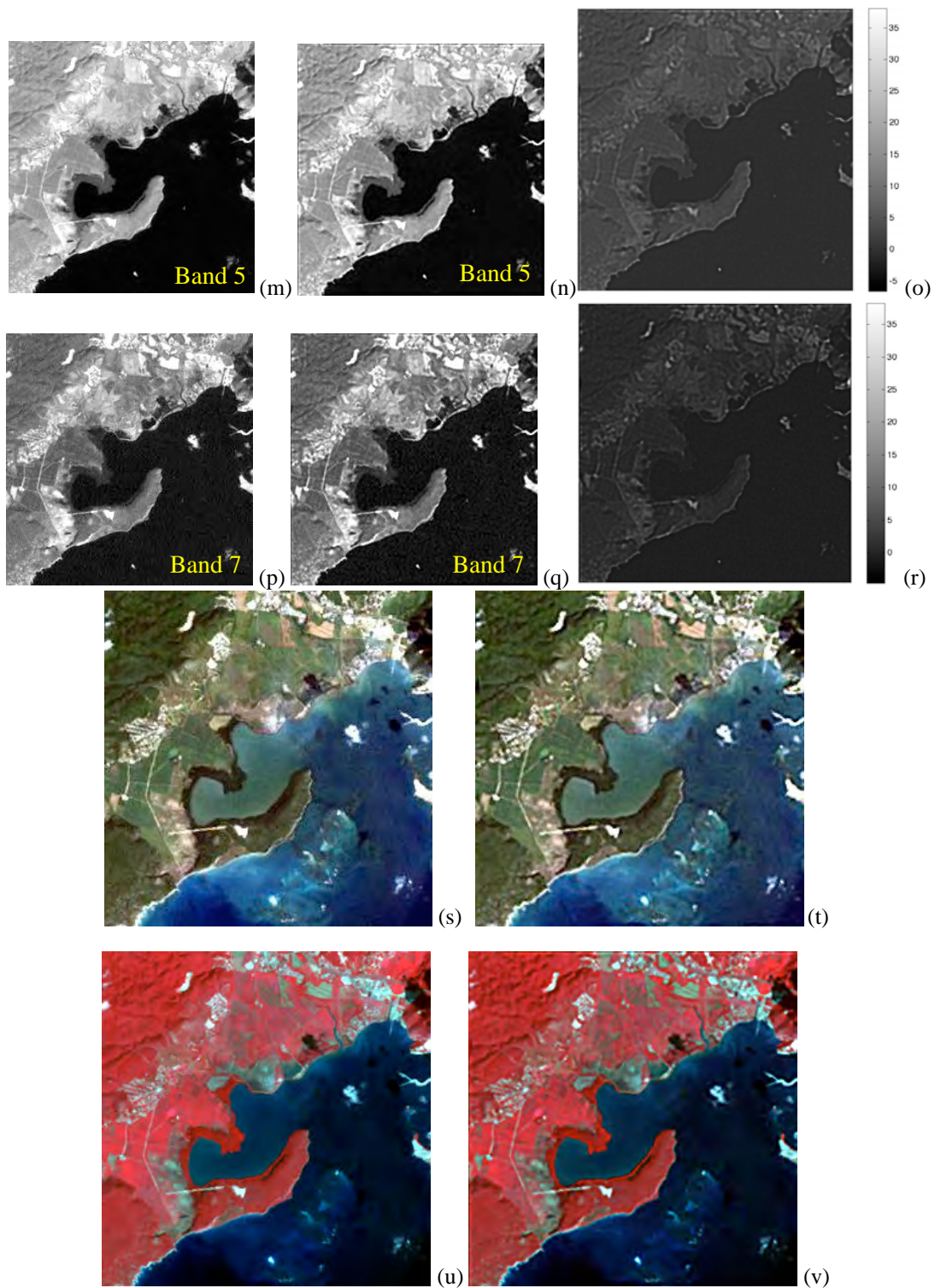


Figure 3.11 Original (a, d, g, j, m, p) and restored (b, e, h, k, n, q) images in grayscale. Difference of the images (c, f, i, l, o, r). Original (s) and Restored (t) image in RGB. Original (u) and Restored (v) image in CIR.

Figure 3.11 show the results with atmospheric corrections of the restored image, band 1-5 and 7 in grayscale with their respective difference figures, RGB and CIR images are presented. If we compare these images, we can see that the borders are better defined in the restored image. For example; the areas that looks like agriculture lands can be defined easily in the restored image. Other enhanced features, are the coastal border and some water bodies on land, the urban regions, and the ridges of the mountains. In the RGB image, the colors are brighter as seen in the results from section 3.4. The geometry of the objects in the image are defined and restored. Visually the image is more clear, the mountains, their shadows and urban areas are much defined than in the original image.

In figure 3.12, we show areas from the original and restored images where the differences were remarkable. We chose a small key located at the southern region of the image, and two different areas from the coast in order to show the image enhancement resulting from the restoration process. It is clear that the shape of the object is more defined in the restored image and it can be seen by the black pixels around the white pixels. Figure 3.12b shows the key, in the restored image, we can better define the structure of this piece of land in the ocean. The center is brighter and consist of four white pixels and not just two as shown in the original image.

The spatial restoration process changes the image as a whole, there are changes in the spatial and in the spectral domain. We have shown changes in the spatial domain, in Figure 3.13 we show results of the changes in the spectral domain. Figure 3.13 shows plots with the spectral profiles before and after restoration. These are characteristic profiles of some features of the image, such as, water, urban areas, pasture and agriculture fields (“Pasture”), and lowland dry semideciduous forest (“Forest”). An average profile along the bands was used to draw the plots; ENVI®

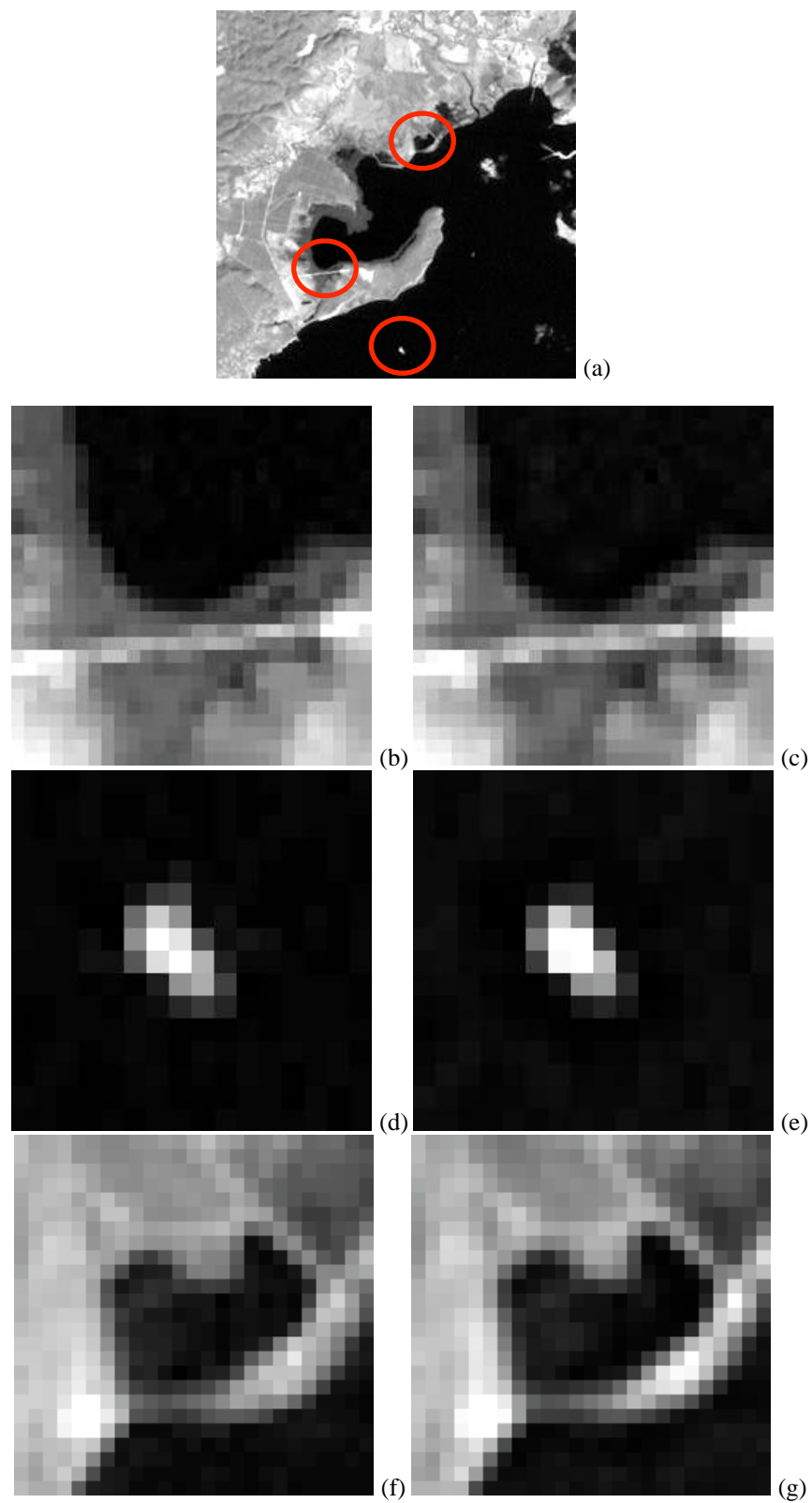


Figure 3.12 Regions of the image where the PSF correction were more notable. Original (b, d, f), restored (c, e, g).

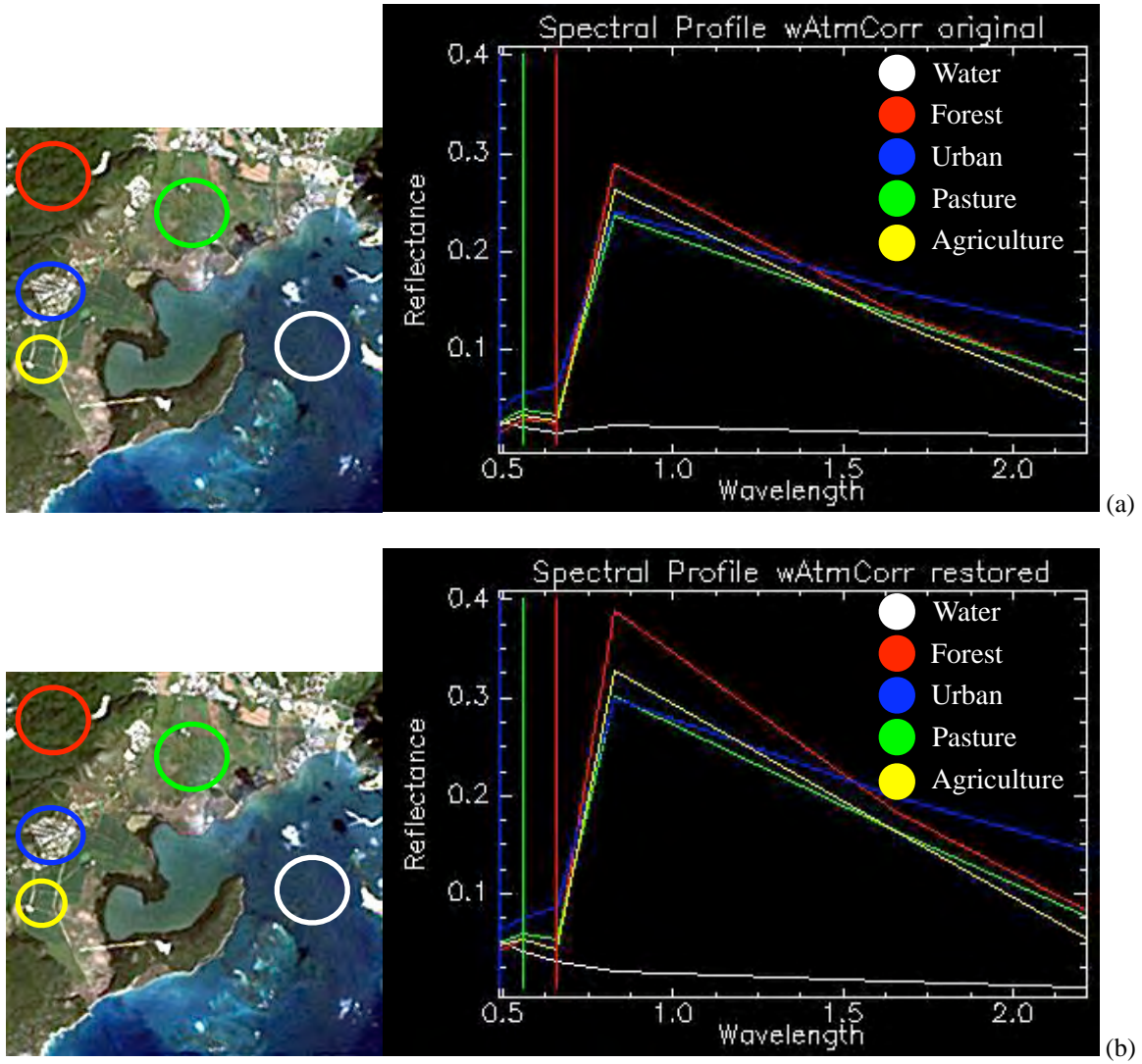


Figure 3.13 Spectral profiles for original (a); and restored (b).

was used to obtain these results. Both plots show spectral reflectance values. These spectral reflectance profiles are unique and different for each feature in an image. We can notice from the latter figure that the reflectance values are higher for the restored image, this can be a result of the removal of the atmospheric effects. For example, the water is not a good reflector, that is why the values from the y-axis are the smallest of them all. Another important change is the features separation and their maximum values, for example, the pasture maximum values are about

0.26 and 0.35 for the original and restored images, respectively. These are some of the changes due to image restoration and atmospheric correction in the spectral domain.

Back in the spatial domain, in Table 3.3, we show the results obtained for the mean and standard deviation of the difference per band between the original and restored images. Also, in the table the correlation coefficient between the bands of both images, original and restored.

Table 3.3 Mean, standard deviation and correlation coefficient in percent of reflectance for the restored image with atmospheric correction.

	Band 1	Band 2	Band 3	Band 4	Band 5	Band 7
Mean	2.747	2.213	1.9041	3.6523	1.7726	0.51643
Standard deviation	0.07344	0.8817	1.2401	4.0357	2.7563	1.9062
Correlation coefficient	0.9849	0.9847	0.9845	0.9938	0.9926	0.9891

Once we have the differences between the images, we developed scatterplots comparing the same bands from the two images (original and restored) as we did in the previous section. Figure 3.14 show the scatterplots comparing the reflectance percentages of the bands from the original and restored images.

Some of the alterations that suffers a restored image can be seen on the pixel reflectance values. Figure 3.15 show plots of the changes in the pixel reflectance values of the bands from the original and restored images. In these plots, we aim to show the enhancement due to the PSF restoration, the red plot is for the reflectance values of the restored image and the blue plot is for the original image. In all the bands the values increased, meaning that the image is brighter after the restoration.

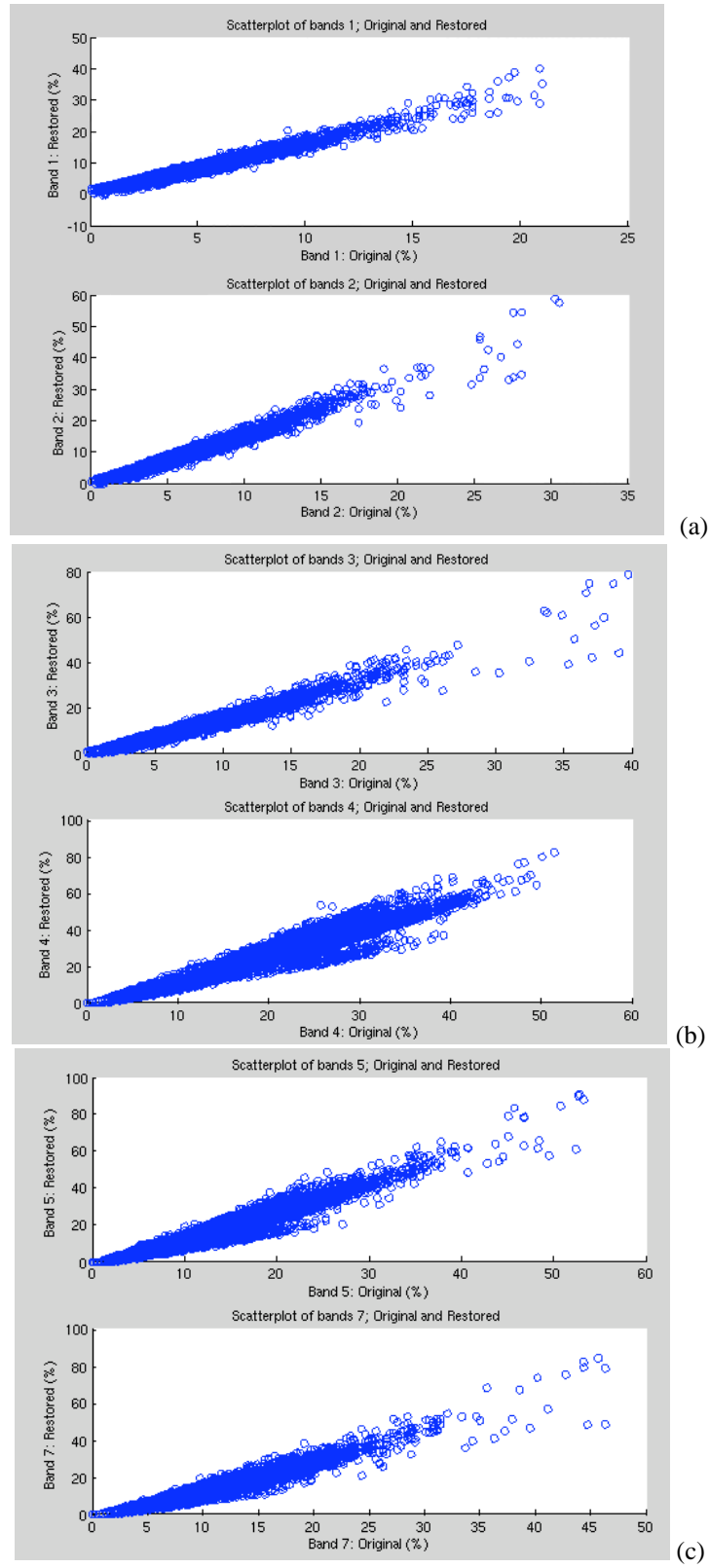


Figure 3.14 Scatterplots per bands, bands 1 and 2 (a), bands 3 and 4 (b) and bands 5 and 7 (c).

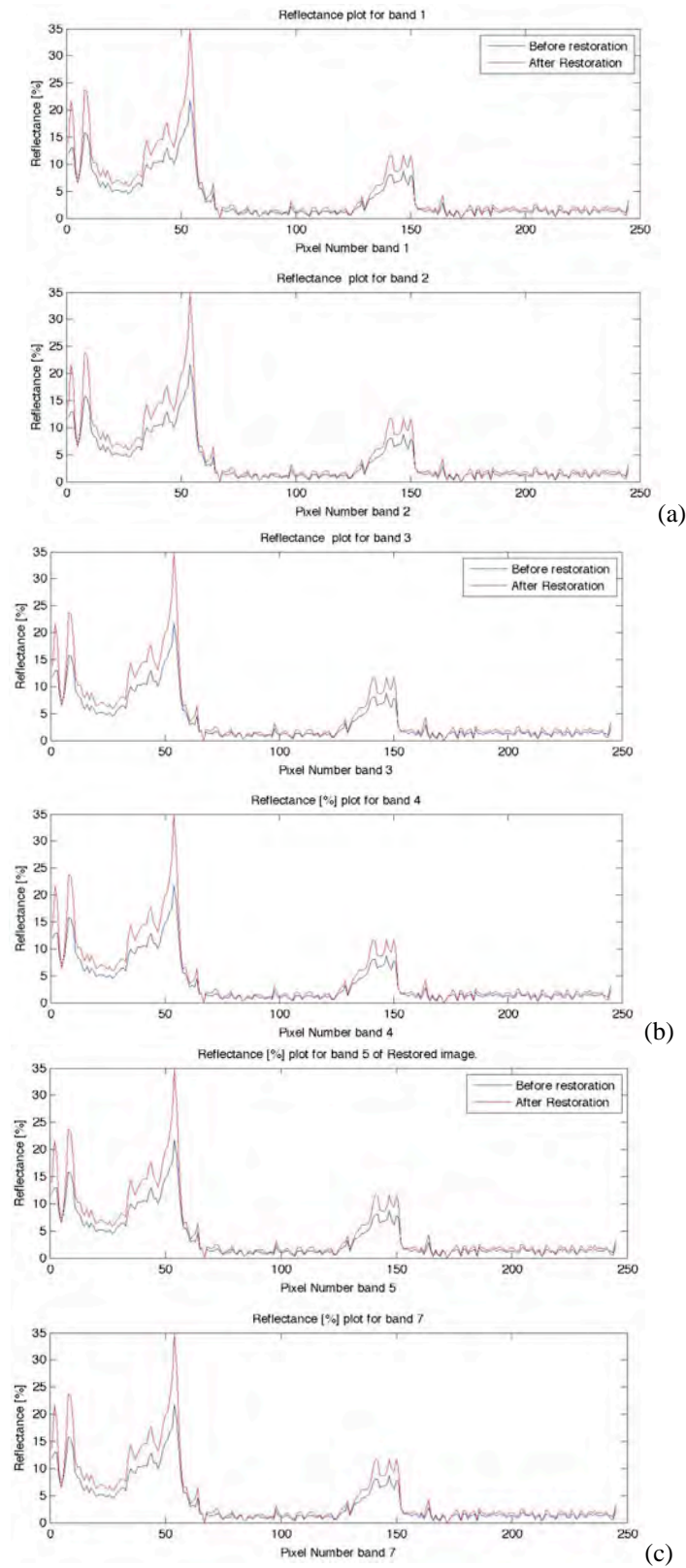
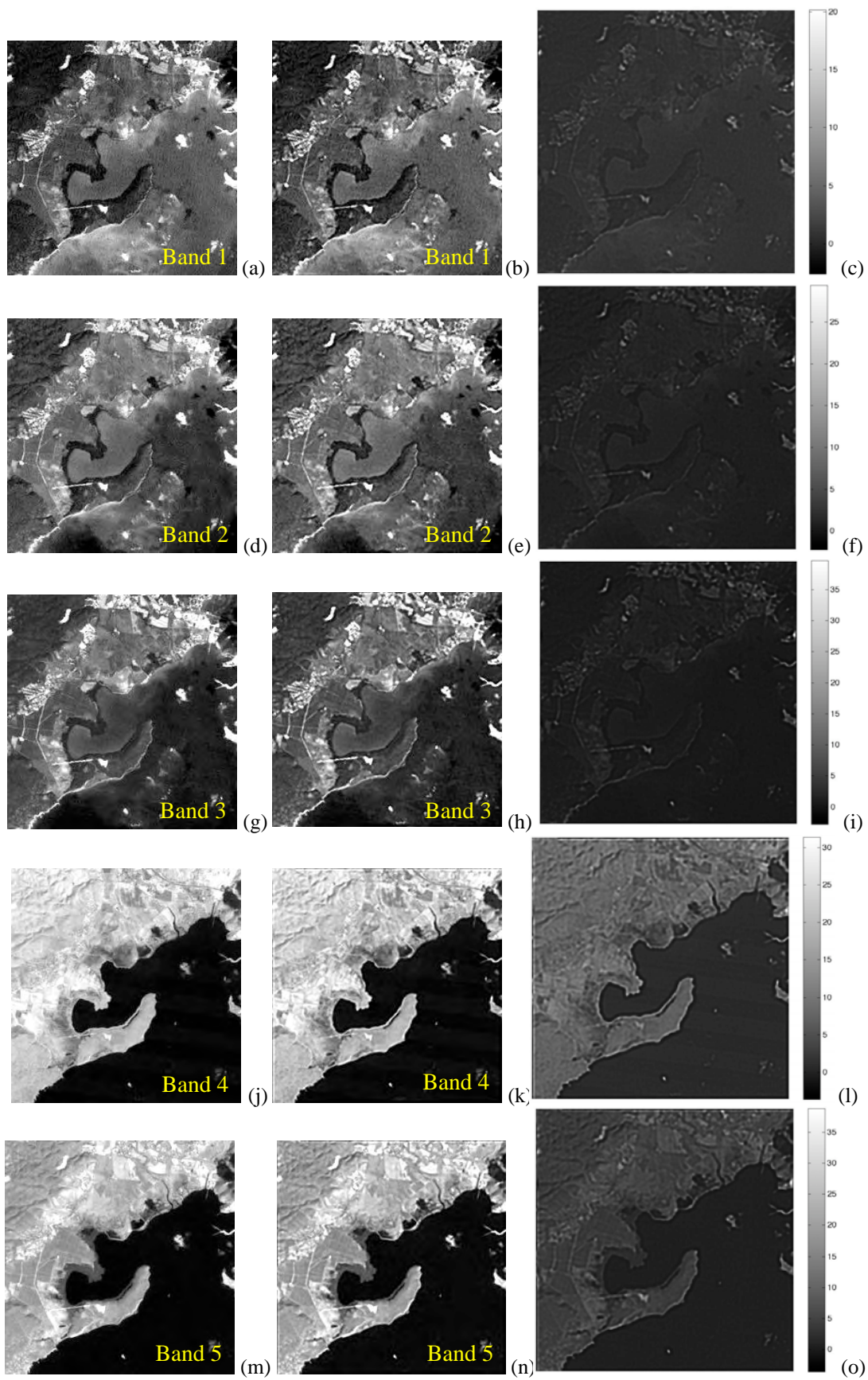


Figure 3.15 Plots of percent of reflectance per bands, bands 1 and 2 (a), bands 3 and 4 (b), and bands 5 and 6 (c), from original and restored images.

3.5 Atmospheric Corrected Original and Restored Images Results

In this section we present results for atmospheric corrected original and restored images. We applied the dark-object method for atmospheric correction to the original image from Section 3.3, then we applied the restoration algorithm. Figure 3.16 shows the results of the restored image, it shows band 1-5 and 7 in grayscale and a figure with the difference of these images (Figure 3.16a-r). Figure 3.16s-t show the RGB image. If we compare these images, we can see that the borders are more defined in the restored image. Details in the original image looks larger than in the restored image, this is due to the blurring. This effect give the impression of a larger objects because of the spread light around it. For example, the keys at the lower right hand corner of the image look larger compared with the restored image, the area agricultural fields can be defined easily in the restored image. Other features, are the coastal border and some water bodies on land, and the urban regions. In the RGB image, the colors are brighter as in the previous sections. Visually the image is more pure, the mountains, their shadows and urban areas are much defined than in the original image.

In Figure 3.17, we show areas from the original and restored images where the restoration improvements were remarkable. We chose the same areas as in the previous section; a small key located at the southern region of the image, and two different areas from the coast. It is clear that the shape of the object is better defined in the restored image and it can be seen by the difference in color tones of the grayscale pixels, from gray to white, and dark gray to black . Figure 3.17b is from a water body at the coast in the upper region of the image. The borders are brighter, and the lower edge is clear compared to the original image.



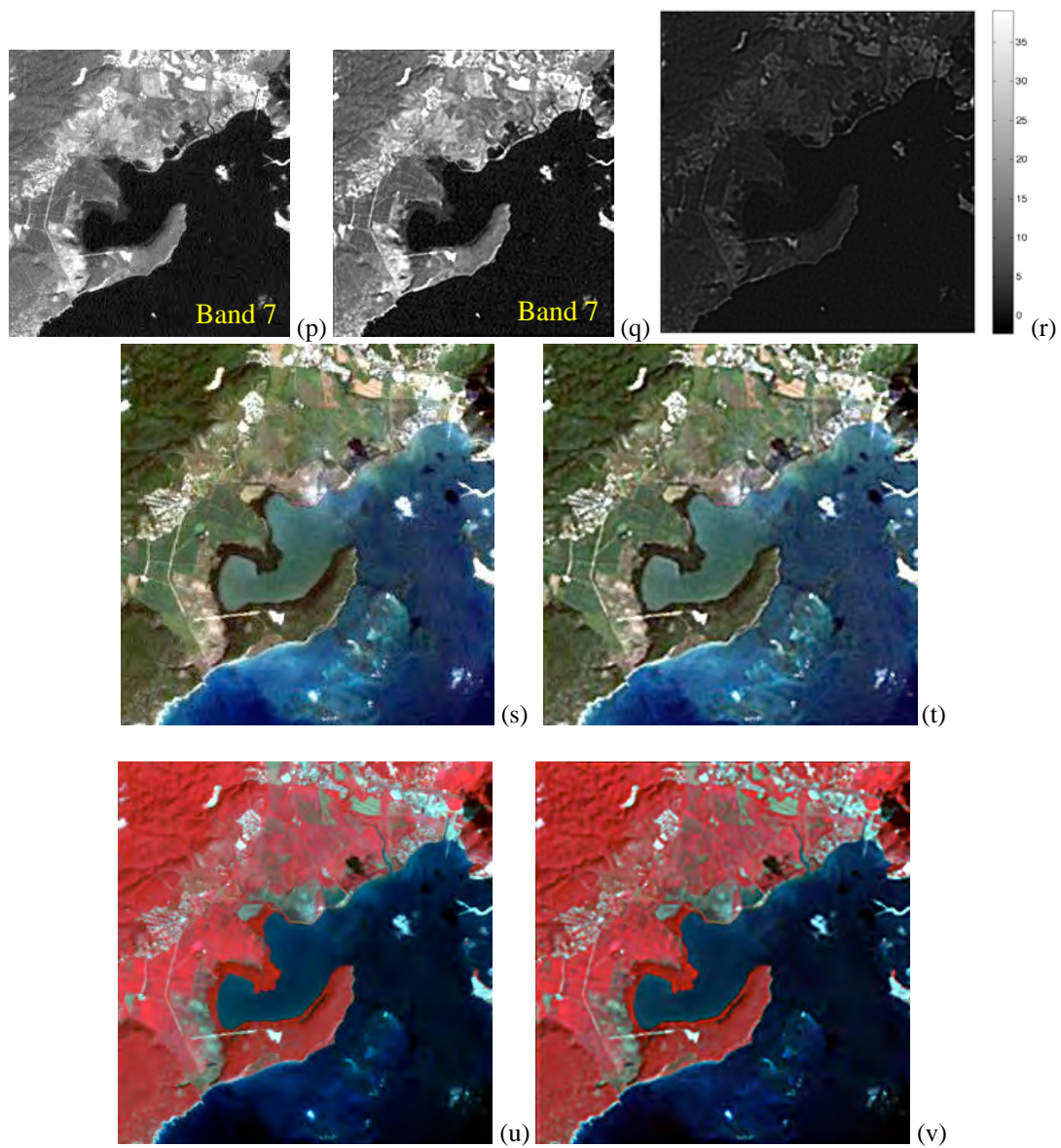


Figure 3.16 Original (a, d, g, j, m, p) and restored (b, e, h, k, n, q) images in grayscale. Difference of the images (c, f, i, l, o, r). Original (s) and Restored (t) image in RGB. Original (u) and Restored (v) image in CIR.

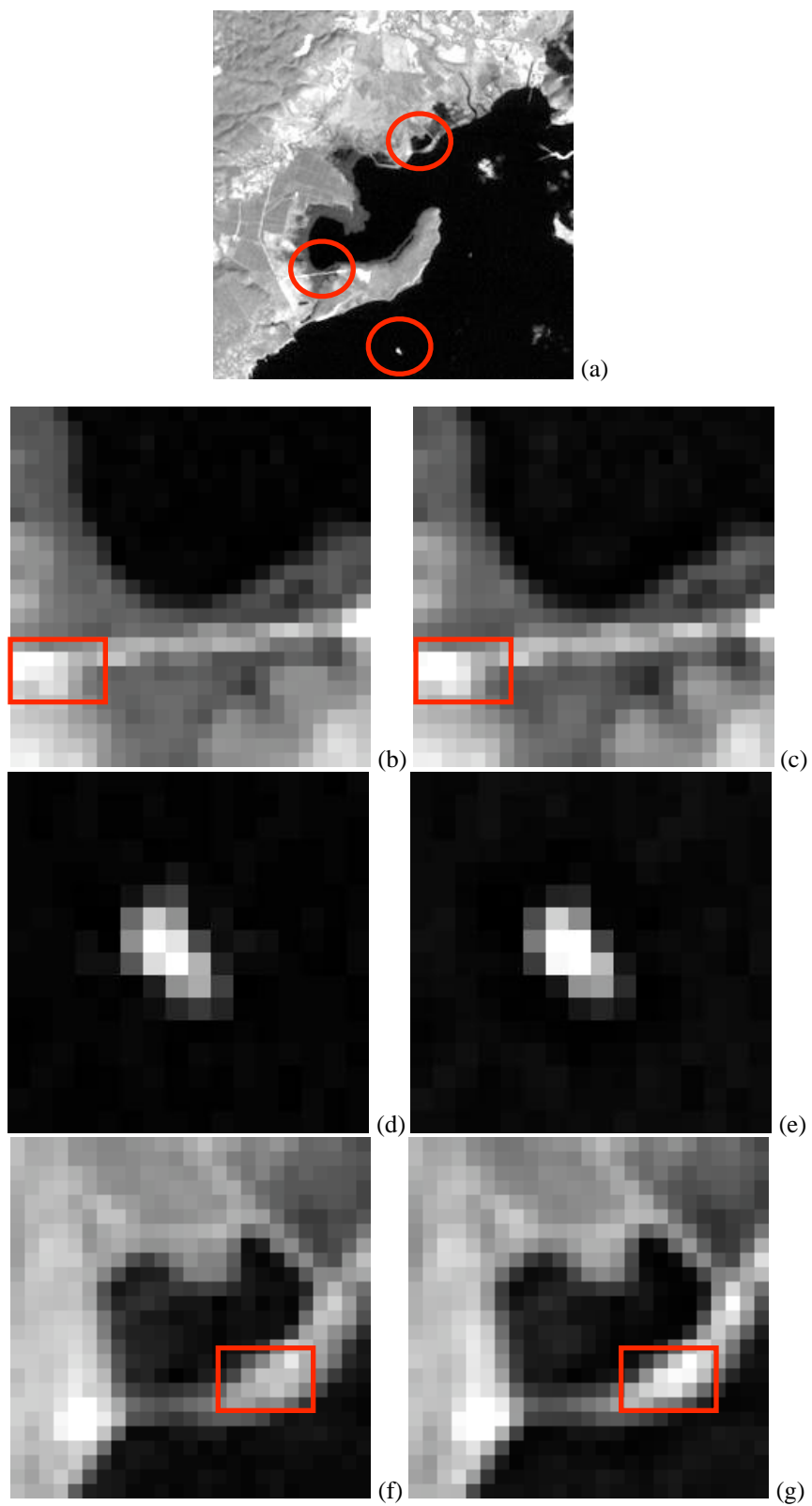


Figure 3.17 Regions of the image where the PSF correction were more notable (a). Original (b, d, f), restored (c, e, g).

When the image restoration algorithm is applied, changes in the spatial and in the spectral domain occur. We have shown changes in the spatial domain, in the previous figures. In the following figures, we show results of the changes in the spectral domain. In the Figure 3.18, we show plots with the spectral reflectance values before and after the restoration process. These curves are unique spectral reflectance profiles of some features of the image, such as, water, urban areas, pasture and agriculture fields (“Pasture”), and lowland dry semideciduous

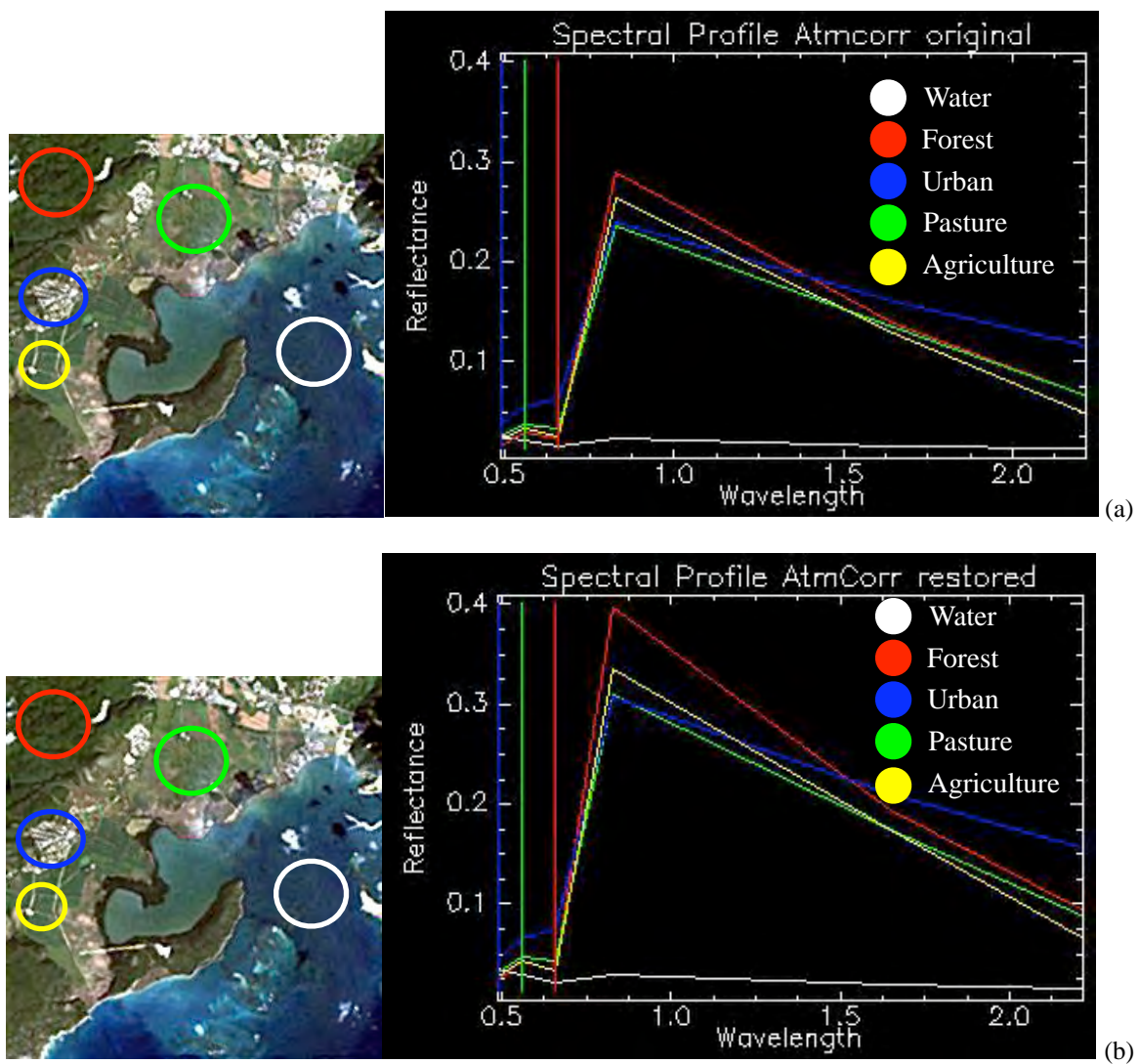


Figure 3.18 Spectral profiles for original (a); and restored (b).

forest (“Forest”). We can notice from the latter figure that the reflectance values are higher for the restored image, this can be a result of the removal of the atmospheric effects. For example, the water is not a good reflector, that is why the values from the y-axis are the smallest of them all. Another important changes are the signature separation and their maximum values, for example, the urban maximum values are about 0.225 and 0.3 for the original and restored images, respectively. These are some of the changes due to the restoration after the atmospheric correction in the spectral domain.

Returning to the spatial domain, in Table 3.4, we show the results obtained for the mean and standard deviation of the difference per band between the original and restored images. We also include the correlation coefficient between the bands of both images, original and restored.

After having the differences between the images bands, we developed scatterplots comparing the same bands from the two images (original and restored). Figure 3.19 show the scatterplots per band of both images.

Table 3.4 Mean, standard deviation and correlation coefficient in percent of reflectance for the atmospheric corrected-restored image.

	Band 1	Band 2	Band 3	Band 4	Band 5	Band 7
Mean	1.91124	1.0642	0.96692	4.4494	2.7041	1.6049
Standard deviation	0.73442	0.88199	1.2394	4.0287	2.7449	1.9158
Correlation coefficient	0.9825	0.9829	0.9826	0.9938	0.9926	0.9891

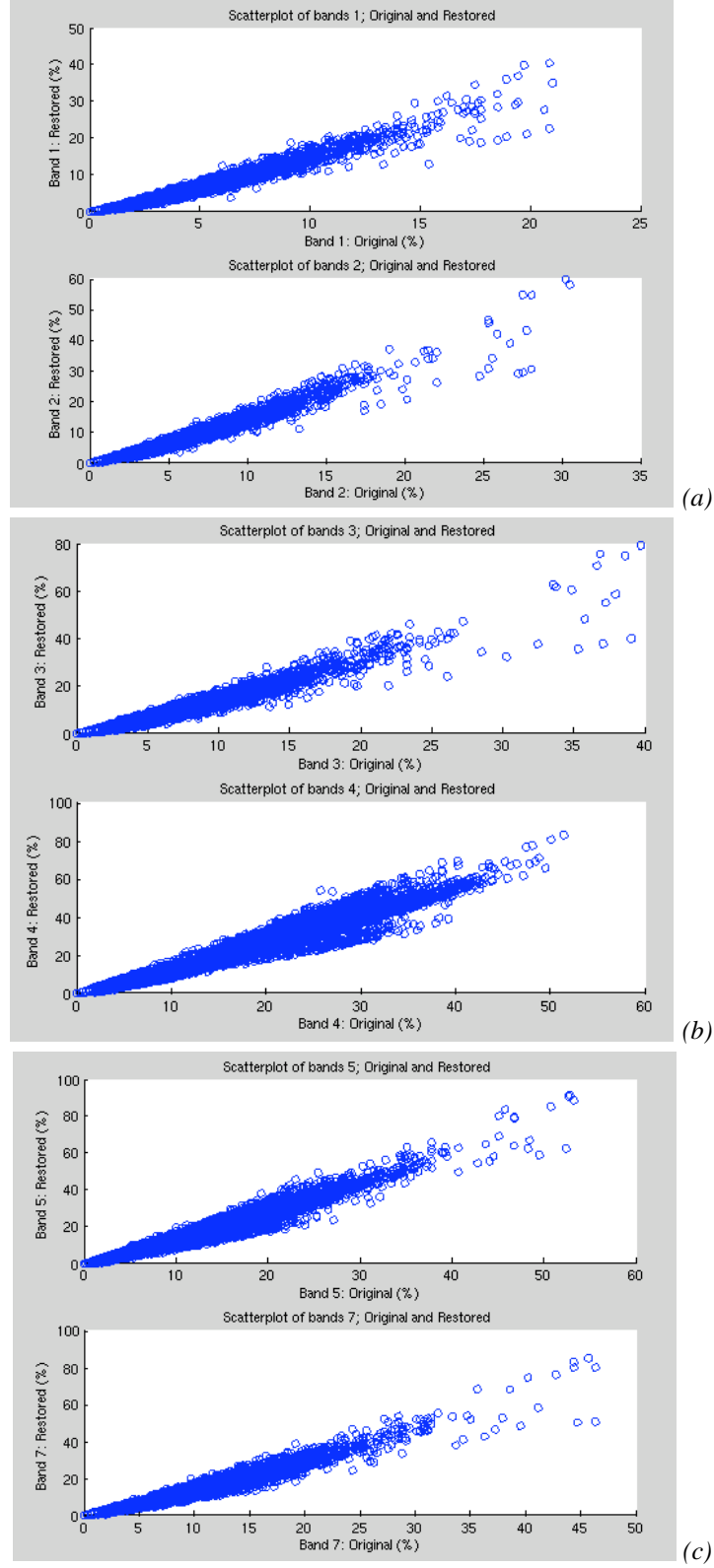


Figure 3.19 Scatterplots per bands, bands 1 and 2 (a), bands 3 and 4 (b) and bands 5 and 7 (c).

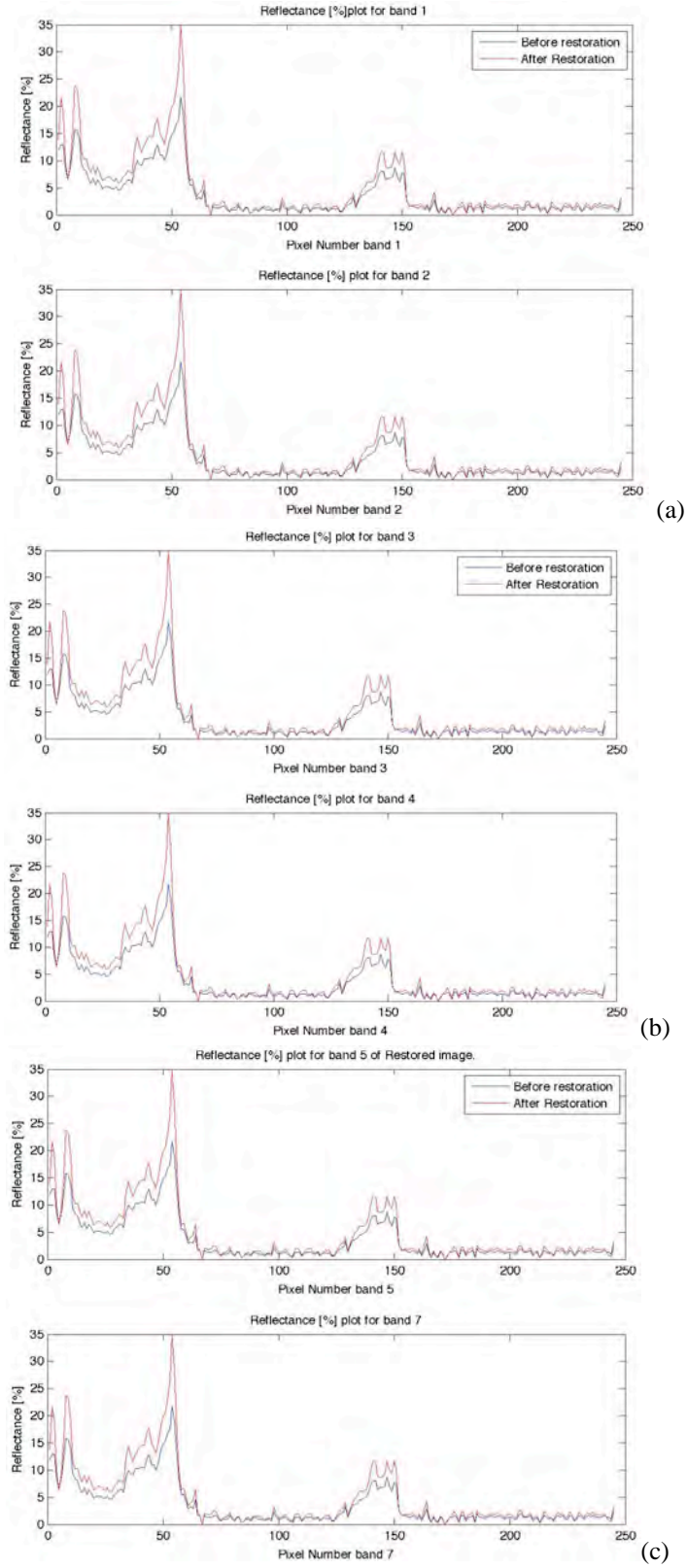


Figure 3.20 Plots of percent of reflectance per bands, bands 1 and 2 (a), bands 3 and 4 (b), and bands 5 and 6 (c), from original and restored images.

Some of the alterations that suffers a restored image can be seen on the pixel reflectance values. Figure 3.20 show plots of the changes in the pixel reflectance values of the bands from the original and restored images. In these plots, we show the enhancement due to the PSF restoration, the red plot is for the reflectance values of the restored image and the blue plot is for the original image. In all the bands the values increase, meaning that the image is brighter after the restoration.

3.6 Effects of Stopping Criteria when Using the Iterative Method

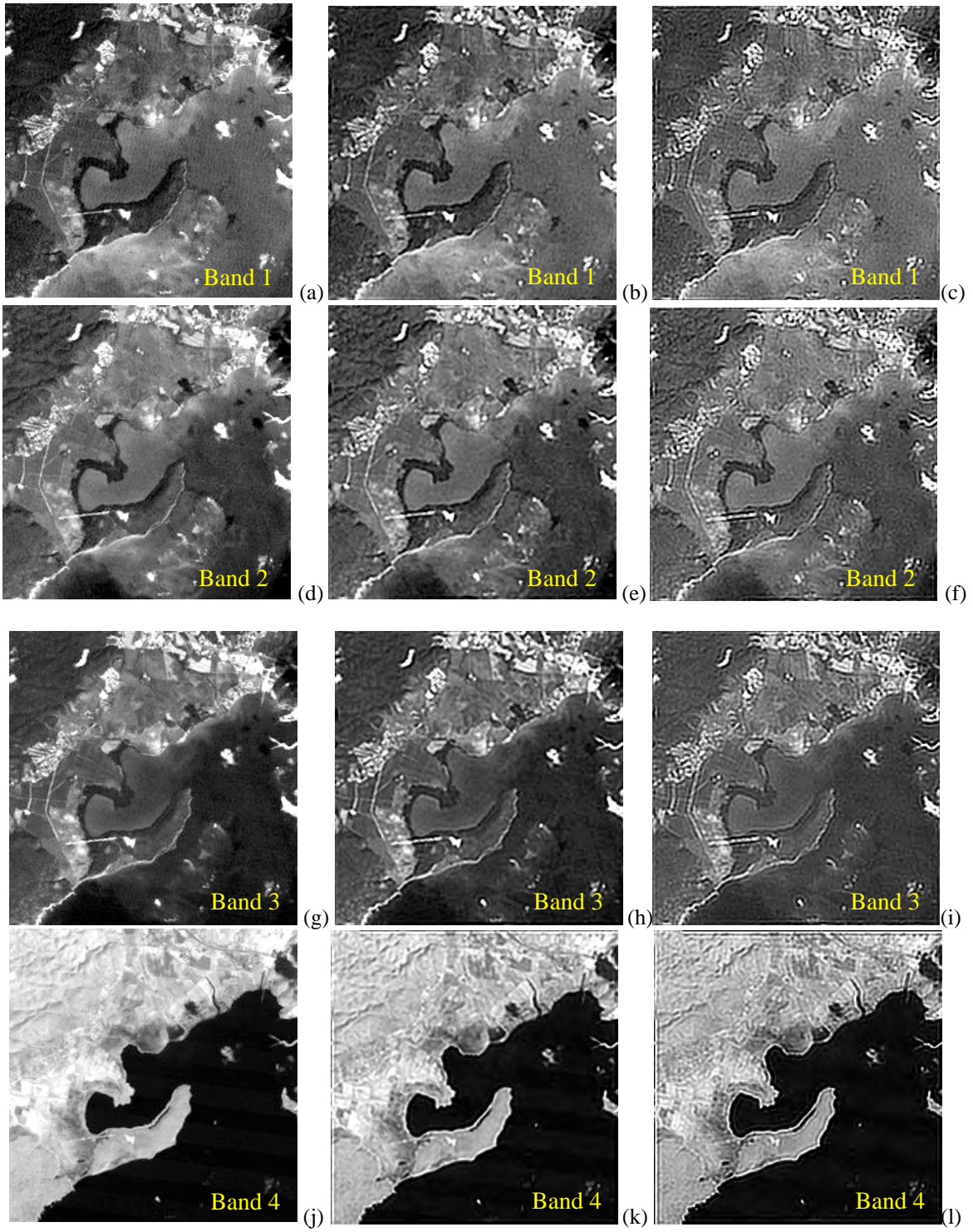
When an iterative method is used to restore images it is necessary to know when to stop the iteration process. We showed in the previous sections results from the third iteration, in this section we will show images from the fifth and tenth iteration in order to illustrate the effect of divergence beyond the third iteration.

We used the image without atmospheric corrections to obtain the figures for the bands in grayscale, RGB and CIR. Figure 3.21 shows the results of the original and restored images in RGB, CIR (bands 4, 3, 2), and from band 1-5 in grayscale for the fifth and the tenth iterations. It can be seen that the method diverges in higher iterations. For visual purposes, the third iteration is better because features such as the coastal lines, urban areas among other features are more geometrically defined. If we compare the figures for both iterations (second and third columns from Figure 3.21) we can notice that the second columns have better visual results than the third column.

In order to measure the performance of the restoration method, we quantify the impact of the PSF by calculating the mean, standard deviation and correlation coefficient of the differ-

ence between the two images, original and restored. In Table 3.5, we show the results for these calculations original and restored with 5 iterations and 10 iterations. As we found for the third iteration, the band four have the higher statistics, meaning that in this band occurred more changes compared with the other bands. Regardless of the divergence introduced, we are still having darker pixel where lighter pixel were at the original image, and vice-versa.

Once we have the differences between the images, we developed scatterplots comparing the same bands from the two images. Figure 3.22 show the reflectance values (%) of the original and restored and the scatterplots for both iterations, 5 and 10. With these scatterplots, we show the expected results when a restoration algorithm is applied to an image, the dark pixels were brighter and bright pixels were less bright when compared to the pixels of the original image. As we discussed in the previous sections, the highlighting changes occurred on the bands 4 and 5. We can see these changes in Figure 3.22(c) and (d) where the plots opens at the center, scattering more point out of the $y=x$ line; if we compare these with Figure 3.22(a) and (b), the points are closer to the line $y=x$, the similar results were obtained for the third iteration. Also, was found that the image become brighter as we advance in iterations.



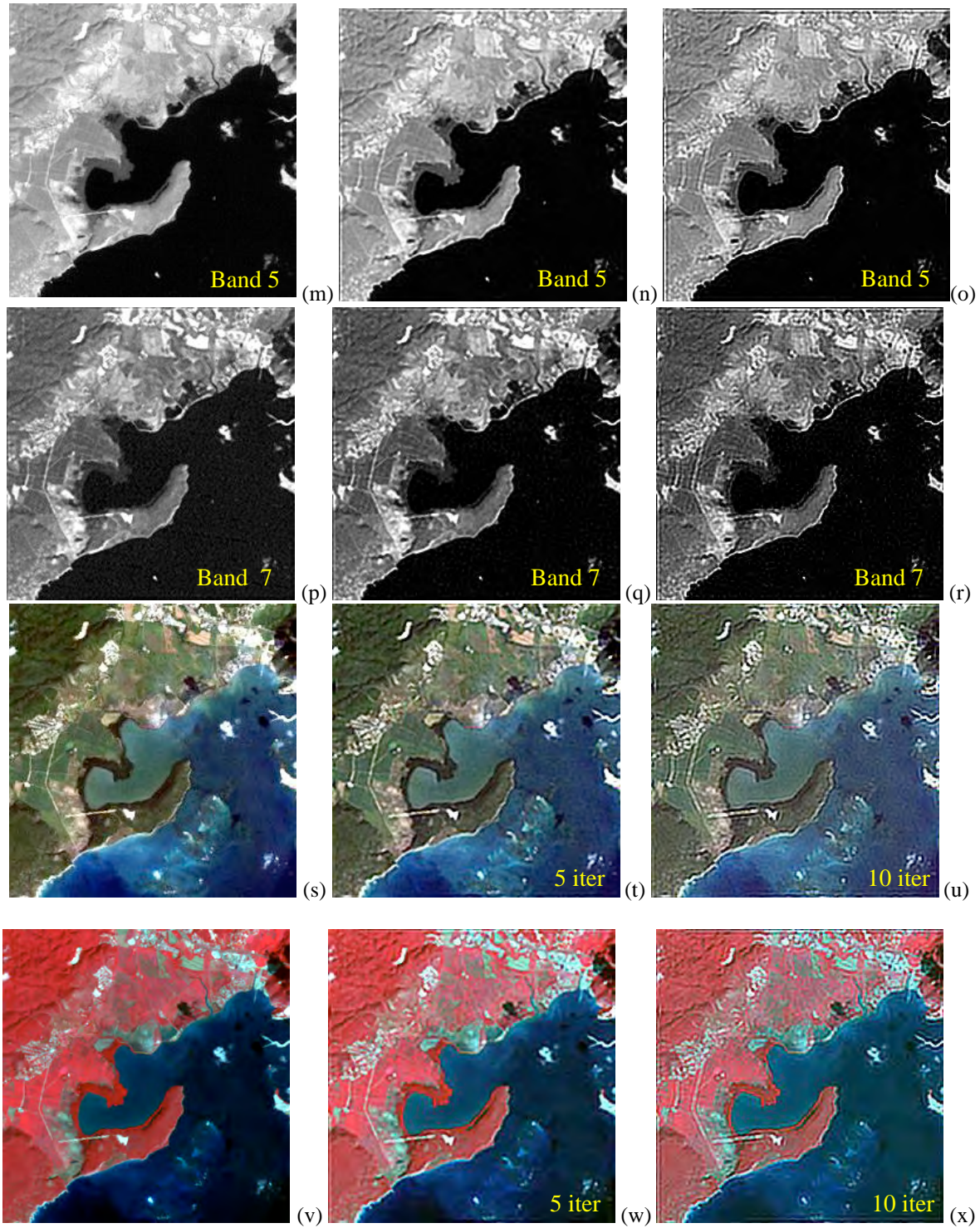


Figure 3.21 Original (a, d, g, j, m, p) and restored (b, e, h, k, n, q) images in grayscale for the fifth iteration. For the tenth iteration (c, f, i l, o, r) are the resulting images. Original (s), Restored with 5 iterations (t), and Restored with 10 iterations (u) images in RGB. Original (v), Restored with 5 iterations (w), and Restored with 10 iterations (x) images in CIR.

Table 3.5 Mean, standard deviation and correlation coefficient in percent of reflectance for the difference between images.

	Band 1		Band 2		Band 3		Band 4		Band 5		Band 7	
	5 iter	10 iter	5 iter	10 iter	5 iter	10 iter	5 iter	10 iter	5 iter	10 iter	5 iter	10 iter
Mean	3.287	3.287	2.196	2.197	1.675	1.675	4.262	4.262	2.486	2.486	1.368	1.368
Standard deviation	0.96	1.593	1.15	1.883	1.63	2.627	4.95	7.43	3.43	5.043	2.47	3.86
Correlation coefficient	0.96	0.856	0.959	0.859	0.957	0.861	0.978	0.921	0.974	0.918	0.964	0.885

The last step of the second stage of the algorithm is dedicated to plot the bands of the images and compare the changes due to the PSF corrections. Figure 3.23 and Figure 3.24 show plots of the changes in reflectance values of the bands from the original and restored images from two different transect in the image. Figure 3.23 show the results for the along-track transect, and Figure 3.24 show the plots for the cross-track transect. In these plots we aim to show the enhancement due to the PSF restoration. In each figure we are comparing the results for the image with 5 (left column) and 10 (right column) iterations. As we discussed earlier, the image with 10 iterations is brighter than the image with 5 iterations, for example looking at Figure 3.23(c) and (d) we can see that the mayor peaks overpasses the 50% for the image with 10 iterations. Similar results are shown in Figure 3.24.

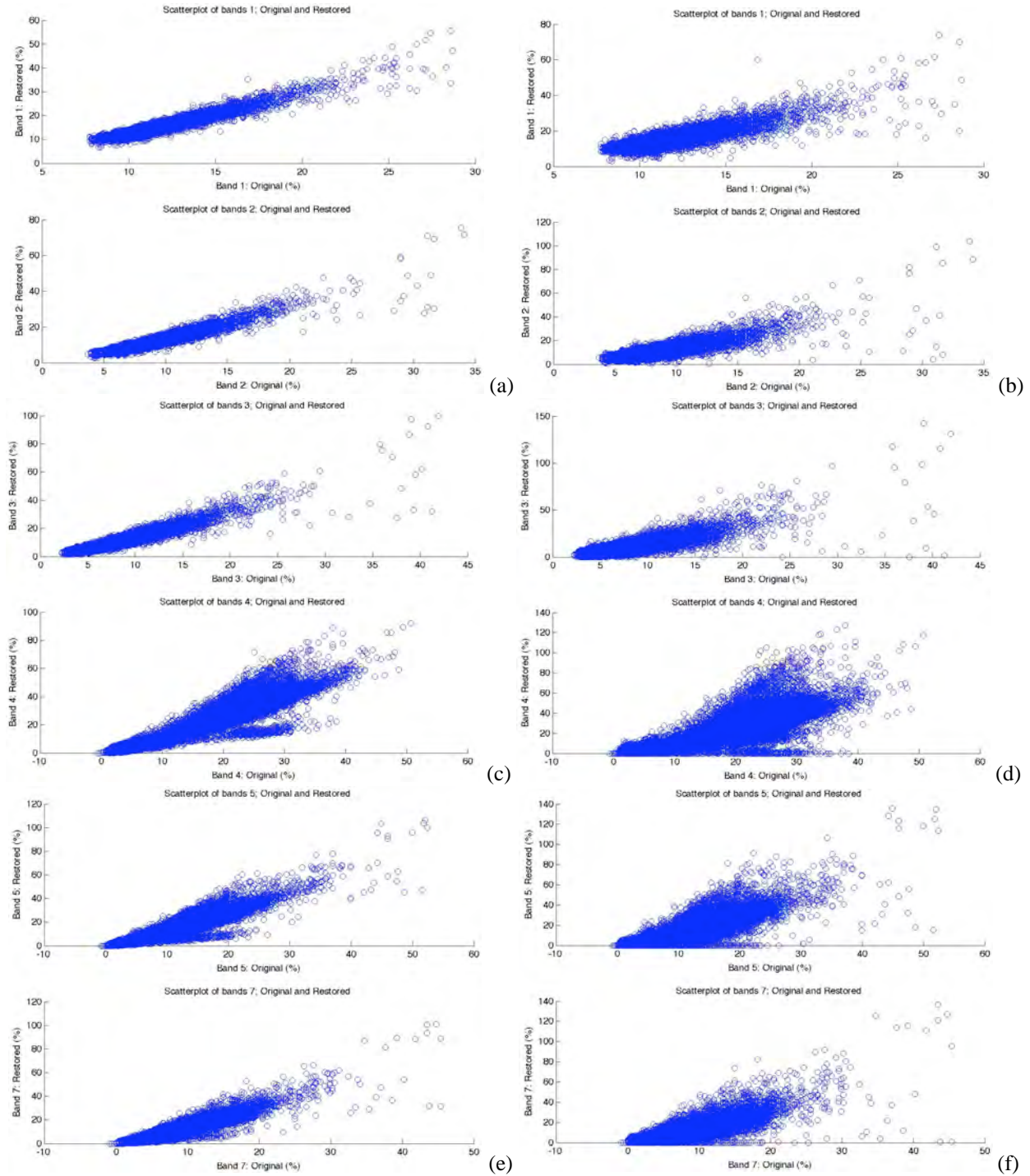


Figure 3.22 Scatterplots per bands, for 5 iterations, bands 1 and 2 (a), bands 3 and 4 (c), bands 5 and 7 (e), and for 10 iterations, bands 1 and 2 (b), bands 3 and 4 (d), and bands 5 and 7 (f).

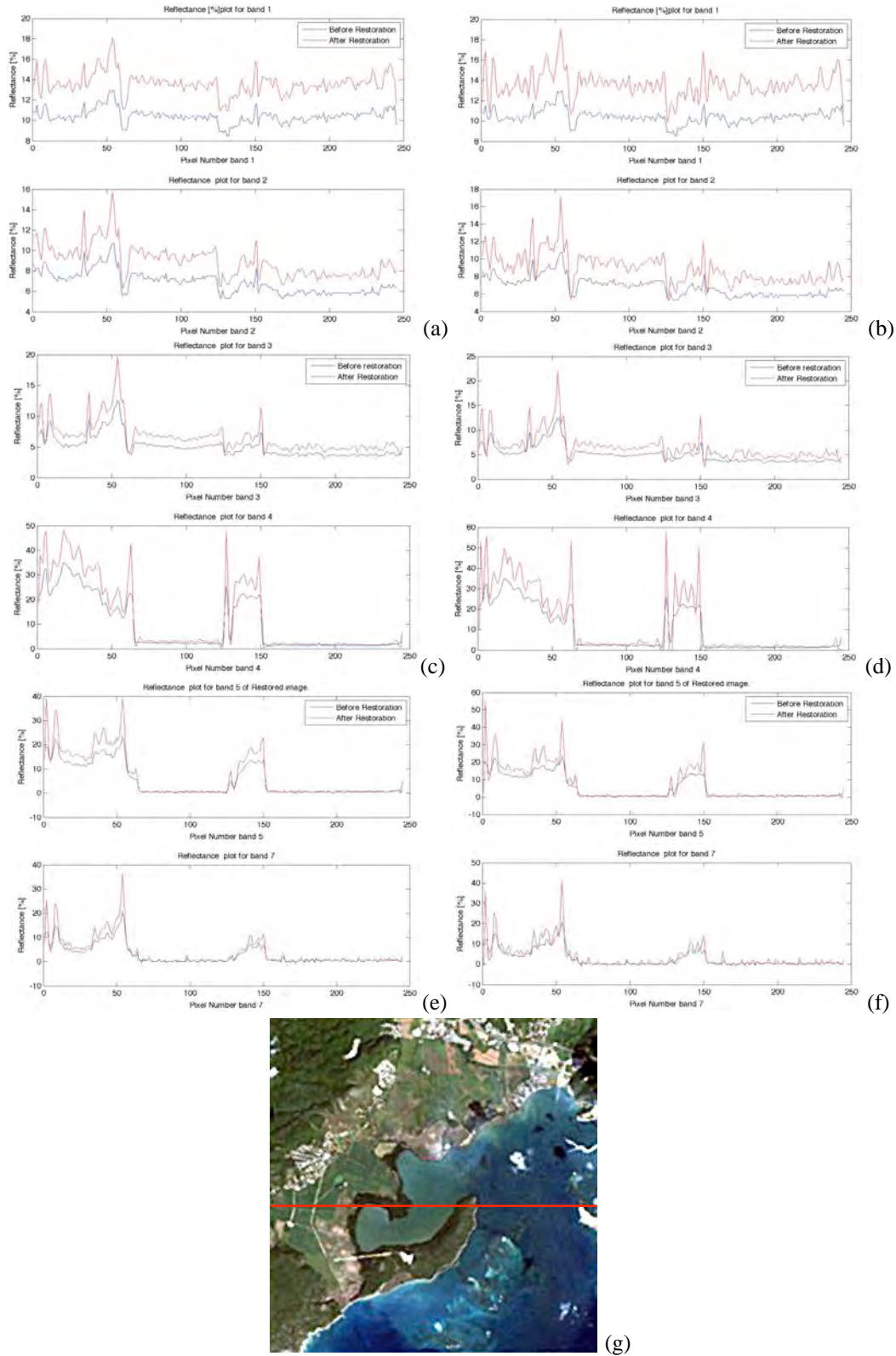


Figure 3.23 Plots of percent of reflectance per bands, for along-track transect of the image with 5 iterations; bands 1 and 2 (a), bands 3 and 4 (c), and bands 5 and 6 (e). Image with 10 iterations, bands 1 and 2 (b), bands 3 and 4 (d), and bands 5 and 6 (f), from original and restored images. Image with the transect used (g).

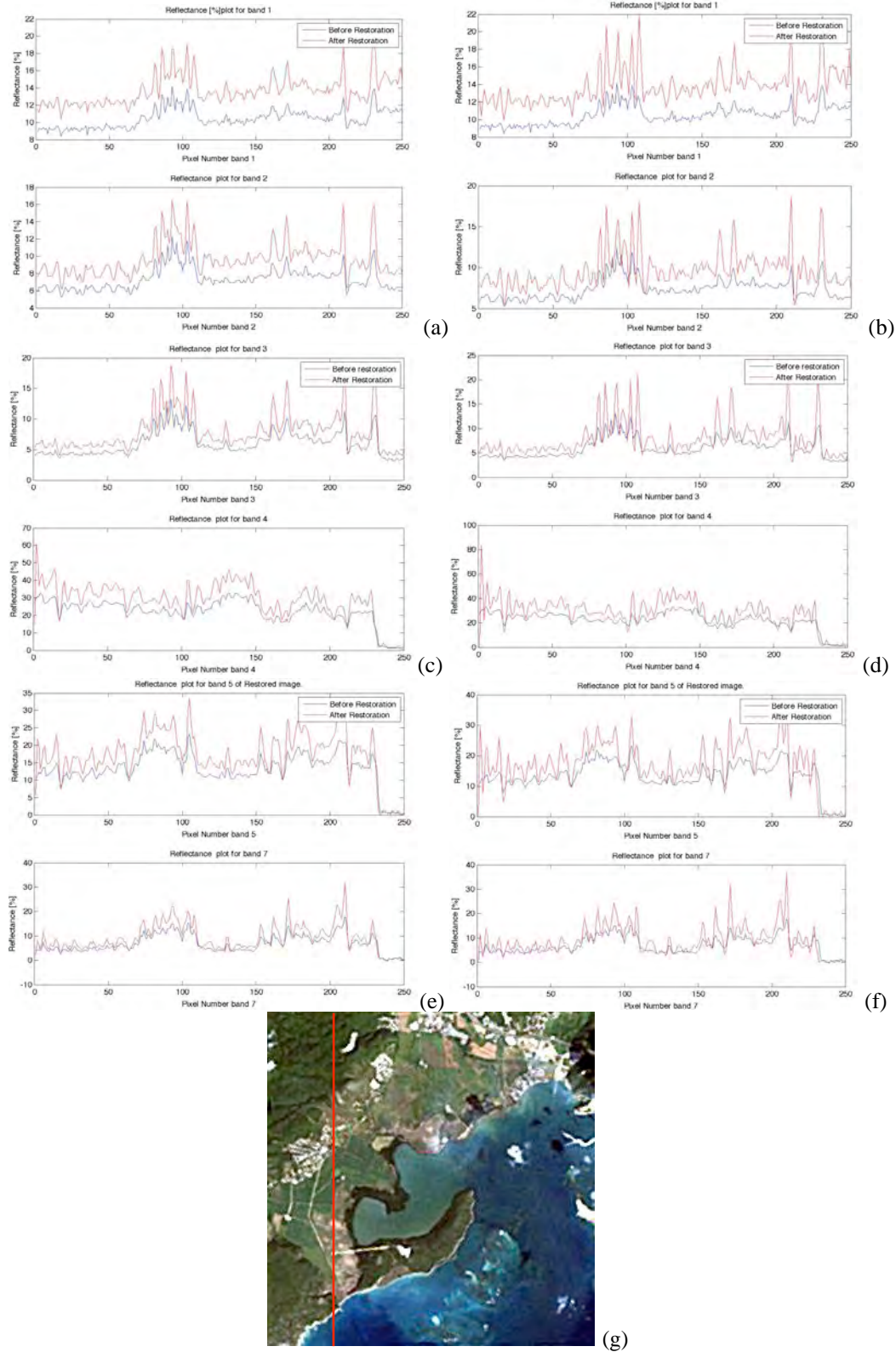


Figure 3.24 Plots of percent of reflectance per bands, for cross-track transect of the image with 5 iterations; bands 1 and 2 (a), bands 3 and 4 (c), and bands 5 and 6 (e). Image with 10 iterations, bands 1 and 2 (b), bands 3 and 4 (d), and bands 5 and 6 (f), from original and restored images. Image with the transect used (g).

3.7 Conclusions

In this chapter we presented results of three images, a restored image, a restored image with atmospheric corrections and an image with atmospheric correction before the restoration algorithm. We showed spectral reflectance profiles of different features found in the image, such as, water, pasture, urban areas and thick vegetation or forested areas. In the last section presented we showed results from two iterations, 5th and 10th. As we expected, the reflectance values for the restored images are higher than the original images, and the restored images are enhanced to brighter colors, or higher percentages of reflectance. This imply that the restoration process was successfully applied.

In the next chapter we will show the results obtained from the classifications before and after the restoration process. We aim to show the differences caused by the PSF on the images under study, when a classification process is applied.

4 Experimental Results: Effects on Classifications

In this chapter, the effects of deblurring on classification performance are studied. The three images presented in Chapter 3 were classified. Results and conclusions are presented in the following sections.

4.1 Description of Classification Process

Classification is defined as the process of assigning labels to objects, features, or area in the image under study [2]. First, we detect the presence or absence of a feature, then we recognize the feature in the image in order to assign a class to it. Finally, we identify the objects, features or areas in an image that can be place in a very specific class.

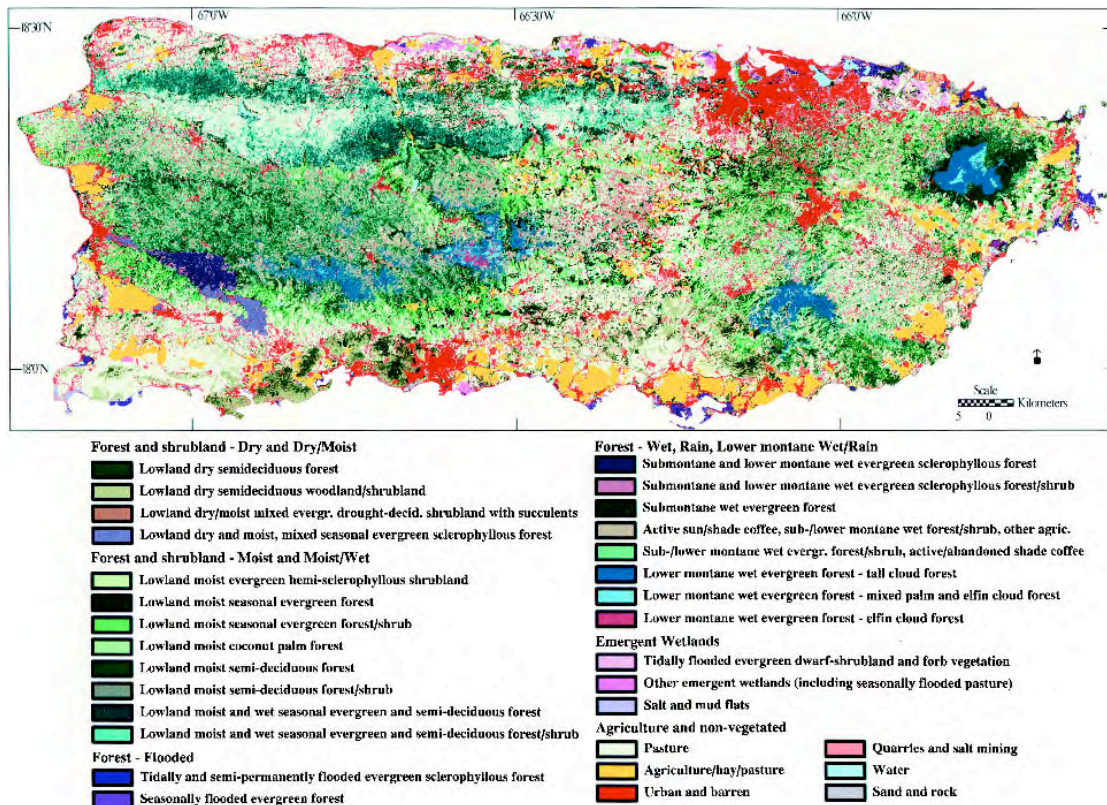


Figure 4.1 Puerto Rico Natural Vegetation and Land Cover, 1991-1992.

We chose six classes based on our knowledge and the descriptions found on the “Puerto Rico Natural Vegetation and Land Cover, 1991-1992” classification map from the International Institute of Tropical Forestry from the USDA Forest Service, San Juan, Puerto Rico. Figure 4.1 illustrates the class map. The classes are:

- Water: This class includes the sea and some water bodies inland.
- Urban and barren: Includes urban areas found inland and in the coastal regions. Also this class includes barren soils across the image.
- Seasonally flooded forest: This class is used to separate mangroves found in the coast from the lowland dry semideciduous forest.

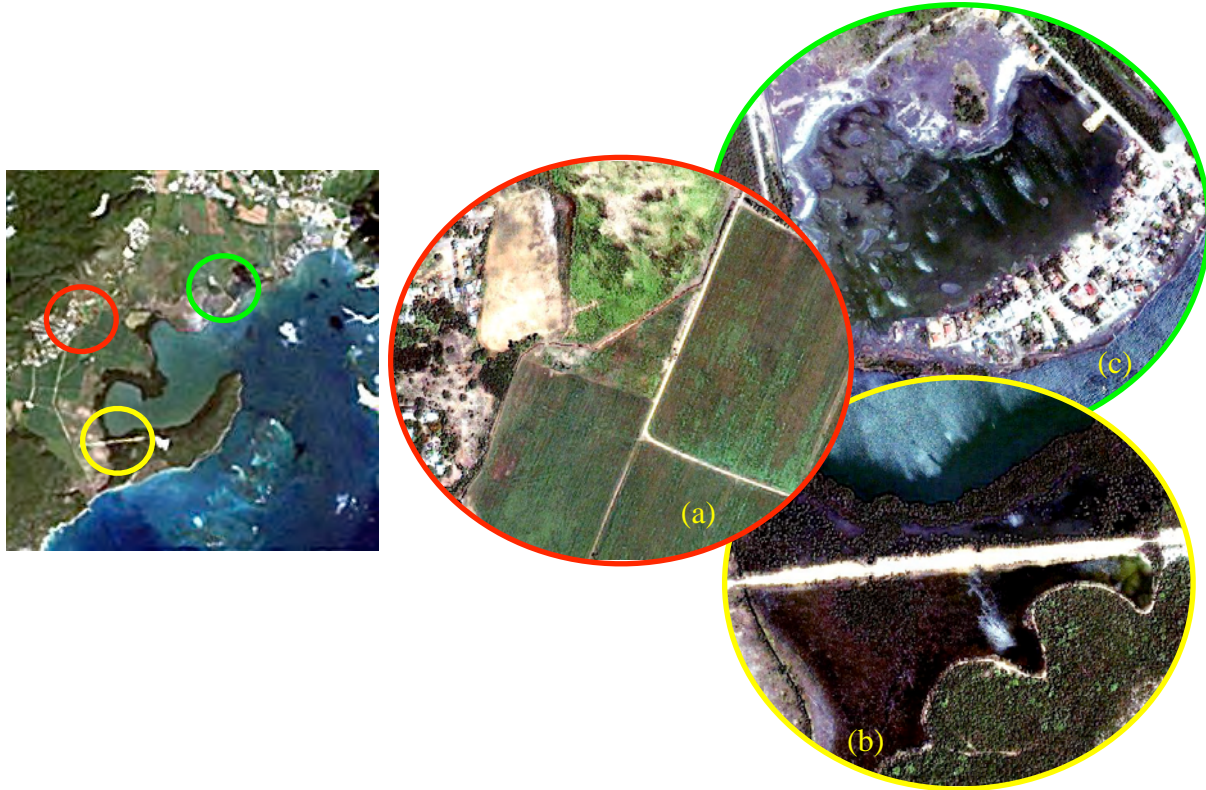


Figure 4.2 Landsat image compared to IKONOS images, urban, barren and agriculture class (a), mangrove, barren, lowland semideciduous forest and water (b), and urban and inland water classes (c).

- Lowland dry semideciduous forest: This class is the one that includes all the thick vegetation found in the image, excluding the mangroves from the coast.
- Agriculture: As its name describe, this class is the one that includes all the agriculture fields in this image.
- Pasture: This class is used to separate fields of agriculture from those fields that just have grass or pasture.

Based on the description of these features, we performed a classifications in the three images described before. Figure 4.2 illustrate the LANDSAT TM 4 image with areas of the image under study taken from an PAN sharpened image acquired by IKONOS. This image is not necessary acquired on the same date as the Landsat TM 4 image, having this in mind is good to mention that the specified areas are not exactly in the same conditions. For example, the agriculture, pasture, seasonally flooded forest and other features may vary from image to image.

ENVI® environment was used to perform the classification process, first we chose the region of interest, then we calculate the classes separability in order to know if the classes are well assigned and do not merge with other classes. Once we have done the latter, we used the Maximum Likelihood (ML) classifier to obtain our results.

The ML method is based on the assumption that the frequency distribution of the class can be approximated by the multivariate normal probability distribution as follows [19],

$$P(\mathbf{x}) = 2\pi^{-0.5p} |\mathbf{S}_i|^{-0.5} \exp\left[-0.5(\mathbf{x} - \boldsymbol{\eta}_i)^T \mathbf{S}_i^{-1}(\mathbf{x} - \boldsymbol{\eta}_i)\right] \quad (1)$$

The latter equation implies that the probability of pixel vector \mathbf{x} of p elements is a member of class i . Where \mathbf{S} is the sample variance-covariance matrix of class i . After some manipulation in (1), we get the following discriminant function.

$$\mathbf{g}_i(\mathbf{x}) = -\left((\mathbf{x} - \boldsymbol{\eta}_i)^T \mathbf{S}_i^{-1}(\mathbf{x} - \boldsymbol{\eta}_i)\right) - \ln |\mathbf{S}_i| \quad (2)$$

The ML classifier is then $\mathbf{x} \in C_i$ if $\mathbf{g}_i(\mathbf{x}) > \mathbf{g}_j(\mathbf{x})$ for all $i \neq j$.

Table 4.1 Testing/training samples used for the classification of the restored image.

Class	Testing (pixels)	Training (pixels)
Water	941	702
Agriculture	311	247
Urban and Barren	106	85
Seasonally flooded forest	301	144
Lowland dry forest	1,219	706
Pasture	143	84
Total	3,021	1,969

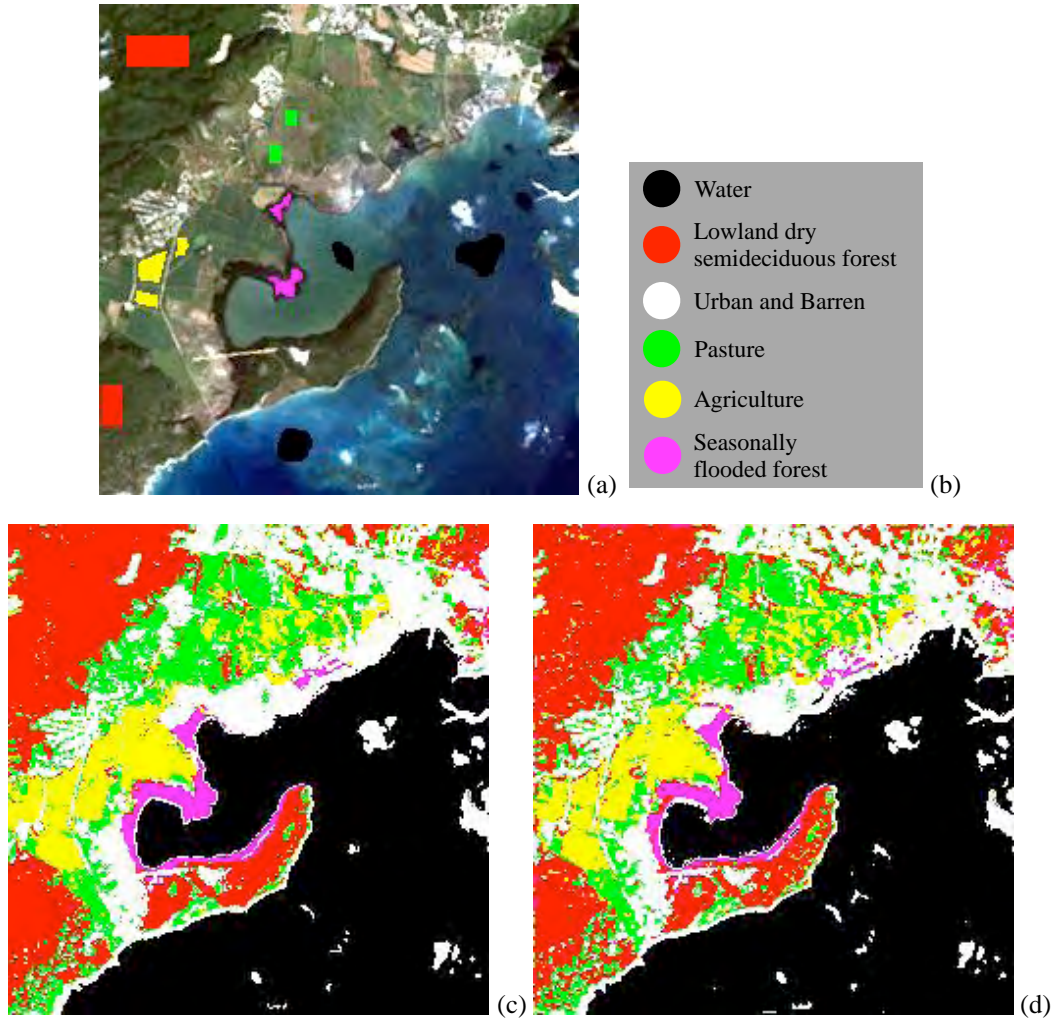


Figure 4.3 Thematic map for the image without atmospheric corrections. Image with ROIs (a), color map of classes (b), original (c) and restored (d) thematic maps.

4.2 Restored Image Classification

In this section, we show the classification results obtained for the restored image. Figure 4.3 show the results comparing the original and the restored images, it also shows, the image with the regions of interest (ROIs) used for the classification. Table 4.1 presents the number of testing/training samples used for each class.

We chose 1,969 pixels out of 61,250, which is the size of the image, as training samples to perform the supervised classification. For the original image, was found that 1,958 of 1,969 pix-

els were classified correctly giving as a result an overall accuracy of 93.44%. In Table 4.2, we present the confusion matrix for this image. Here we will see the pixels that were correctly classified and those that were classified under other classes. For example, 4 pixels from the pasture class were classified as agriculture (2) and as urban and barren (2), resulting in 80 pixels correctly classified as pasture. For the restored image, was found that 1,943 of 1,969 pixels were classified correctly giving as a result an overall accuracy of 98.68%. In Table 4.3, we present the confusion matrix for this image.

If we look Figure 4.3, we can notice some changes in the classification products, for example in the peninsula we can see that the classifier improve significantly. Pixels that were not classified on the original image, now are classified on the restored image. Figure 4.4 shows a cropped image from a lagoon located at the north side of the peninsula compared with an IKONOS image. Looking at the latter image, we can recognize some water pixels (black pixels) that were not

Table 4.2 Confusion matrix for the original image without atmospheric correction.

Class	Water	Agriculture	Urban and Barren	Seasonally flooded forest	Lowland dry forest	Pasture
Water	702	0	0	0	0	0
Agriculture	0	244	0	0	1	2
Urban and Barren	0	0	83	0	0	2
Seasonally flooded forest	0	0	0	144	0	0
Lowland dry forest	0	1	0	0	705	0
Pasture	0	2	2	0	0	80
Total	702	247	85	144	706	84

Table 4.3 Confusion matrix for the restored image without atmospheric correction.

Class	Water	Agriculture	Urban and Barren	Seasonally flooded forest	Lowland dry forest	Pasture
Water	702	0	0	0	0	0
Agriculture	0	237	0	0	5	2
Urban and Barren	0	0	81	0	1	2
Seasonally flooded forest	0	0	0	144	1	0
Lowland dry forest	0	7	0	0	699	0
Pasture	0	3	4	0	0	80
Total	702	247	85	144	706	84

found in the original image. This shows that the restoration method can retrieve features lost because of degradation since now the spatial features in the image are more defined, like edges, borders among other characteristics. Another region of interest is shown on Figure 4.5, here we show another lagoon. Once again we include an IKONOS image in order to show that in this area exist the presence of water.

In the following sections, we will show the results obtained for the restored image with atmospheric correction and the restored image with the atmospheric correction before the restoration process. Results are similar to these presented in this section, having this in mind we will show just the classification images and some comments explaining the results.

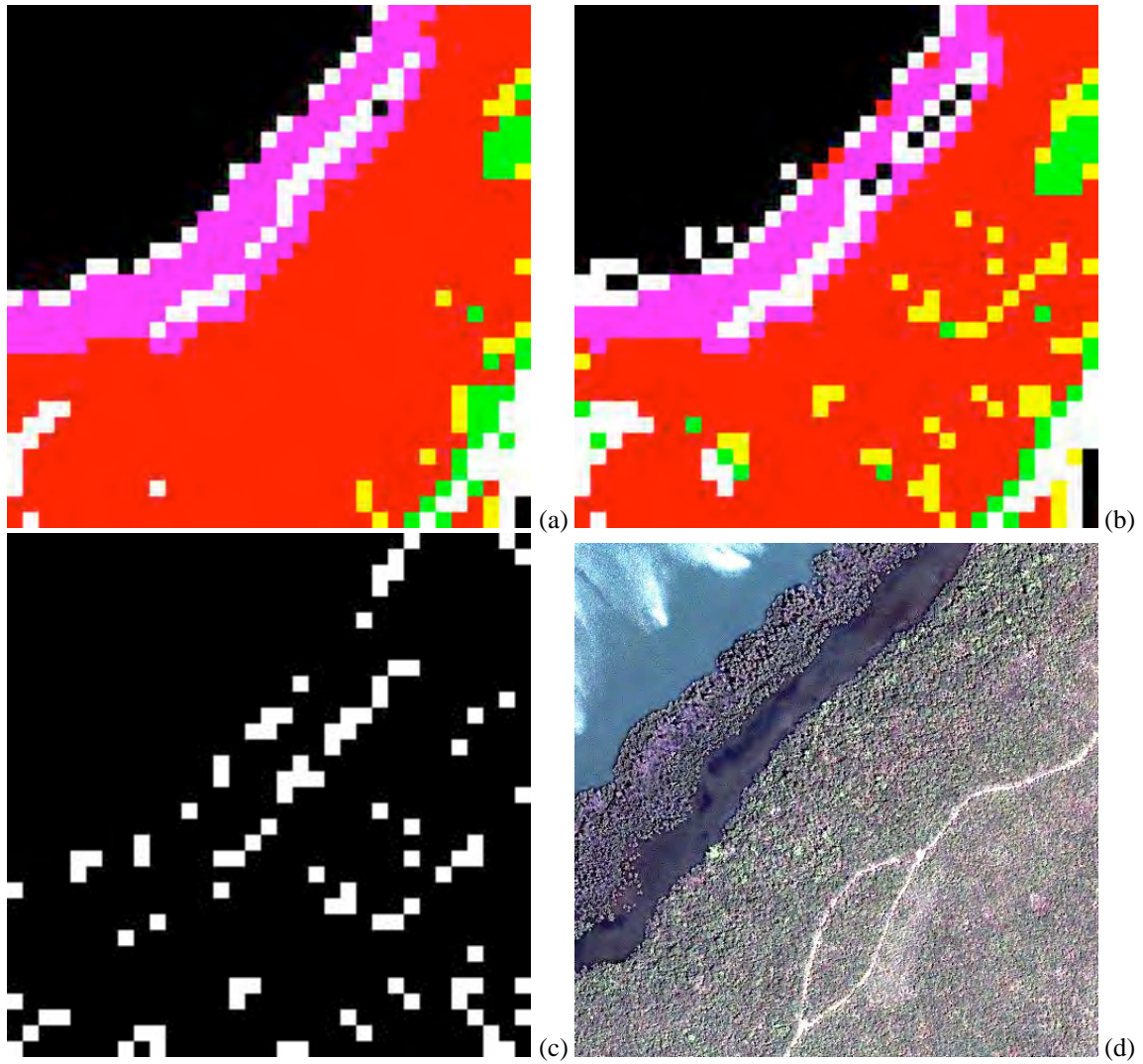


Figure 4.4 Original (a), Restored (b), difference between images (c) and IKONOS image.

4.3 Restored Image with Atmospheric Corrections Classification

The classification products obtained for the restored image with atmospheric correction after the restoration process are similar to those shown in the previous section. In this image, we applied the dark subtraction method for atmospheric correction described in Section 3.4. All pixels in the image are the same correction. Knowing this we will expect the same classification results as for the image without atmospheric correction.

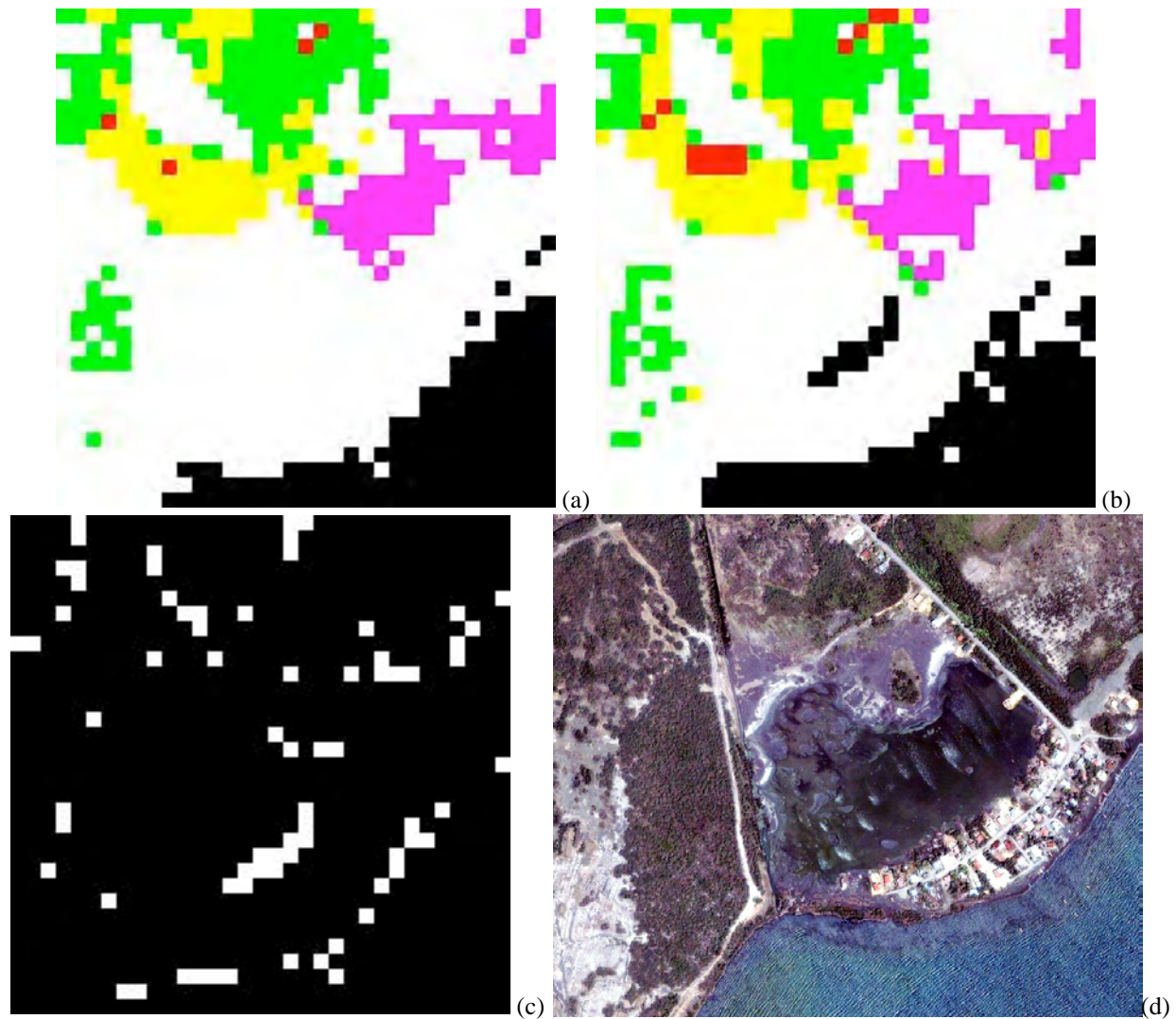


Figure 4.5 Original (a), Restored (b), difference between images (c) and IKONOS image.

Figure 4.5 show the thematic map for this image. If we compare Figure 4.5 with Figure 4.2 we will notice that are the same figures or at least have the same features. Maybe is not that clear, but in Table 4.4 and Table 4.5 we show the confusion matrix obtained for the original and restored image, respectively. We used the same ROIs as testing/training samples that we used for the image described Section 4.2. The overall accuracy for the original and restored image are, 93.44% and 98.68%. respectively, the same as the percents obtained for the image without atmospheric correction.

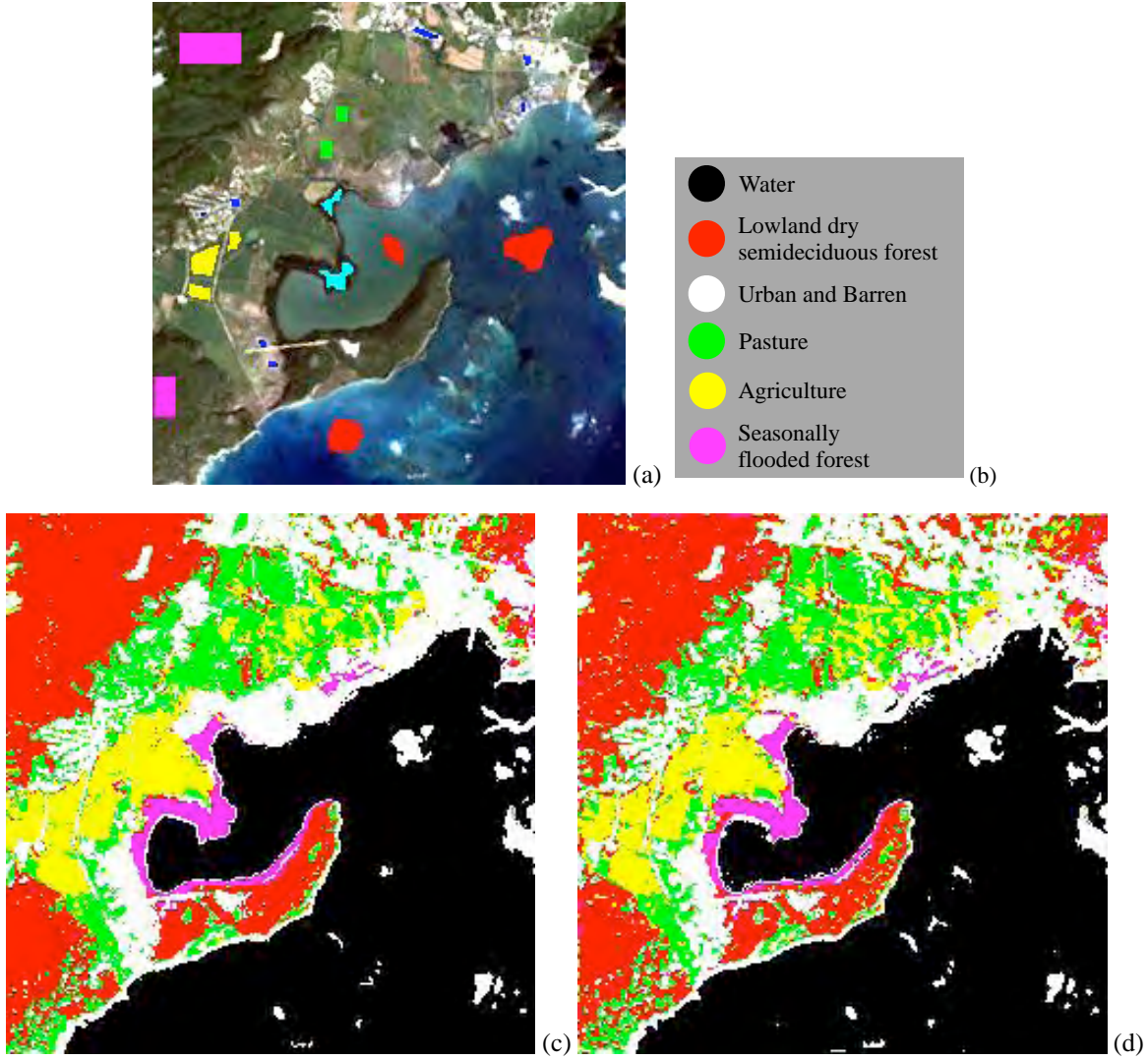


Figure 4.5 Thematic map for the image with atmospheric correction. Image with ROIs (a), color map of classes (b), original (c) and restored (d) thematic maps.

4.4 Atmospheric Corrected-Restored Image Classification

In this section, results for the image with atmospheric corrections before the restoration process are presented. In Section 3.5, we described the process to obtain this image, we correct for the atmosphere with the dark subtract method, then we applied the restoration algorithm. As mentioned in the previous section, a uniform correction do not affect the classification results. Once again, we have the same results as in section 4.2. Refer to this section to see the classification products.

Table 4.4 Confusion matrix for the original image with atmospheric correction.

Class	Water	Agriculture	Urban and Barren	Seasonally flooded forest	Lowland dry forest	Pasture
Water	702	0	0	0	0	0
Agriculture	0	244	0	0	1	2
Urban and Barren	0	0	83	0	0	2
Seasonally flooded forest	0	0	0	144	0	0
Lowland dry forest	0	1	0	0	705	0
Pasture	0	2	2	0	0	80
Total	702	247	85	144	706	84

Table 4.5 Confusion matrix for the restored image with atmospheric correction.

Class	Water	Agriculture	Urban and Barren	Seasonally flooded forest	Lowland dry forest	Pasture
Water	702	0	0	0	0	0
Agriculture	0	237	0	0	5	2
Urban and Barren	0	0	81	0	1	2
Seasonally flooded forest	0	0	0	144	1	0
Lowland dry forest	0	7	0	0	699	0
Pasture	0	3	4	0	0	80
Total	702	247	85	144	706	84

4.5 Effects on Classification of Stopping Criteria

In this section, we will show classification results for those images presented in Section 3.6. These images are examples of what happens if an iterative method is not stopped at the right point. The images presented are not very clear for the human eye, but when they are classified everything is different. Figure 4.6 shows the classification results for images with 5 and 10 iterations, compared with the original image.

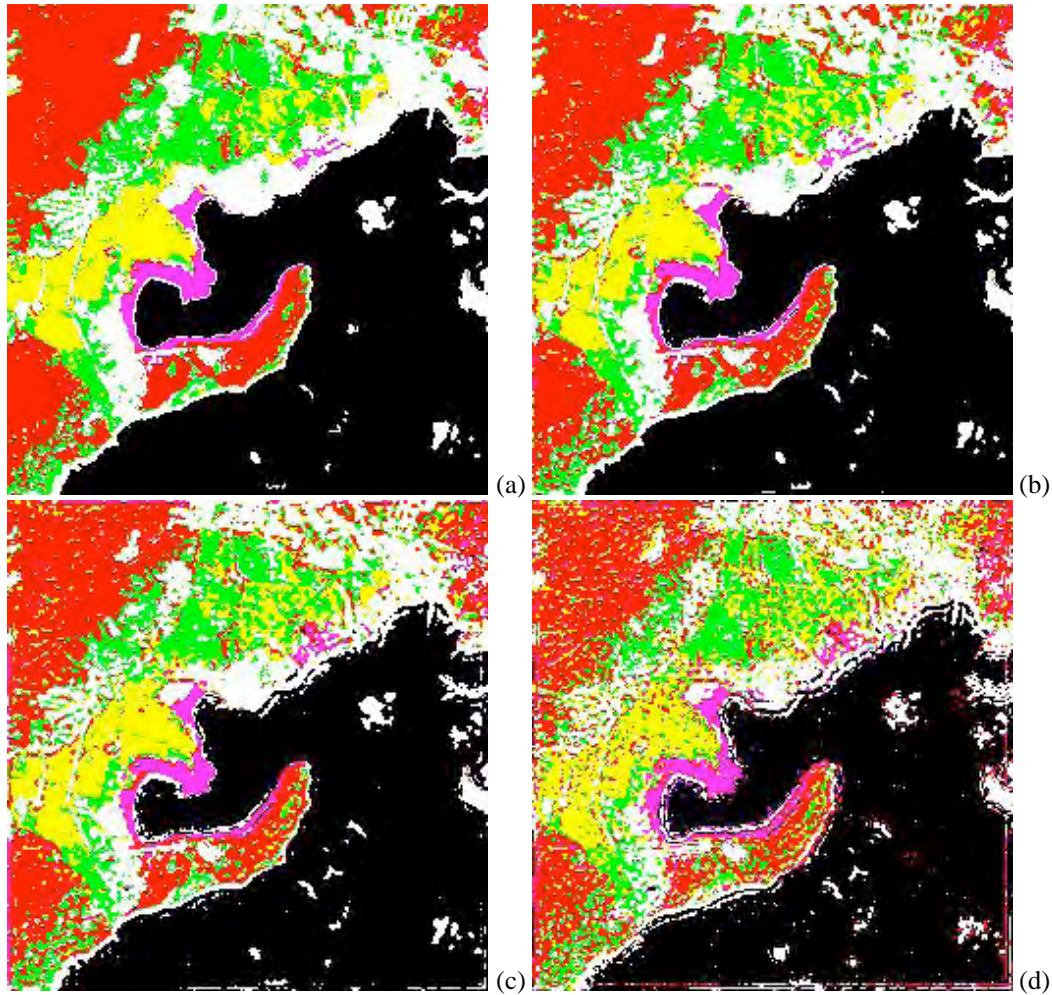


Figure 4.6 Thematic map for the images with 5 and 10 iterations. Thematic map of the original (a), 3 iterations (b), 5 iterations (c) and 10 iterations (d) images.

If we look closer at these images, we can notice that the classification is good in the 3rd iteration but improve significantly in the 5th iteration and in the 10th iterations, because features such as small water bodies, urban areas and coastal lines are better defined, but in the tenth iteration divergence introduces features that are not present in the previous iterations. Divergence introduces parallel lines or curves around the features (coastal line, urban areas, agriculture regions, etc). Figure 4.7 and 4.8 show highlighting changes in these classifications.

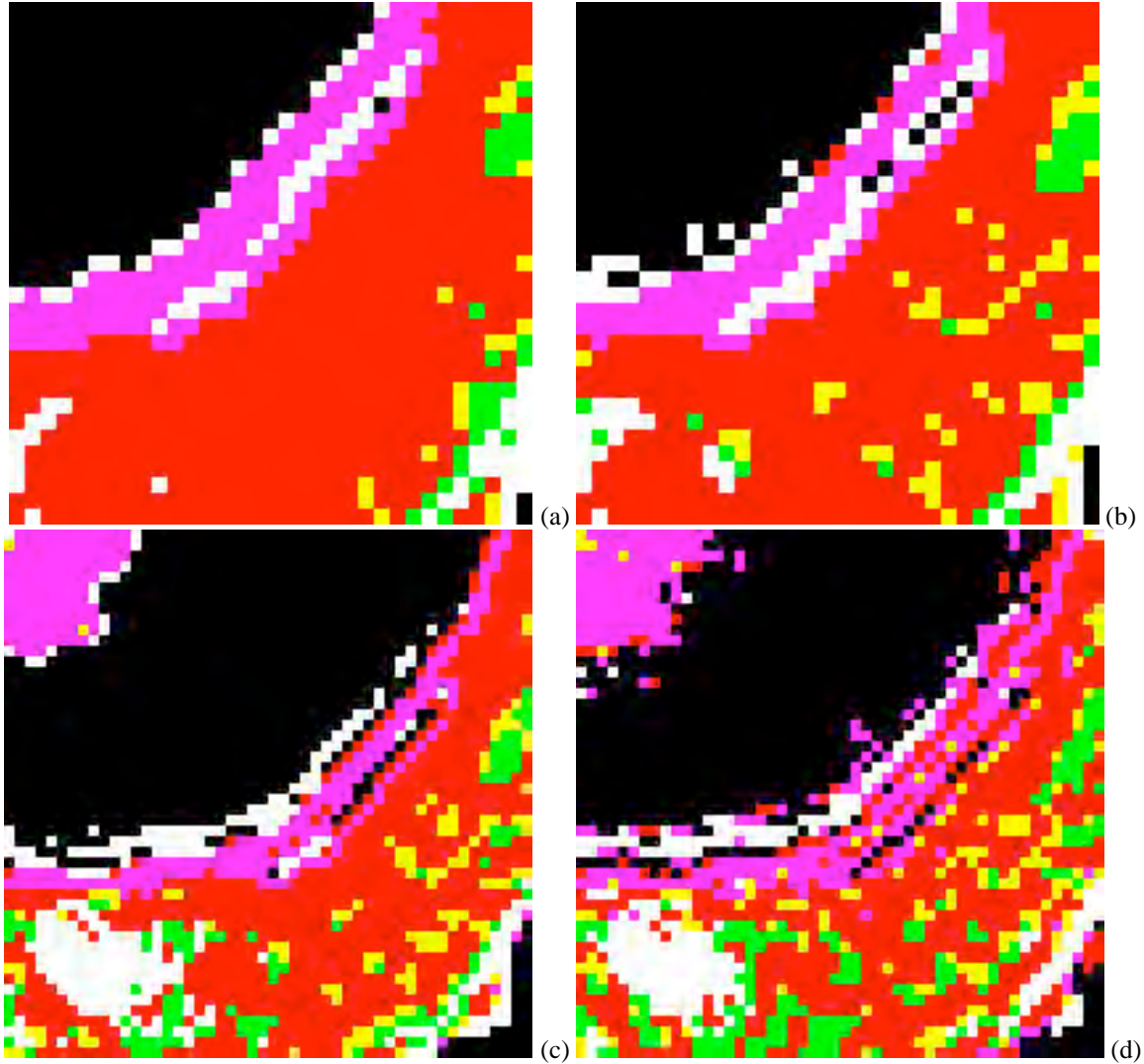


Figure 4.7 Zoom of the thematic map for the images with 3, 5 and 10 iterations. Original (a), 3 iterations (b), 5 iterations (c) and 10 iterations (d) images.

We chose 1,969 pixels out of 61,250, which is the size of the image, as training samples to perform the supervised classification. For the original image, it was found that 1,958 of 1,969 pixels were classified correctly giving as a result an overall accuracy of 93.44%. For the 5 iteration and 10 iterations images were found that the overall accuracy was 97.10 % and 91.98%, respectively. In Table 4.6 and Table 4.7, we present the confusion matrix for the 5th and 10th iterations images. In these tables we can see the pixels well classified and the ones classified under

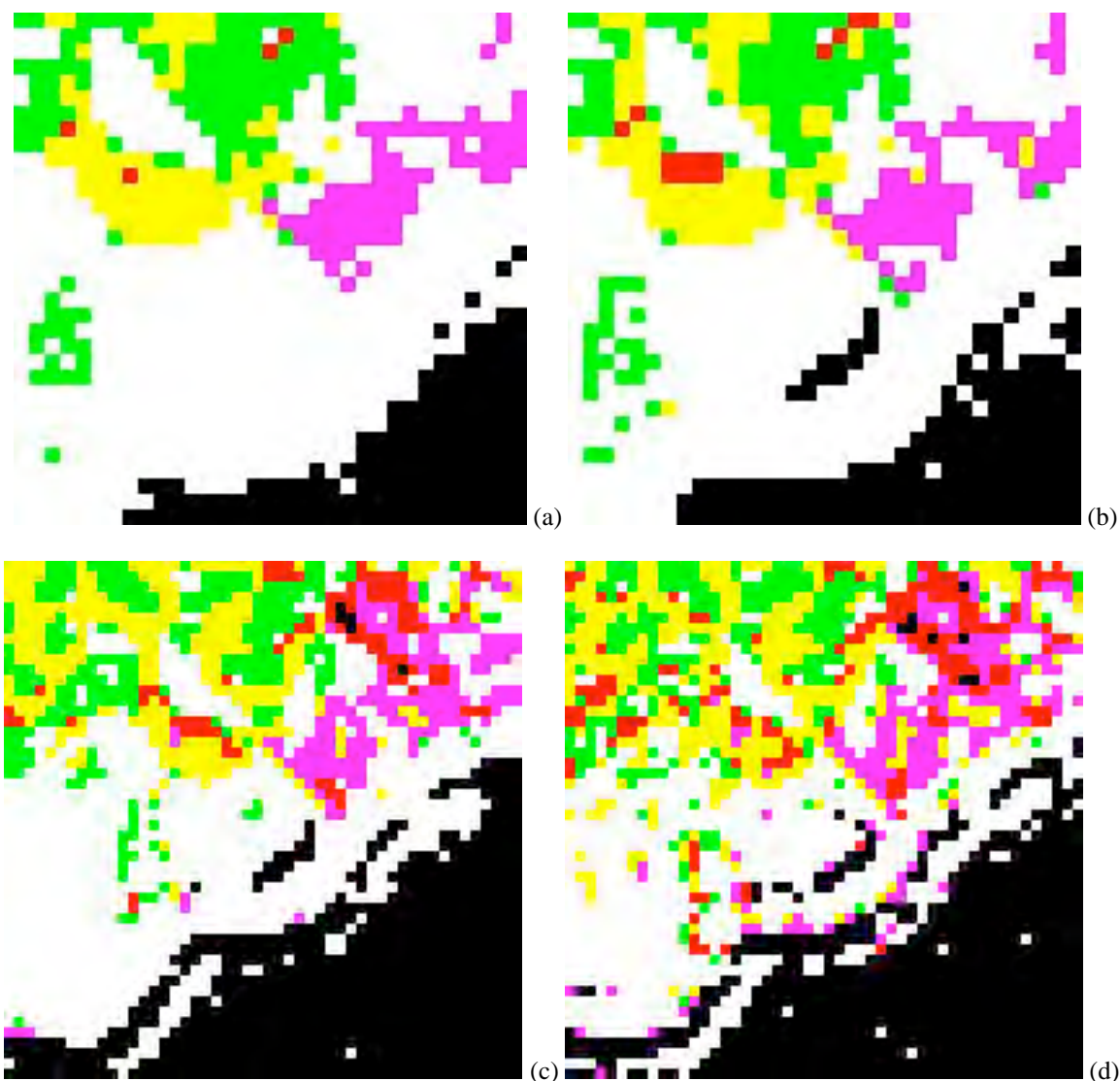


Figure 4.8 Zoom of the thematic map for the images with 3, 5 and 10 iterations. Original (a), 3 iterations (b), 5 iterations (c) and 10 iterations (d) images.

other classes, for example, in Table 4.6 we chose 702 pixels as training samples for Water and 702 were classified as Water. In the other hand, we chose 247 pixels for Agriculture, 229 were classified as Agriculture, but 18 were classified as Lowland dry forest (15 pixels) and Pasture (3 pixels). In Table 4.7 we also chose 702 pixels as training samples for Water, but 698 were classified as Water, and 4 as Urban and Barren (3 pixels) and Seasonally flooded forest (1 pixel). For Agriculture, 192 were well classified, but 55 pixels were classified under the following classes: Urban and Barren (2), Seasonally flooded forest (3), Lowland dry forest (27) and Pasture (23).

This classification results can be caused by the divergence introduced when the algorithm is not stopped at the right point. For further results refer to these tables.

Table 4.6 Confusion matrix for the restored image with 5 iterations.

Class	Water	Agriculture	Urban and Barren	Seasonally flooded forest	Lowland dry forest	Pasture
Water	702	0	0	0	0	0
Agriculture	0	229	2	1	19	6
Urban and Barren	0	0	80	0	2	0
Seasonally flooded forest	0	0	0	143	2	0
Lowland dry forest	0	15	1	0	679	0
Pasture	0	3	2	0	4	79
Total	702	247	85	144	706	85

Table 4.7 Confusion matrix for the restored image with 10 iterations.

Class	Water	Agriculture	Urban and Barren	Seasonally flooded forest	Lowland dry forest	Pasture
Water	698	0	0	0	0	0
Agriculture	0	192	2	2	51	6
Urban and Barren	3	2	78	0	0	0
Seasonally flooded forest	1	3	0	138	19	0
Lowland dry forest	0	27	1	4	627	1
Pasture	0	23	4	0	9	78
Total	702	247	85	144	706	85

4.6 Conclusions

Results of supervised classification of the three images were presented. Classification improvements were obtained on the restored images as expected. Also, we found that the dark sub-

traction method did not changed. The overall accuracy percent for the original and restored image are 99.44% and 98.68%, respectively. Higher accuracy percentages were expected for the restored image, but due to the conditions of small ROIs, these were lower. In the other hand, the distribution or classification of small spatial features improved significantly, nevertheless these percentages were lower. Areas where some features were not classified on the original image, were classified on the restored image (Figures 4.3 and 4.4). We also presented classification results for the image with 5 and 10 iterations. For these images we used the same ROIs as for the previous images. Best results were obtained with further iterations (5 and 10), once again the overall accuracies were lower but when zoomed the images the features were well classified, based on the map class used as ground truth information.

5 CONCLUSIONS AND FUTURE WORK

5.1 Summary

The main objective of this project was to implement restoration algorithms for multispectral imagery and to study the effect of restoration in classification accuracy. Other objectives were to create and develop a software application for multispectral image restoration and study restoration and classification performance with and without atmospheric corrections. We studied three images derived from the Landsat 4 image from a region located at the south of Puerto Rico (18.1°N, 66.2°W), an image with an without atmospheric correction after the restoration process and an image with atmospheric correction before the restoration process algorithm. In this project, we used the Lucy-Richardson reconstruction algorithm to correct for the PSF and the dark subtraction method for the atmospheric correction. Once we applied the restoration algorithm we classified the images to study the effects in each image.

5.2 Conclusions

The blurring caused by instrument collection system characterized by its PSF affects the quality of satellite image and its use for land cover characterization. The acquired image is distorted by the PSF and atmospheric contributions that produces distorted images. The use of the Lucy-Richardson method for multispectral image restoration revealed the expected results, to have a brighter image, and improve classification products revealing small spatial features hidden by the blur.

The image was enhanced significantly after the restoration process, refer to Figures 3.6, 3.11, and 3.16 to see the results. On Figures 3.8, 3.13, and 3.18 we showed spectral reflectance profiles of five features from the image. The spectral reflectance profiles, also, showed remarkable changes on the three images. The features were shifted to higher reflectance values on the restored image. Scatterplots were developed in order to see the changes in brightness before and after the restoration process, it was found that after the restoration process pixels that were brighter became darker and darker pixels became brighter, as expected (See Figures 3.10, 3.14, and 3.19). Also, we plotted the reflectance percentages per bands to see this brightness changes (Figures 3.11, 3.15, and 3.20). Means and standard deviations of the differences between the “original” and restored images were calculated, and found that bands 4 and 5 were the bands with more enhancement than the other four bands (bands 1,2,3, and 7) with standard deviations of approximately 3% and 4% for the three images.

Supervised classification was performed on the three images, and similar results were found. We chose six classes to perform classification, water, lowland dry semideciduous forest, seasonally flooded forest, urban and barred, agriculture, and pasture. The image was basically com-

posed of these six features. We classified the three images, the “original” and the restored, and we found that the changes were significant. Spatial features that were not correctly classified on the original image were correctly classified on the restored image, refer to Figures 4.3 and 4.4 to see the results. The overall accuracy percent for the original and restored image are 99.44% and 98.68%, respectively. We found that the dark pixels atmospheric correction method does not affect the classification process, because the method applied a uniform correction to the image. However, the dark pixel method does affect the restoration process, it was found that gives better results when the atmospheric correction is applied after the restoration process.

We found that the application of a restoration algorithm to multispectral images is very important as a pre-processing technique because the restored image revealed features that were not clear in the raw image. We also found, that the classification process improved significantly after the restoration algorithm was applied. Furthermore we found that the atmospheric correction was not necessary to fulfill the main objective of this project.

5.3 Future Work

In this project, we presented results of multispectral image restoration only for a Landsat 4 image, this let to future work in the following topics to be studied:

- More experimentation with images with ground truth for validation of the restoration algorithms. In addition to this, work with other multispectral sensors and compare results.
- More experimentation with non-uniform atmospheric correction methods, before and after the restoration process.

- Perform the same methodology used in this project on hyperspectral imagery. Repeat the process combining spatial and spectral domain restoration.

BIBLIOGRAPHY

1. Banham, M. R., Katsaggelos, A. K., (1997). "Digital Image Restoration". *IEEE Signal Processing Magazine*. 24-41.
2. Campbell, J. B., (2002). *Introduction to Remote Sensing*. 3rd ed. Guilford Press, NY.
3. Carnahan, B., Luther, H. A., Wilkes, J., (1969). *Applied Numerical Methods*. Krieger Publishing Company-Malabar, Florida.
4. Chung, F., Jian-wen, MA., and Jian-ping, Ch., (2004). "The PSF Correction method for Satellite Image Restoration". *Proceedings of the Third International Conference on Image and Graphics (ICIG'04)*.
5. Davis, P. J. and Rabinowitz P.,(1983). *Methods of Numerical Integration*. 2nd ed., Academic Press.
6. F.D. van der Meer and S.M. de Jong, (2006). *Remote Sensing Analysis: Including the Spatial Domain*, Springer.
7. Galatsanos, N. P., Chin, R., (1989). "Digital Restoration of Multichannel Images". *IEEE Transactions on Acoustics, Speech and Signal Processing*, Vol. 37. No. 3, 415-421.
8. Gonzalez, R. C., Woods, R. E., (2002). *Digital Image Processing*. Prentice Hall, NJ.
9. Huang Ch., Townshend, J. R. G., Liang, Sh., Kalluri, S. N. V., (2002). "Impacts of sensor's point spread function on land cover characterization: assessment and deconvolution". *Remote Sensing of Environment*, Vol. 80, 203-212.
10. Jansson, P. A., (1997). *Deconvolution of images and spectra*. Academic Press, Inc., San Diego.
11. Kruse F. A. 1999. "Visible-Infrared Sensor and Case Studies". *Remote Sensing for the Earth Sciences: Manual of Remote Sensing*. 3.
12. Kruse F. A., Boardman, J. W., Huntington, J. F, Mason, P. and Quigley, M. A. 2002. "Evaluation and Validation of EO-1 Hyperion for Geologic Mapping. *IEEE International Geoscience and Remote Sensing Symposium*, 2002.1: 593-595.
13. Langrebe, D. A., (2003). *Signal Theory Methods in Multispectral Remote Sensing*. John Wiley & Sons.
14. Liang, S., (2004). *Quantitative Remote Sensing of Land Surfaces*. John Wiley & Sons.
15. Markham, B. L., (1985). "The Landsat Sensors' Spatial Responses". *IEEE Transactions on Geoscience and Remote Sensing*, Vol. GE-23, No. 6, 864-875.
16. Mather, P. M. 2004. *Computer Processing of Remotely-Sensed Images: An Introduction*. 3rd ed. John Wiley and Sons.
17. Modestino, J. W., and Fries, R. W., (1980). "Construction and Properties of a Useful Two-Dimensional Random Field". *IEEE Transactions on Information Theory*, Vol. IT-26, No. 1, 44-50.

18. Schowengerdt, R. A., (2006). *Remote Sensing: Models and Methods for Image Processing*. 3rd ed., Elsevier.
19. Townshend, J. R. G., Huang Ch., Kalluri, S. N. V., Defries, R. S., and Liang, S., (2000). "Beware of per-pixel characterization of land cover". *Int. J. Remote Sensing*, Vol. 21, No. 4, 839-843.
20. Umaña-Díaz, A and Vélez-Reyes, M., (2006). "Restoration of hyperspectral imagery". In *Proceedings of SPIE: Algorithms and Technologies for Multispectral, Hyperspectral, and Ultraspectral Imagery XII*, Vol. 6233.
21. Wu, H. H. P., Schowengerdt, R. A., (1993). "Improved Estimation of Fraction Images Using Partial Image Restoration". *IEEE Transactions on Geoscience and Remote Sensing*, Vol. 31, No. 4, 771-778.
22. http://en.wikipedia.org/wiki/Point_spread_function
23. http://www.au.af.mil/au/awc/space/primer/multispectral_imagery.pdf
24. <http://www.btopper.com/Optics.pdf>
25. <http://documents.wolfram.com/applications/digitalimage/UsersGuide/ImageTransforms/ImageProcessing8.7.html>

Appendix A

MATLAB Algorithm for the image without atmospheric corrections

```
% This algorithm opens a Landsat TM 4 image by using "multibandread", show the
% image per band. Then it calculates the PSF matrix to use it with
% Lucy-Richarson algorithm in order to restore the image.

clear all, clc;
for j = 1:4

    band(j) = j;
    SI = multibandread('/users/carlosemoralesarroyo/Desktop/Veronica/MATLAB71/NAC6 original Re-
flectance',[250 245 6], 'float32',0,'bsq','ieee-be');

    % figure
    % imshow(SI(:, :, band(j)), []); % especifico el numero de bandas q quiero mostrar. Cuando quiero usar
    solo una banda
    % str = sprintf('%s %d', 'Guanica, band', band(j));
    % title(str);
    % saveas(gcf, str, 'jpg');

    % =====
    % Sigma values for bands 1 thru 4:
    % =====
    sigmax = 35.9;
    sigmay = 32.1;

    delta = 30;    %Landsat spatial resolution in [m]

    Cx = 1./ (sqrt((2*pi*sigmax^2)));
    fx1 = (delta/2)*Cx*exp(-2/(2*(sigmax/delta)^2));
    fx2 = (delta)*Cx*exp(-1/(2*(sigmax/delta)^2));
    fx3 = fx2;
    fx4 = fx2;
    fx5 = fx1;

    Cy = 1./ (sqrt((2*pi*sigmay^2)));
    fy1 = (delta/2)*Cy*exp(-2/(2*(sigmay/delta)^2));
    fy2 = (delta)*Cy*exp(-1/(2*(sigmay/delta)^2));
    fy3 = fy2;
    fy4 = fy2;
    fy5 = fy1;

    % =====
    % Generating the five vectors with the values for sigma.
    % =====
```

```

PSFx1 = [fx1 fx2 fx3 fx4 fx5];

PSFy1 = [fy1 fy2 fy3 fy4 fy5]';

% =====
% Creating the Transfer function for the PSF. Lo hago y*x para que genere
% la matriz que quiero.
% =====

PSF1 = PSFy1*PSFx1;

Blurred = SI(:,band(j));      % Defining the SI image as the blurred data. In this case is the Landsat
image.
%figure, imshow(Blurred(:,band(j)),[]);

% =====
% Image restoration using Richard-Lucy
% Running Lucy-Richardson algorithm with 1 to 3 iterations.
% =====

RLucy = zeros([size(Blurred), 3]);
for i = 1:3
    iter(i) = i;
    RLucy(:,i) = deconvlucy(Blurred, PSF1, iter(i));
%     str = sprintf('%s %d', 'Restored Image, (band ',band(j),' with Lucy-Richardson,', iter(i), ' itera-
tions');
%     figure; imshow(RLucy(:,i), []); title(str)
%     saveas(gcf,str,'jpg')
end

% =====
% Guardando la imagen usando multibandwrite, me va a generar una imagen de 3 bandas,
% donde estas bandas son las 3 iteraciones de Lucy-Richardson.
% =====

filename = sprintf('%s%d%s','Restored NAC6 Band', band(j), '.img');
multibandwrite(RLucy, filename, 'bsq');

outstr = sprintf('ENVI\ndescription = {Imported by HIAT}\nsamples = %s\nlines = %s\nbands =
%s\nheader offset = %s\ndata type = %s\ninterleave = %s\n byte order = %s\n', '245', '250', '3', '0', '5',
'bsq', '1');
filename = sprintf('%s%s',filename, '.hdr');
fid = fopen(filename,'w');
fwrite(fid,outstr, 'char');
fclose(fid);

end

% *****
% This part of the algorithm is for band 5.
% The values for sigmax and sigmay are different from the bands 1-4.
% *****

for k = 5:6

```

```

band(k) = k;

% =====
% Sigma values for band 5 and 7:
% =====

sigmax = 35.7;    %one sigma in [m], crosstrack.
sigmay = 33.3;    %one sigma in [m], alongtrack.

delta = 30;      %Landsat spatial resolution in [m]

Cx = 1./(sqrt((2*pi*sigmax^2)));
fx1 =(delta/2)*Cx*exp(-2/(2*(sigmax/delta)^2));
fx2 = (delta)*Cx*exp(-1/(2*(sigmax/delta)^2));
fx3 = fx2;
fx4 = fx2;
fx5 = fx1;

Cy = 1./(sqrt((2*pi*sigmay^2)));
fy1 =(delta/2)*Cy*exp(-2/(2*(sigmay/delta)^2));
fy2 = (delta)*Cy*exp(-1/(2*(sigmay/delta)^2));
fy3 = fy2;
fy4 = fy2;
fy5 = fy1;

% =====
% Generating the five vectors with the values for sigma.
% =====

PSFx1 = [fx1 fx2 fx3 fx4 fx5];

PSFy1 = [fy1 fy2 fy3 fy4 fy5]';

% =====
% Creating the Transfer function for the PSF. Lo hago y*x para que genere
% la matriz que quiero.
% =====

PSF1 = PSFy1*PSFx1;

Blurred = SI(:,band(k));      % Defining the SI image as the blurred data. In this case is the Landsat
                               % image.
%figure, imshow(Blurred(:,band),[]);

% =====
% Image restoration using Richard-Lucy
% Running Lucy-Richardson algorithm with 1 to 3 iterations.
% =====

RLucy = zeros([size(Blurred), 3]);
for i = 1:3
    iter(i) = i;
    RLucy(:,i) = deconvlucy(Blurred, PSF1, iter(i));

```

```

%      str = sprintf('%s %d', 'Restored Image, (band ',band,') with Lucy-Richardson,', iter(i), ' itera-
tions');
%      figure; imshow(RLucy(:,:,i), []); title(str)
%      saveas(gcf,str,'jpg')

end

% =====
% Guardando la imagen usando multibandwrite, me va a generar una imagen de 10 bandas,
% donde estas bandas son las 3 iteraciones de Lucy-Richardson.
% =====

filename = sprintf('%s%d%s','Restored NAC6 band', band(k), '.img');
multibandwrite(RLucy, filename, 'bsq');

outstr    = sprintf('ENVI\ndescription = { Imported by HIAT}\nsamples = %s\nlines = %s\nbands =
%s\nheader offset = %s\nndata type = %s\ninterleave = %s\n byte order = %s\n', ...
    '245', '250', '3', '0', '5', 'bsq', '1');
filename   = sprintf('%s%s',filename, '.hdr');
fid        = fopen(filename,'w');
fwrite(fid,outstr, 'char');
fclose(fid);

end

% =====
% Abrir la imagen corregida y la original con las seis bandas.
% =====

NOAtmCorr = multibandread('/users/carlosemoralesarroyo/Desktop/Veronica/MATLAB71/NAC6 origi-
nal Reflectance',[250 245 6],...
    'float32',0,'bsq','ieee-be');

RLUCY = multibandread('/users/carlosemoralesarroyo/Desktop/Veronica/MATLAB71/NAC6 restored
Reflectance',[250 245 6],...
    'float32',0,'bsq','ieee-be');

% =====
% Crear las bandas en vectores para hacer los scatterplots.
% =====

bandOriginal = zeros(250,245,6);
bandRestored = zeros(250,245,6);
std_dev_Band = zeros(6,1);
mean_Band = zeros(6,1);

for m = 1:6          %Total number of bands is 6.

    bandOriginal(:,:,m) = NOAtmCorr(:,:,m)*100;
    bandRestored(:,:,m) = RLUCY(:,:,m)*100;

    err = reshape((bandOriginal(:,:,m)-bandRestored(:,:,m)),250*245,1);
    std_dev_Band(m) = std(err);
    mean_Band(m) = mean(err);

```

```

figure; imshow(NOAtmCorr(:,:,m),[]), colorbar
str = sprintf('%s %d', 'AtmCorr Original band',m);
title(str);
saveas(gcf,str,'jpg')

figure; imshow(RLUCY(:,:,m),[]), colorbar
str = sprintf('%s %d', 'AtmCorr Restored band',m);
title(str);
saveas(gcf,str,'jpg')

% =====
% Diferencia entre imagenes original y corregida por la atmosfera
% =====

Difference = RLUCY - NOAtmCorr;
%figure
%plot(Difference(1,:,1))

figure
imshow(Difference(:,:,1),[]), colorbar
str = sprintf('%s %d', 'Difference between restored and original image, band', 1);
title(str);
saveas(gcf,str,'jpg')
%figure
%imshow(Difference(:,:,[]), colorbar      % Grafica las cinco bandas en una figura.
%str = sprintf('%s %d', 'Difference between restored and original images');
%title(str);
%saveas(gcf,str,'jpg')

end

% =====
% Sacatterplots entres las bandas de las imagenes original y restaurada.
% =====

figure
subplot(2,1,1)
scatter(reshape(bandOriginal(:,:,1),245*250,1),reshape(bandRestored(:,:,1),245*250,1)),
str = ('Scatterplot of bands 1; Original and Restored ');
title(str)
ylabel('Band 1: Restored (%)'), xlabel('Band 1: Original (%)')
subplot(2,1,2)
scatter(reshape(bandOriginal(:,:,2),245*250,1),reshape(bandRestored(:,:,2),245*250,1)),
str = ('Scatterplot of bands 2; Original and Restored ');
title(str)
ylabel('Band 2: Restored (%)'), xlabel('Band 2: Original (%)')
saveas(gcf,'Scatterplot of bands 1, 2 ; Original and Restored','jpg')

figure
subplot(2,1,1)

```

```
scatter(reshape(bandOriginal(:,:,3),245*250,1),reshape(bandRestored(:,:,3),245*250,1)),str = ('Scatterplot  
of bands 3; Original and Restored ');  
title(str)  
ylabel('Band 3: Restored (%)'), xlabel('Band 3: Original (%)')  
subplot(2,1,2)  
scatter(reshape(bandOriginal(:,:,4),245*250,1),reshape(bandRestored(:,:,4),245*250,1)),str = ('Scatterplot  
of bands 4; Original and Restored ');  
title(str)  
ylabel('Band 4: Restored (%)'), xlabel('Band 4: Original (%)')  
saveas(gcf,'Scatterplot of bands 3, 4 ; Original and Restored','jpg')
```

[illegible]

```
figure
subplot(2,1,1);
plot(bandOriginal(161,:,3)), xlabel('Pixel Number band 3'), ylabel('Reflectance [%]')
title('Reflectance plot for band 3')
hold on
plot(bandRestored(161,:,3),'r'), xlabel('Pixel Number band 3'), ylabel('Reflectance [%]')
legend('Before restoration','After Restoration')
subplot(2,1,2);
plot(bandOriginal(161,:,4)), xlabel('Pixel Number band 4'), ylabel('Reflectance [%]')
title('Reflectance plot for band 4')
```


Appendix B

MATLAB Algorithm for the image with atmospheric corrections

```
% This code open the Restored w/AtmCorr image to calculate the difference
% between images (restored and original) in order to plot it. Also, plot
% scatterplots comparing same band from different images.

% =====
% Abrir la imagen corregida y la original con las cinco bandas.
% =====

wAtmCorr = multibandread('/users/carlosemoralesarroyo/Desktop/Veronica/MATLAB71/wAtmCorr 6R
Original',[250 245 6], 'float32',0,'bsq','ieee-be');

wAtmCorrRestored =
multibandread('/users/carlosemoralesarroyo/Desktop/Veronica/MATLAB71/wAtmCorr 6R Restored',[250
245 6], 'float32',0,'bsq','ieee-be');

% =====
% Crear las bandas en vectores para hacer los scatterplots.
% =====

bandOriginal = zeros(250,245,6);
bandRestored = zeros(250,245,6);
std_dev_Band = zeros(6,1);
mean_Band = zeros(6,1);

for l = 1:6      %Total number of bands is 5.

    bandOriginal(:,:,l) = wAtmCorr(:,:,l)*100;
    bandRestored(:,:,l) = wAtmCorrRestored(:,:,l)*100;

    err = reshape((bandOriginal(:,:,l)-bandRestored(:,:,l)),250*245,1);
    std_dev_Band(l) = std(err);
    mean_Band(l) = mean(err);

    figure; imshow(wAtmCorr(:,:,l),[]), colorbar
    str = sprintf('%s %d', 'AtmCorr Original band',l);
    title(str);
    saveas(gcf,str,'jpg')

    figure; imshow(wAtmCorrRestored(:,:,l),[]), colorbar
    str = sprintf('%s %d', 'AtmCorr Restored band',l);
    title(str);
    saveas(gcf,str,'jpg')

% =====
% Diferencia entre imagenes original y corregida por la atmosfera
% =====
```

```

Difference = wAtmCorrRestored - wAtmCorr;
%figure
%plot(Difference(1, :, 1))

figure
imshow(Difference(:, :, 1), [], colorbar
str = sprintf('%s %d', 'Difference between restored and original image, band', 1);
title(str);
saveas(gcf, str, 'jpg')

end

% =====
% Sacatterplots entres las bandas de las imagenes original y restaurada.
% =====

figure
subplot(2, 1, 1)
scatter(reshape(bandOriginal(:, :, 1), 245*250, 1), reshape(bandRestored(:, :, 1), 245*250, 1)),
str = ('Scatterplot of bands 1; Original and Restored ');
title(str)
ylabel('Band 1: Restored (%)'), xlabel('Band 1: Original (%)')
subplot(2, 1, 2)
scatter(reshape(bandOriginal(:, :, 2), 245*250, 1), reshape(bandRestored(:, :, 2), 245*250, 1)),
str = ('Scatterplot of bands 2; Original and Restored ');
title(str)
ylabel('Band 2: Restored (%)'), xlabel('Band 2: Original (%)')
saveas(gcf, 'Scatterplot of bands 1, 2 ; Original and Restored', 'jpg')

figure
subplot(2, 1, 1)
scatter(reshape(bandOriginal(:, :, 3), 245*250, 1), reshape(bandRestored(:, :, 3), 245*250, 1)), str = ('Scatterplot
of bands 3; Original and Restored ');
title(str)
ylabel('Band 3: Restored (%)'), xlabel('Band 3: Original (%)')
subplot(2, 1, 2)
scatter(reshape(bandOriginal(:, :, 4), 245*250, 1), reshape(bandRestored(:, :, 4), 245*250, 1)), str = ('Scatterplot
of bands 4; Original and Restored ');
title(str)
ylabel('Band 4: Restored (%)'), xlabel('Band 4: Original (%)')
saveas(gcf, 'Scatterplot of bands 3, 4 ; Original and Restored', 'jpg')

figure
subplot(2, 1, 1)
scatter(reshape(bandOriginal(:, :, 5), 245*250, 1), reshape(bandRestored(:, :, 5), 245*250, 1)),
str = ('Scatterplot of bands 5; Original and Restored ');
title(str)
ylabel('Band 5: Restored (%)'), xlabel('Band 5: Original (%)')
subplot(2, 1, 2)
scatter(reshape(bandOriginal(:, :, 6), 245*250, 1), reshape(bandRestored(:, :, 6), 245*250, 1)),
str = ('Scatterplot of bands 7; Original and Restored ');
title(str)
ylabel('Band 7: Restored (%)'), xlabel('Band 7: Original (%)')

```

```
saveas(gcf,'Scatterplot of band 5 and 7 ; Original and Restored','jpg')
```

```
figure
subplot(2,1,1);
plot(bandOriginal(161,:,1)), xlabel('Pixel Number Band 1'), ylabel('Reflectance [%]')
title('Reflectance plot for band 1')
hold on
plot(bandRestored(161,:,1),'r'), xlabel('Pixel Number band 1'), ylabel('Reflectance [%]')
legend('Before restoration','After Restoration')
hold off
subplot(2,1,2);
plot(bandOriginal(161,:,2)), xlabel('Pixel Number band 2'), ylabel('Reflectance [%]')
title('Reflectance plot for band 2')
hold on
plot(bandRestored(161,:,2),'r'), xlabel('Pixel Number band 2'), ylabel('Reflectance [%]')
hold off
saveas(gcf,'Reflectance plots band 1 and 2','jpg')
```

```
figure
subplot(2,1,1);
plot(bandOriginal(161,:,5)), xlabel('Pixel Number band 5'), ylabel('Reflectance [%]')
title('Reflectance [%] plot for band 5 of Original image.')
hold on
plot(bandRestored(161,:,5),'r'), xlabel('Pixel Number band 5'), ylabel('Reflectance [%]')
title('Reflectance [%] plot for band 5 of Restored image.')
legend('Before restoration','After Restoration')
hold off
subplot(2,1,2);
plot(bandOriginal(161,:,6)), xlabel('Pixel Number band 7'), ylabel('Reflectance [%]')
title('Reflectance [%] plot for band 7')
hold on
plot(bandRestored(161,:,6),'r'), xlabel('Pixel Number band 7'), ylabel('Reflectance [%]')
hold off
saveas(gcf,'Reflectance [%] plots band 5 and 7','jpg')
```

Appendix C

MATLAB Algorithm for the image with atmospheric corrections before restoration

```
% This algorithm opens a Landsat TM 4 image by using "multibandread", show the
% image per band. Then it calculates the PSF matrix to use it with
% Lucy-Richarson algorithm in order to restore the image.

clear all, clc;

SI = multibandread('/Applications/MATLAB71/AtmCorr 6R Original',[250 245 6],...
    'float32',0,'bsq','ieee-be');

for j = 1:4
    band(j) = j;

% figure
% imshow(SI(:,5),[]); % especifico el numero de bandas q quiero mostrar. Cuando quiero usar solo
una banda
% str = sprintf('%s %d', 'Guanica, band', band(j));
% title(str);
% saveas(gcf,str,'jpg');

%
=====
=
% If I want to show the image in RGB I used this portion of algorithm.
%
=====
=

%SI = multibandread('/Applications/MATLAB71/PR_Landsat-7_S_12_13_05.htm',[843 883 5],...
    'uint8=>uint8',0,'bsq','ieee-le',{ 'Band','Direct',[3 2 1]});
%figure,imshow(SI)

% =====
% Sigma values for bands 1 thru 4:
% =====
sigmax = 35.9;
sigmay = 32.1;

delta = 30;    %Landsat spatial resolution in [m]

Cx = 1./sqrt((2*pi*sigmax^2));
fx1 =(delta/2)*Cx*exp(-2/(2*(sigmax/delta)^2));
fx2 = (delta)*Cx*exp(-1/(2*(sigmax/delta)^2));
fx3 = fx2;
fx4 = fx2;
fx5 = fx1;

Cy = 1./sqrt((2*pi*sigmay^2));
fy1 =(delta/2)*Cy*exp(-2/(2*(sigmay/delta)^2));
```

```

fy2 = (delta)*Cy*exp(-1/(2*(sigmay/delta)^2));
fy3 = fy2;
fy4 = fy2;
fy5 = fy1;

% =====
% Generating the five vectors with the values for sigma.
% =====

PSFx1 = [fx1 fx2 fx3 fx4 fx5];

PSFy1 = [fy1 fy2 fy3 fy4 fy5]';

% =====
% Creating the Transfer function for the PSF. Lo hago y*x para que genere
% la matriz que quiero.
% =====

PSF1 = PSFy1*PSFx1;

Blurred = SI(:,band(j));      % Defining the SI image as the blurred data. In this case is the Landsat
image.
%figure, imshow(Blurred(:,band(j)),[]);

% =====
% Image restoration using Richard-Lucy
% Running Lucy-Richardson algorithm with 1 to 3 iterations.
% =====

RLucy = zeros([size(Blurred), 3]);
for i = 1:3
    iter(i) = i;
    RLucy(:,i) = deconvlucy(Blurred, PSF1, iter(i));
%     str = sprintf('%s %d', 'Restored Image, (band ',band(j),') with Lucy-Richardson,', iter(i), ' itera-
%     tions');
%     figure; imshow(RLucy(:,i), []); title(str)
%     saveas(gcf,str,'jpg')
end

% =====
% Guardando la imagen usando multibandwrite, me va a generar una imagen de 3 bandas,
% donde estas bandas son las 3 iteraciones de Lucy-Richardson.
% =====

filename = sprintf('%s%d%s','Atm Corr 6R Restored Band', band(j), '.img');
multibandwrite(RLucy, filename, 'bsq');

outstr = sprintf('ENVI\ndescription = {Imported by HIAT}\nsamples = %s\nlines = %s\nbands =
%s\nheader offset = %s\nndata type = %s\ninterleave = %s\n byte order = %s\n', ...
    '245', '250', '3', '0', '5', 'bsq', '1');
filename = sprintf('%s%s',filename, '.hdr');
fid = fopen(filename,'w');
fwrite(fid,outstr, 'char');
fclose(fid);

```

end

```
%
*****

%
% This part of the algorithm is for band 5.
% The values for sigma_x and sigma_y are different from the bands 1-4.
%
*****

for k = 5:6
    band(k) = k;

    %SI = multibandread('/Applications/MATLAB71/Atm Corr Original',[250 245 5],...
    %'uint8',0,'bsq','ieee-le');
    % figure
    % imshow(SI(:,5),[]); % especifico el numero de bandas q quiero mostrar. Cuando quiero usar solo
    % una banda
    % str = sprintf('%s %d', 'Guanica, band', band(k));
    % title(str);

    % saveas(gcf,str,'jpg');

    % =====
    % Sigma values for band 5 thru 7:
    % =====

    sigma_x = 35.7; %one sigma in [m], crosstrack.
    sigma_y = 33.3; %one sigma in [m], alongtrack.

    delta = 30; %Landsat spatial resolution in [m]

    Cx = 1./sqrt((2*pi*sigma_x^2));
    fx1 = (delta/2)*Cx*exp(-2/(2*(sigma_x/delta)^2));
    fx2 = (delta)*Cx*exp(-1/(2*(sigma_x/delta)^2));
    fx3 = fx2;
    fx4 = fx2;
    fx5 = fx1;

    Cy = 1./sqrt((2*pi*sigma_y^2));
    fy1 = (delta/2)*Cy*exp(-2/(2*(sigma_y/delta)^2));
    fy2 = (delta)*Cy*exp(-1/(2*(sigma_y/delta)^2));
    fy3 = fy2;
    fy4 = fy2;
    fy5 = fy1;

    % =====
    % Generating the five vectors with the values for sigma.
    % =====
```

```

PSFx1 = [fx1 fx2 fx3 fx4 fx5];

PSFy1 = [fy1 fy2 fy3 fy4 fy5]';

% =====
% Creating the Transfer function for the PSF. Lo hago y*x para que genere
% la matriz que quiero.
% =====

PSF1 = PSFy1*PSFx1;

Blurred = SI(:,band(k));      % Defining the SI image as the blurred data. In this case is the Landsat
image.
figure, imshow(Blurred(:,band),[]);

% =====
% Image restoration using Richard-Lucy
% Running Lucy-Richardson algorithm with 1 to 3 iterations.
% =====

RLucy = zeros([size(Blurred), 3]);
for i = 1:3
    iter(i) = i;
    RLucy(:,i) = deconvlucy(Blurred, PSF1, iter(i));
%     str = sprintf('%s %d', 'Restored Image, (band ',band,') with Lucy-Richardson,', iter(i), ' iterations');
%     figure; imshow(RLucy(:,i), []); title(str)
%     saveas(gcf,str,'jpg')
end

% =====
% Guardando la imagen usando multibandwrite, me va a generar una imagen de 10 bandas,
% donde estas bandas son las 3 iteraciones de Lucy-Richardson.
% =====

filename = sprintf('%s%d%s','Atm Corr 6R Restored Band', band(k), '.img');
multibandwrite(RLucy, filename, 'bsq');

outstr = sprintf('ENVI\ndescription = { Imported by HIAT}\nsamples = %s\nlines = %s\nbands =
%s\nheader offset = %s\ndata type = %s\ninterleave = %s\n byte order = %s\n', ...
    '245', '250', '3', '0', '5', 'bsq', '1');
filename = sprintf('%s%s',filename, '.hdr');
fid = fopen(filename,'w');
fwrite(fid,outstr, 'char');
fclose(fid);

end

% =====
% Abrir la imagen corregida y la original con las cinco bandas.
% =====

```

```

AtmCorr = multibandread('/users/carlosemoralesarroyo/Desktop/Veronica/MATLAB71/AtmCorr 6R
Original',[250 245 6],...
    'float32',0,'bsq','ieee-le');

AtmCorrRestored = multibandread('/users/carlosemoralesarroyo/Desktop/Veronica/MATLAB71/AtmCorr
6R Restored',[250 245 6],...
    'double',0,'bsq','ieee-be');

% =====
% Crear las bandas en vectores para hacer los scatterplots.
% =====
bandOriginal = zeros(250,245,6);
bandRestored = zeros(250,245,6);
std_dev_Band = zeros(6,1);
mean_Band = zeros(6,1);

for m = 1:6                %Total number of bands is 5.

    bandOriginal(:,:,m) = AtmCorr(:,:,m)*100;
    bandRestored(:,:,m) = AtmCorrRestored(:,:,m)*100;

    err = reshape((bandRestored(:,:,m)-bandOriginal(:,:,m)),250*245,1);
    std_dev_Band(m) = std(err);
    mean_Band(m) = mean(err);

    figure; imshow(bandOriginal(:,:,m),[]), colorbar
    str = sprintf('%s %d', 'AtmCorr Original band',m);
    title(str);
    saveas(gcf,str,'jpg')

    figure; imshow(bandRestored(:,:,m),[]), colorbar
    str = sprintf('%s %d', 'AtmCorr Restored band',m);
    title(str);
    saveas(gcf,str,'jpg')

% =====
% Diferencia entre imagenes original y corregida por la atmosfera
% =====

Difference = (AtmCorrRestored - AtmCorr)*100;
%figure
%plot(Difference(1,:,1))

figure
imshow(Difference(:,:,m),[]), colorbar
str = sprintf('%s %d', 'Difference between restored and original image, band',m);
title(str);
saveas(gcf,str,'jpg')

end

```



```

legend('Before restoration','After Restoration')
hold off
subplot(2,1,2);
plot(bandOriginal(161,:,2)), xlabel('Pixel Number band 2'), ylabel('Reflectance [%] ')
title('Reflectance [%] plot for band 2')
hold on
plot(bandRestored(161,:,2),'r'), xlabel('Pixel Number band 2'), ylabel('Reflectance [%]')
hold off
saveas(gcf,'Reflectance [%] plots band 1 and 2','jpg')

figure
subplot(2,1,1);
plot(bandOriginal(161,:,3)), xlabel('Pixel Number band 3'), ylabel('Reflectance [%]')
title('Reflectance [%] plot for band 3')
hold on
plot(bandRestored(161,:,3),'r'), xlabel('Pixel Number band 3'), ylabel('Reflectance [%]')
legend('Before restoration','After Restoration')
hold off
subplot(2,1,2);
plot(bandOriginal(161,:,4)), xlabel('Pixel Number band 4'), ylabel('Reflectance [%]')
title('Reflectance [%] plot for band 4')
hold on
plot(bandRestored(161,:,4),'r'), xlabel('Pixel Number band 4'), ylabel('Reflectance [%]')
hold off
saveas(gcf,'Reflectance [%] plots band 3 and 4','jpg')

figure
subplot(2,1,1);
plot(bandOriginal(161,:,5)), xlabel('Pixel Number band 5'), ylabel('Reflectance [%]')
title('Reflectance [%] plot for band 5 of Original image.')
hold on
plot(bandRestored(161,:,5),'r'), xlabel('Pixel Number band 5'), ylabel('Reflectance [%]')
title('Reflectance [%] plot for band 5 of Restored image.')
legend('Before restoration','After Restoration')
hold off
subplot(2,1,2);
plot(bandOriginal(161,:,6)), xlabel('Pixel Number band 7'), ylabel('Reflectance [%]')
title('Reflectance [%] plot for band 7')
hold on
plot(bandRestored(161,:,6),'r'), xlabel('Pixel Number band 7'), ylabel('Reflectance [%]')
hold off
saveas(gcf,'Reflectance [%] plots band 5 and 7','jpg')

% #####
% Termina el codigo para trabajar con la imagen corregida por atmosfera.
% #####

```